NTNU

Norwegian University of
Science and Technology

Experimental Determination of Losses in MgB2 Superconductors for Wind Turbine Applications

Lars-Erik Moslått

Master of Energy and Environmental Engineering
Submission date: June 2017
Supervisor: Arne Nysveen, IEL
Co-supervisor: Niklas Magnusson, SINTEF Energi

Norwegian University of Science and Technology
Department of Electric Power Engineering

NORGES TEKNISK-NATURVITENSKAPELIGE UNIVERSITET

NTNU

M A S T E R T H E S I S

Name of the candidate	:	Lars-Erik Moslått
Main topic	:	**ELECTRICAL POWER ENGINEERING**
Title (Norwegian)	:	Eksperimentell testing av tap i MgB_2 superledere for vindturbinapplikasjoner
Title (English)	:	Experimental determination of losses in MgB_2 superconductors for wind turbine applications

Problem description:
Superconducting rotor windings are considered for large offshore wind turbine generators to reduce weight, size and cost. Superconductors carry DC currents loss-free, when cooled down to low temperatures, and their current densities are about 100 times higher than in copper conductors. However, when exposed to an AC magnetic field, the superconductor exhibit energy losses.

Although the rotor windings of a generator is operated with DC current, there will inevitably be a ripple AC magnetic field superimposed on the large DC magnetic field. The level of the losses appearing under these conditions will partly determine both the capacity and the design of the cooling system.

The master thesis study will include:

- To develop a calorimetric system for measurement of AC losses due to low AC magnetic fields on a bias DC magnetic field.
- To perform measurements of AC losses.

The DC magnetic field in the 0.5 – 1 T range will be generated by a superconducting coil developed in previous projects. The AC circuit and the measurement equipment are to be designed, built and incorporated in the existing cooling system.

Further details to be clarified with the supervisors.

Project start-up	: 15. January 2017
Project revision	: 15. June 2017
Project submission deadline	: 18. June 2017 :
Carried out at	: Dep. of Electric Power Engineering/NTNU
Co-supervisor	: Niklas Magnusson, SINTEF Energi
Responsible supervisor	: Professor Arne Nysveen

Trondheim, 15. June2017

Arne Nysveen
Responsible supervisor

Preface

This master thesis is written at the Department of Electrical Power Engineering at the Norwegian University of Science and Technology (NTNU) in collaboration with SINTEF Energy Research during spring semester 2017.

The master project is a part of the European Union research project INNWIND.EU. The INNWIND.EU has an overall goal of an innovative design of a beyond-state-of-the-art high performance offshore wind turbine in the range of 10-20MW. SINTEF in collaboration with NTNU have during the EU project produced a hardware demonstrator of a rotor field winding for a superconducting generator. During this master project, custom made equipment have been made and assembled with the DC field winding to experimentally determine AC losses in a MgB_2 superconductor.

I am grateful to get the opportunity to participate in research on this cutting-edge technology in the exciting field of superconductivity. I want to thank my supervisors for the involvement in this project, Professor Arne Nysveen at NTNU and Niklas Magnusson at SINTEF. I also want to thank Svein Magne Hellesø for great collaboration in the lab and to the assistance of the workers at the NTNU workshop.

Trondheim, June 18. 2017

Lars-Erik Moslått

Abstract

Superconducting generator field windings are suggested for the next generation of wind turbines. The foreseen wind turbines with power ratings greater than 10 MW give raise to technical challenges. Superconducting field windings can produce strong magnetic fields with a compact design. Generators with field windings made of superconducting MgB_2 wire could potentially reduce weight, material requirements, maintenance requirements and power losses, compared to conventional wind turbine generators.

Losses in the superconductors increase the cooling costs of the system, hence these losses affect the economic feasibility of applying superconductor technology for wind turbine applications. Superconductors in a rotor field winding will be exposed to a strong DC magnetic field with an AC magnetic field ripple. A theoretical model of the AC losses in the superconducting material MgB_2 predicts increasing losses when the strength of the DC and AC magnetic field increase. However, experimental testing is required to determine the magnitude of the losses in a MgB_2 superconductor.

A superconductive MgB_2 generator field winding demonstrator has been developed by SINTEF Energy Research in collaboration with NTNU, as part of the research project INNWIND.EU. The field winding is used to produce a strong background DC magnetic field during testing of AC losses. Custom hardware have been designed, produced and installed to produce a controlled AC field ripple and to measure the losses in a 10 cm sample of a MgB_2 superconducting wire. The losses are measured using a calorimetric measurement method. The test equipment is installed in the air gap of the field winding, in the existing cryogenic cooling environment of the field winding. During testing, the field winding and the wire sample is cooled to temperatures of about 20 K.

Losses are measured for different AC magnetic fields up to 21 mT peak, with different background DC fields up to 0.35 T. The losses measured increase with the 2nd power of the AC magnetic field, regardless of the strength of the background field applied. For a fixed AC field with different background fields, the AC losses peak at about 0.1 T DC field and are lowest at the highest field value of 0.35 T. After the first strong magnetization of the wire sample, it was found a significant difference in the AC losses as a function of the DC background field. Considering the magnitude and the loss patterns, it is assumed that the losses at the tested field strengths are dominated by eddy current losses and hysteresis losses in the copper and the nickel in the superconducting wire, not superconductor losses in the MgB_2.

Sammendrag

Superledende generator-feltviklinger er en mulig teknologi for neste generasjon vindturbiner. De forespeilede vindturbinene med effekt over 10 MW fører med seg nye tekniske utfordringer. Superledende feltviklinger kan indusere sterke magnetiske felt med en kompakt konstruksjon. Generatorer med feltviklinger laget av MgB_2 superledere kan potensielt redusere vekt, materialbehov, vedlikehold og effekttap, sammenlignet med konvensjonelle generatorer.

Tap i superlederne vil øke kjølekostnaden til systemet, dermed vil tapene påvirke hvorvidt det er økonomisk lønnsomt å benytte superlederteknologi i vindturbingeneratorer. Superledere i en rotorfeltvikling vil være eksponert for et sterkt DC-magnetfelt med en AC-ripple. I en teoretisk modell av AC tapene i MgB_2 er det beregnet at tapene vil øke når styrken til DC- og AC-magnetfeltet øker. For å avgjøre de faktiske effekttapene i en MgB_2 superleder er det nødvendig å gjøre eksperimentelle målinger.

SINTEF Energi i samarbeid med NTNU har utviklet og produsert en demonstrator av en superledende MgB_2 feltvikling. Dette er utført gjennom det europeiske forskningsprosjektet INNWIND.EU. Denne feltviklingen benyttes for å indusere et sterk bakgrunnsfelt under testing av AC-tap. For å lage en AC-magnetfeltripple og for å måle AC-tap i en 10 cm testbit av MgB_2 superleder, har spesialutstyr blitt designet, produsert og installert. AC tapene måles ved hjelp av en kalorimetrisk målemetode. Testutstyret er installert i det eksisterende kryogeniske kjølesystemet til feltviklingen. Under testing blir feltviklingen og superleder-testbiten nedkjølt til temperaturer på ca 20 K.

AC-tapene er målt for AC-magnetfelt opp til 21 mT amplitude, med ulike DC-felt opp til 0.35 T. De målte tapene øker eksponentielt med AC-magnetfeltet, med en eksponent på 2. Denne eksponentielle økningen måles ved alle testede bakgrunnsfeltstyrker. For et gitt AC-felt med ulike bakgrunnsfelt måles de høyeste AC-tapene ved 0.1 T og de laveste ved det høyeste DC-feltet på 0.35 T. Etter første sterke magnetisering av testbiten er det en stor forskjell i AC-tapene ved ulike bakgrunnsfelt. Basert på mønsteret og verdiene til tapene er det antatt at ved de feltstyrker benyttet i testene domineres tapene i superlederen av virvelstrømstap og hysteresetap i kobberet og i nikkelet i superlederen, ikke av superleder AC-tap i MgB_2.

Contents

List of Figures

List of Tables

Chapter 1

Introduction

A new generation of offshore wind turbines with power ratings greater than 10 MW is envisioned. New challenges arise as the power ratings increase. Important aspects subject to research are wind turbine weight, use of raw materials and power losses. On the pathway towards the next generation of wind turbines a huge EU project, INNWIND.EU, is carried out. 27 nations are participating through different innovative research projects on different fields of wind turbine technology.

SINTEF is part of INNWIND.EU with a research project on a superconducting field winding. The last two years an MgB_2 superconducting field winding demonstrator has been designed and produced at SINTEF with assistance from master students at NTNU. The field winding is race-track shaped, and is half a meter wide and 1 m long. It is designed to carry a current of 200 A. Superconducting MgB_2 field windings are considered for large wind turbine generators. This is due to the superconductors' capacity to carry current densities 25-50 times larger than copper, with approximately no power losses. A superconducting field winding can produce a strong magnetic field with a compact design. Superconducting generators are studied as a possible solution to the next generation of wind turbines, as it has the potential to reduce weight, size, power losses and price of the generator.

If superconducting field windings are to be applied in wind turbines, its economical feasibility has to be proven. The cost of cooling systems and cooling power could strongly impact the overall costs when applying superconductor technology. Power losses increase the total required cooling power for the superconductors. Hence, addressing the losses in the superconductors is necessary to evaluate its economic feasibility compared to other technologies. In real applications of a superconducting rotor field winding, the superconductors will be exposed to a strong DC magnetic field induced by the winding itself and an AC magnetic field ripple from AC harmonics and AC equipment disturbance. When exposed to AC magnetic fields, superconductors experience power losses.

This master thesis regards experimental testing of AC losses in a MgB_2 superconductor. To experimentally test these losses, a strong DC magnetic field is required, as well

as a controlled AC magnetic field disturbance and a system to measure losses in a superconducting wire sample. The pre-produced DC field winding demonstrator is used to produce the DC magnetic field, while the hardware for the AC magnetic field and the system for loss measurements are custom-made in this project. After production and mounting of the equipment, losses are measured systematically for different combinations of DC magnetic field and AC magnetic field strength.

Chapter 2

Theory

2.1 A brief history of superconductivity

The Dutch physicist Heike Kamerlingh Onnes was the first to discover the phenomenon of superconductivity in 1911. He observed that the resistance of mercury suddenly vanished below a critical temperature, $T_c \backsimeq 4.2$ K. No one had predicted this result and it took physicists almost half a century to figure out an explanation for the phenomenon, and ever since physicists have realized they still cannot fully explain superconductivity.

Since the discovery in 1911, superconductivity has been an important scientific area of physics with continuing surprises. This first discovery in mercury was a result of advancements in low temperature physics, as Kammerlingh Onnes was the first to achieve to liquefy helium. The achievement made it possible to cool materials to temperatures close to the absolute zero (-273 °C/0 K) and study their properties.

In 1933, the Meissner effect was discovered by the German physicists Walter Meissner and Robert Ochsenfeld. The Meissner effect is a property of all superconductors. When a superconductor exposed to a magnetic field is cooled below its transition temperature, all or part of the magnetic field in the conductor is expelled.

Despite a strong motivation to find superconducting materials with a high transition temperature, until the 1980s the highest T_c found was 23 K in Nb_3Ge. In 1986, Karl Alexander Müller and Johannes Georg Bednorz discovered superconducting properties at 35 K; 12 K higher than the highest T_c known at that time. What made the finding even more remarkable was that the material used was a ceramic, more commonly known for its insulating properties. The discovery triggered a variety of research on different compounds, eventually resulting in the discovery of high-temperature superconductors (HTS). The critical temperature of HTS can be reached by using liquefied nitrogen with a boiling point of 77.4 K instead of helium. This makes the cooling process significantly easier and cheaper. HTS seemed to offer a promising future for the use of superconductors in practical applications. However, the prophecies of the applications of superconductors are

still not fulfilled. A century after the first discovery of superconductivity the applications of both LTS and HTS are still limited to mainly MRI machines and physics research equipment at CERN.

2.2 Application of superconductors in offshore wind power

In 2017, the interest in offshore wind power production is huge and it is increasing. With an annual offshore wind power installation of 2.2 GW in 2016, the world total installed capacity reached 14.6 GW [5]. In 2016, the total offshore wind power investments in Europe increased by 40%. Due to stronger and more stable winds at sea, wind power production offshore has a huge potential. More predictable and powerful winds increase the capacity factor for each turbine, which in turn lowers the levelized cost of electricity (LCOE) compared to onshore installations. Along with the increasing interest in wind power, there is an increasing interest in bigger wind turbines. In 2004, the average size of offshore wind turbine was 2 MW, while in 2014 the average size was increased to 3.6 MW [2] and in 2016, the first 8 MW wind turbine was installed. Bigger wind turbines reduce the LCOE due to higher capacity factors and lower operation and maintenance (O&M) costs per produced unit. Thus, the growth is expected to continue. A 6 MW wind turbine has 17 % lower LCOE than a 3 MW wind turbine [3]. As the LCOE is reduced, offshore wind power gets more competitive to other energy sources and can be expected to expand its market share.

Currently, the dominating companies are developing wind turbines in the range of 6-9 MW, mainly using permanent magnet generators. Geared doubly-fed induction generators are most commonly used, whereas direct drive train generators are less used. As the size of wind turbines are growing, direct drive technology could become a more feasible solution. By omitting the generator, the possibility of gear failure is avoided, reducing the O&M costs. A consequence of omitting the gear is that the generator gets increasingly huge, because the generator rotates with the same frequency as the turbine blades. Furthermore, the optimal blade rotation frequency (ω) gets lower for bigger turbines with more power (P). Correspondingly, the torque (M) increases strongly by the relation [11],

$$P = M\omega \rightarrow M \propto V \cdot \sigma \rightarrow \sigma \propto A \cdot B. \tag{2.1}$$

The torque is linear to the product of the rotor volume (V) and the shear stress (σ), thus the rotor size depends on the torque. The shear stress is linear to the product of the average air-gap magnetic field (B) and the linear current density (A). In conventional generators σ is limited as B usually will not exceed about 1.2 T due to magnetic saturation of the permanent magnet, and A is restricted by physical properties of the stator. If the permanent magnet or the copper field windings of a conventional generator is replaced by superconducting field windings, B can reach values of 2-3 T. Moreover, the armature teeth

can be removed. This leaves more space for the stator windings which allows for A to be increased. Hence, superconducting rotor windings have the potential of increasing the shear stress, which in turn increases the torque and thereby the power without increasing the volume of the generator.

2.3 Electromagnetism in superconductors

Two remarkable properties are observed when a material becomes superconductive. The DC resistivity of the material drops to zero. Hence, there are no resistive losses in the conductor. The other is that the conductor takes the property of a perfect diamagnet, to perfectly repel an external magnetic field. To try to understand the phenomenon of superconductivity, it is inevitable to end up in the field of quantum mechanics. Although there are several theories explaining the fundamental quantum mechanics of superconductivity, none of them are fully approved. These quantum mechanical theories will not be discussed in this report, as this is considered to be beyond the scope of this thesis. For practical applications of superconductivity, understanding the phenomenon in terms of electromagnetism is more relevant and is how it will be explained in the following.

2.3.1 The Superconductive state

Superconducting materials are only superconducting when operated within a certain range of magnetic field (B), temperature (T) and current density (J). The highest temperature in which the material is superconducting is the critical temperature (T_c) and depends on the value of B and J. The upper limit of the current in a superconductor is given by the critical current density (J_c), while the critical magnetic field (B_c) is the highest magnetic field density in which the material remains superconducting. If any of the three limits are exceeded, the material enters the normal state and ceases to be superconducting. The limits of the variables T, J and B for superconduction are interdependent, hence the upper limit of one of them depends on the value of the two remaining ones. Due to this relation, the temperature of a superconductor during operation is typically held well below the Tc. When temperatures are below the Tc, the superconductor can carry a higher current and withstand a higher magnetic field, without losing the superconductive abilities. The values of the critical limits of B, J and T depend on the superconducting material. By plotting the critical limits of a superconductor as a function of B, J and T in a three-dimensional graph, the critical limits form a continuous surface. This surface is known as the critical surface and is shown in the generic form in Figure 2.1

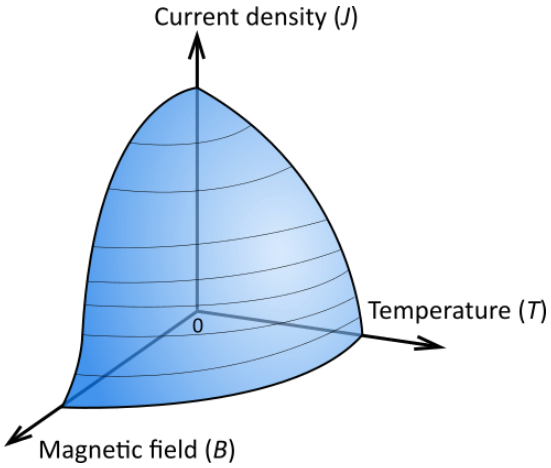

Figure 2.1: Generic critical surface of a superconductor.

In the transition from the superconductive state to the normal state, i.e. when crossing the critical surface, the resistance of the superconducting material changes from zero to a finite value. This transition is not infinitely sharp. The resistance increases continuously, hence the voltage across the superconductor increases gradually as the critical current (I_c) is exceeded. Due to this continuous transition in superconducting wires, a definition of the critical current is necessary. The critical current is defined as the current value of the superconductor when the dc electric field across the wire exceeds a specified value, E_0. The critical electrical field value for the MgB_2 wire in this project is set to $E_0 = 1 \cdot 10^{-4}$ V/m. In the transition from zero resistance to a finite resistance, the electric field can be approximated by the following relation between the conductor current (I) and the longitudinal dc magnetic field of the conductor (E_{dc}):

$$E_{dc}(I) = E_0 \left(\frac{I}{I_c} \right)^N . \tag{2.2}$$

I_c is the critical current of the conductor, E_0 is the specified value corresponding to the critical current and N is the exponent of the factor between the superconductor current and the critical current. The N-value is a parameter differing for different types of superconductors. A typical N-value for a MgB_2 wire is 20. A high N-value corresponds to a steep transition curve between the superconducting state and the normal state and is an indicator of quality.

There is a variation to the parameter critical current density (J_c) of a superconductor, called the engineering critical current density (J_e). J_c refers to the critical current density, with respect to the cross-section of only the superconducting material, e.g. the cross-section area of MgB_2 in a MgB_2 wire, even though the wire consists of additional materials for reinforcement. The J_e is the critical current density for the cross-section area of the whole wire, including the area of non-conducting materials. The engineering critical current density is often provided by the wire manufacturers as the actual wire cross-section is more relevant for practical engineering challenges.

2.3.2 The Meissner effect

22 years after Kammerlingh's discovery of zero electrical resistivity, Meissner and Ochsenfeld discovered another property of materials in the superconducting state. They found that materials in the superconducting state also exhibits the property of perfect diamagnet. Hence, the superconductor perfectly repels an applied magnetic field (B) below the critical temperature, T_c. The B-field inside the material becomes zero. By the expression of the B-field in terms of the magnetic field strength (H), the magnetization of the material (M) and the vacuum permeability constant (μ_0),

$$B = \mu_0(H + M) = 0, \tag{2.3}$$

it is found that for the B-field in the superconductor to become zero,

$$H = -M. \tag{2.4}$$

Hence, the resulting magnetic susceptibility (χ) is:

$$\chi = \frac{dM}{dH} = -1 \tag{2.5}$$

which is the value of a perfect diamagnetic material.

When a superconducting material with a temperature above T_c is exposed to a B-field, the field passes through the material as if it were vacuum. By decreasing the temperature of the material, it can be observed that as the temperature drops below T_c, the B-field suddenly passes the material on the outside. As the material enters the superconducting state, a shield current arise on the surface of the conductor. The magnitude and direction of this current is such that the corresponding B-field exactly cancels the initial field in the superconductor. The shield current also produces a B-field on the outside of the superconductor enforcing the initial field. A superconductor is said to be in the Meissner state, or the superconductive state, if it is not exposed to field values or temperatures such that the superconductor is penetrated by the magnetic field.

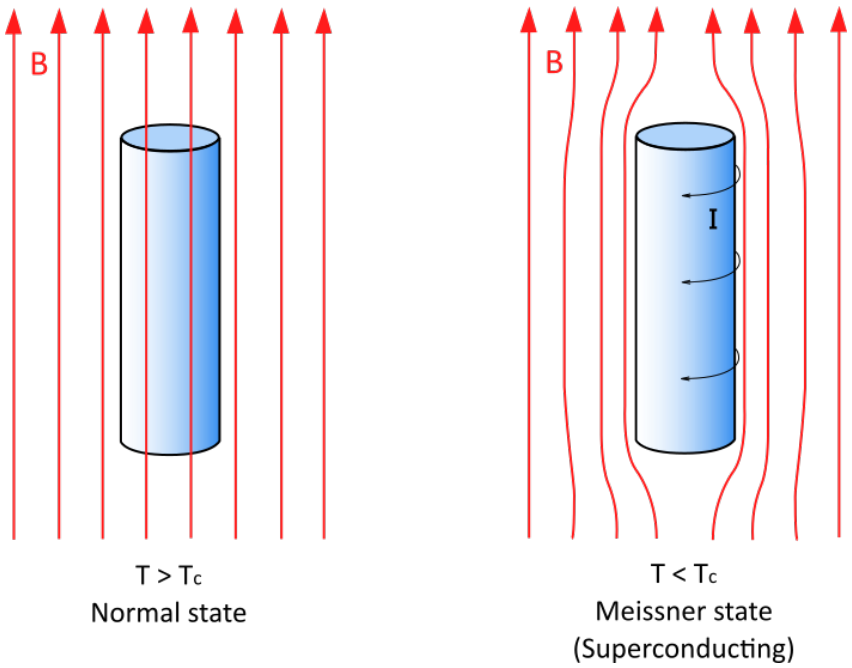

Figure 2.2: The Meissner effect. When the temperature is below the critical temperature currents are induced in the superconductor, repelling the external field.

2.3.3 Type I and type II superconductors

Superconductors are classified the categories Type I and Type II, depending on their transition characteristics between the superconductive state and the normal state. A superconductor has a critical field strength (H_c or H_{c1}) determined by the material. If the applied field exceeds the critical field of the superconductor, the Meissner effect breaks down and the magnetic field starts penetrating the superconductor.

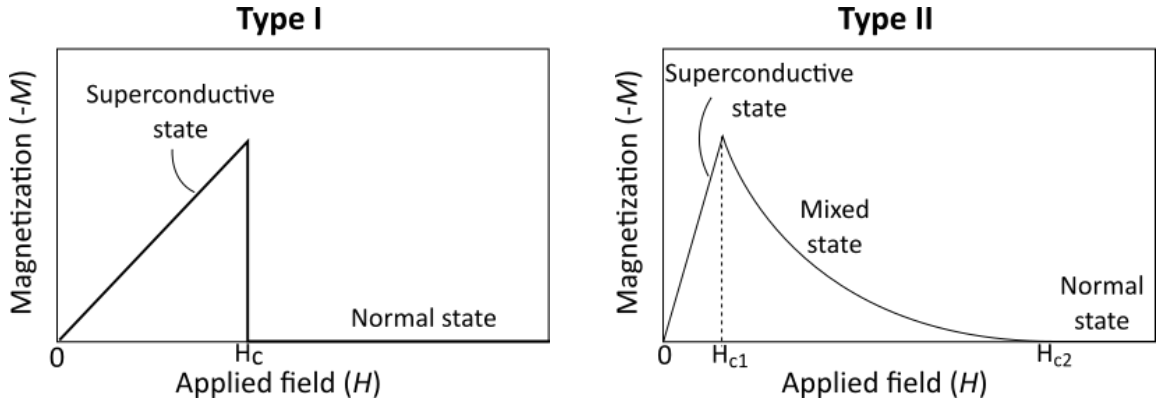

Figure 2.3: Transition from the superconductive state to the normal state. Typical curves of the applied field and magnetization in Type I and Type II superconductors.

In some superconductors, the magnetic field fully penetrates the superconductor abruptly when the applied field exceeds H_c. These superconductors instantly switch between the superconductive state and the normal state. These materials are called Type I superconductors. In Type II superconductors, the Meissner effect decays gradually when the applied field exceeds H_{c1}. As the applied field increases further, the superconductor material continuously loses the ability to withstand the external field until it reaches H_{c2} and the superconductor enters the normal state.

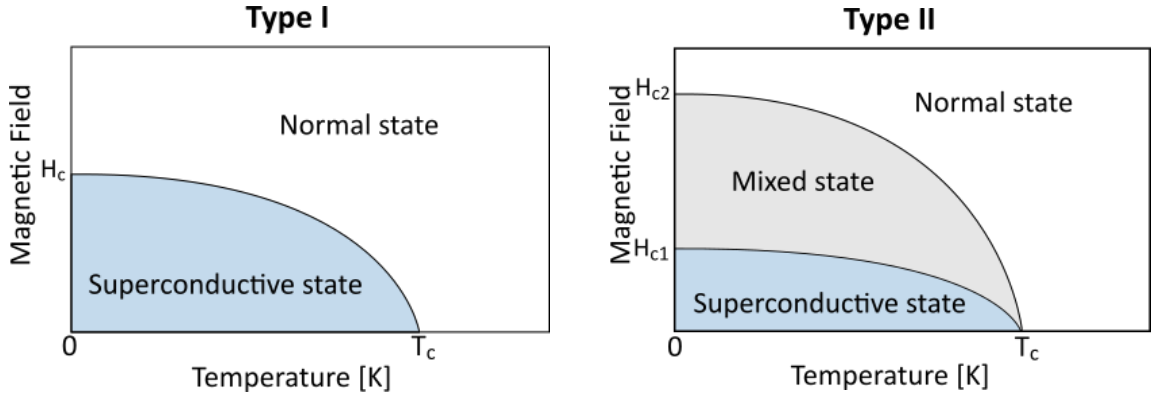

Figure 2.4: Transition from the superconductive state to the normal state. Typical curves of the magnetic field and temperature in Type I and Type II superconductors.

2.4 Magnesium diboride (MgB_2) superconductor

MgB_2 was first discovered to be superconducting by a Japanese research group in 2001. This simple and long known binary compound of magnesium and boron was found to switch to the superconducting state at a remarkably high temperature of 39 K. While the T_c of MgB_2 is relatively high, the transition characteristics is more like an LTS than an HTS. These characteristics makes it a credible competitor to other superconductors for low-temperature applications (below 25 K). The cost of the raw materials magnesium and boron is also relatively cheap. As the manufacturing of MgB_2 superconductors reaches economies of scale, these conductors will be more cost competitive compared to its alternatives.

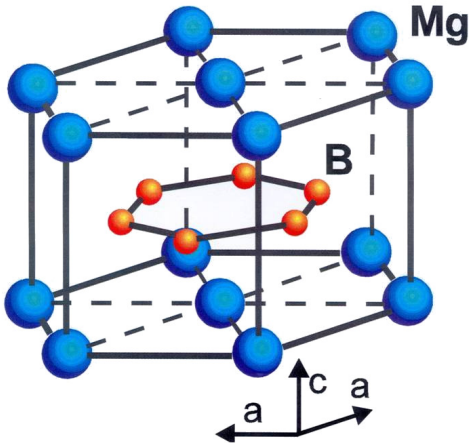

Figure 2.5: MgB_2 molecule structure [13].

The preparation process of MgB_2 for practical applications is carried out using either the powder in tube (PIT) technique or by Mg diffusion. Using these techniques, MgB_2 can be shaped into tape or wire, and potentially be used to manufacture equipment such as MRI-magnets, cables, superconducting induction heaters, fault current limiters, motors coils and generator coils.

2.4.1 Properties of the MgB_2 superconductor by *Columbus Superconductors*

The superconducting wire used in this project is manufactured by the Italian company Columbus Superconductors. Columbus Superconductors is one of the world leading manufacturing companies of MgB_2 superconductors, with an annual production of more than 3000 km of wire.

Columbus Superconductors is manufacturing wire using the PIT ex-situ process technique. Pre-reacted powder of MgB_2 is packed into a long tube shaped strip of metal, before it is shaped into a monofilament wire. Furthermore, a variable number of monofilament MgB_2 wires are packed into another tube of metal among with additional wire constituents and shaped into a conductor. The superconductor in the wire used in this project consists of 19 monofilament MgB_2 wires. To maximize the critical current and improve the superconducting properties of the multifilament wire, it is heat treated to sinter the MgB_2 grains. A benefit from the PIT ex-situ processing is the mechanical properties of the wire. With this technique, the wire can be winded, for instance to a coil, after the final heat treatment.

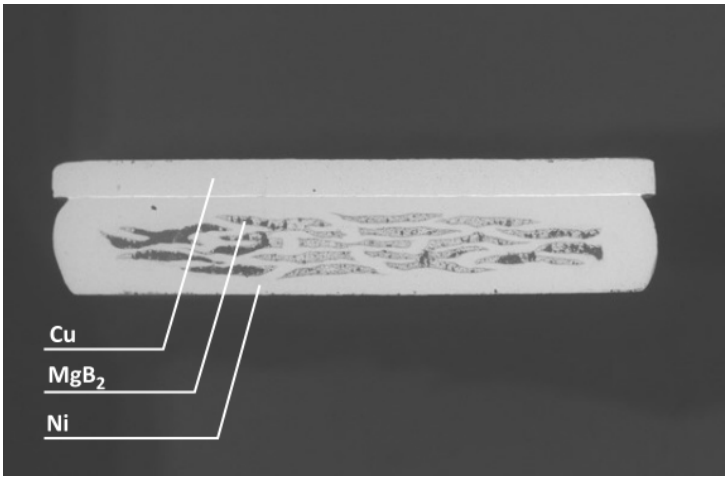

Figure 2.6: Cross-section of a 19 filament MgB_2 wire by Columbus Superconductors [1].

Figure 2.6 shows the cross-section of a multifilament MgB_2 wire similar to the wire used in this project. The cross-section area of the conductor is 3.00mm×0.50mm. In addition, there is a copper lamination layer of 3.00mm×0.20mm. The total cross-section area of the conductor is 1.50 mm^2 and consists of 0.30 mm^2 MgB_2 and 1.20 mm^2 Ni. A sheath of nickel is used to protect the superconducting MgB_2 filaments. The copper lamination serves as a mechanical reinforcement to stabilize the wire. In case of a quench the copper lamination can also reduce the risk of damage of the wire by conducting current. If subjected to mechanical stress the wire could easily break or lose its superconducting ability at the impact zone. Minimum bending diameter is specified by the manufacturer to be 150 mm.

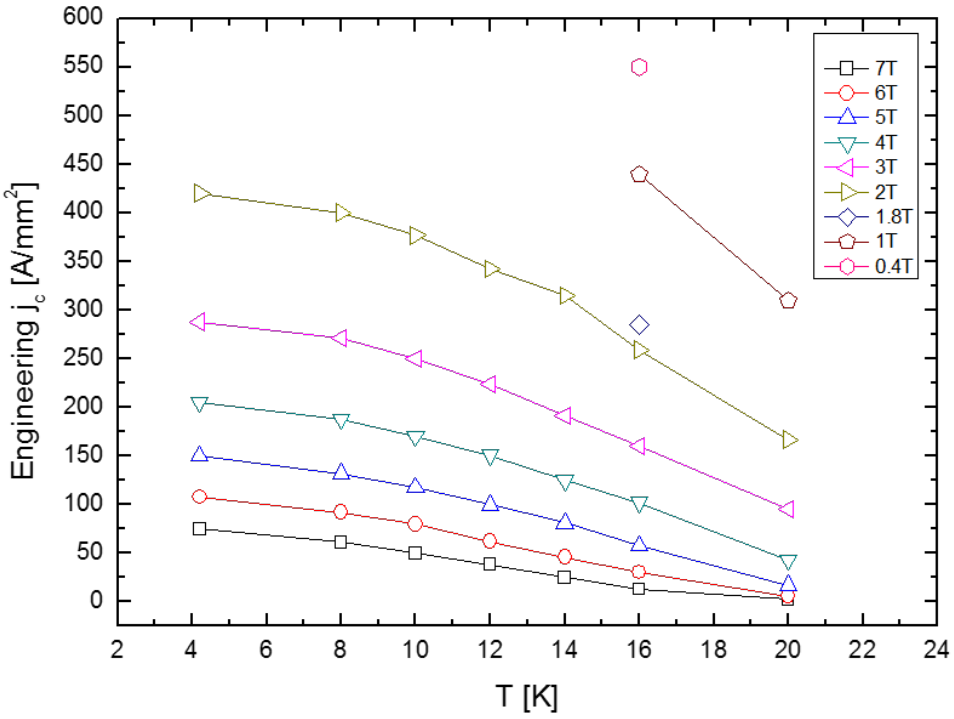

Figure 2.7: Critical engineering current density as a function of temperature for Columbus Superconductor's MgB_2 wire. Each curve corresponds to a different magnetic field density [1].

The operation range of the superconductor is specified in Figure 2.7. Each plot curve corresponds to the critical surface of the superconductor for a fixed magnetic field density. For temperatures above 20 K the critical current density and critical magnetic field tends to be strongly limited according to the curves. This indicates that the superconductor is not suited for applications at such temperatures. There is an increasing capacity of current density and magnetic field density at temperatures below 20K, suggesting operating temperatures in this range.

2.5 BSCCO superconductor by Sumitomo Electric

BSCCO wires consist of the materials bismuth (Bi), strontium (Sr), calsium (Ca), copper (Cu) and oxygen (O). BSCCO is a high-temperature superconductor with different T_c for different composition ratios. A Bi-2223 superconductor is used in this project. 2223 refers to the composition ratio of the chemical elements (except Oxygen which can take various values), $Bi_2Sr_2Ca_2Cu_3O_{10+x}$. The wire dimensions are 4.5mm×0.34mm, with a

reinforcing layer of a copper alloy on both sides with a thickness of 50μm. A cross-section of the wire is shown in Figure 2.8

Figure 2.8: Cross-section of BSCCO superconductor by Sumitomo Electrics [14].

The critical temperature of Bi-2223 is 110 K. In this project, the BSCCO superconductor is used to conduct current from the outer section of the cryostat to the field winding in the centre of the cryostat. In the outer section of the cryostat, the expected temperatures are in the range of 50-100 K. The temperature of the field winding should be below 20 K. Temperatures in the outer section is above the T_c of the MgB_2 superconductor, which requires another conductor to be used in this section. To reduce the heat transfer trough the current injection conductor, a superconductor is beneficial. The high current density of a superconductor allows it to inject high currents trough a small cross-section. This reduces heat conduction trough the conductor. As the T_c of the BSCCO is higher than the operating temperatures in the outer section of the cryostat the BSCCO superconductor is a suited conductor to carry current from this section into the field winding.

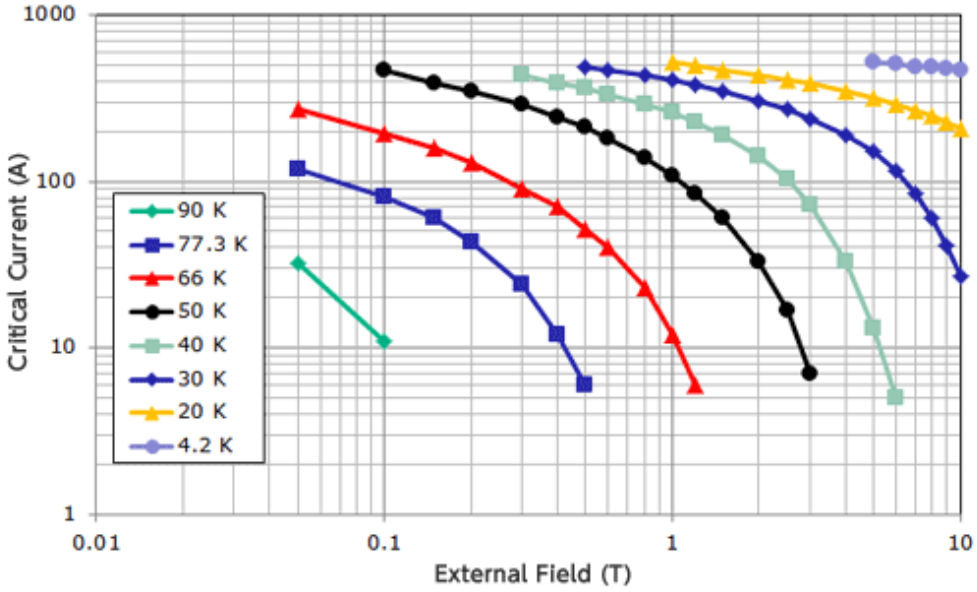

Figure 2.9: The critical current as a function of external magnetic field for the BSCCO superconductor by Sumitomo Electric. Each curve corresponds to different temperatures. [7].

Values of the critical surface of the BSCCO superconductor provided by the manufacturer is shown in Figure 2.9. To assure a buffer to the critical limits of the superconductor three

BSCCO wires are connected in parallel on both sides of the winding, to lower the current through each of them.

2.6 AC losses in a superconductor

2.6.1 Critical state model

By the critical state model, also referred to as the Bean model, it is stated that the current density in a superconductor is either equal to the critical current J_c or zero. Considering a superconductor type II in an external magnetic field; if the applied field is stronger than B_{c1}, the magnetic field gradually starts penetrating the superconductor. As the magnetic field is increased, more vortices enter the superconductor. (A vortex is a single unit of flux.) Inside the superconductor a pinning force, f_p, acts on the vortices, preventing them from floating freely. The strength of the pinning force is determined by the impurity of the superconductor. When vortices first enter the superconductor, most of the vortices are pinned close to the surface of the material. If the strength of the magnetic field applied is increased, the density of vortices increases and more vortices penetrates deeper into the superconductor. The resulting magnetic field in the superconductor has approximately linearly decreasing field strength from the surfaces perpendicular to the magnetic field towards the centre of the superconductor.

According to Ampère's law, such a flux density gradient requires a current density by the relation,

$$\nabla \times B = \mu_0 J \tag{2.6}$$

In a superconductor a current density (J) greater than the critical current density (J_c) would impose a Lorentz-like force on the vortices that is stronger than the pinning force. In that case the vortices would move and power would dissipate [9]. A current density of less than J_c would imply that the pinning force is only partly acting on the vortices. In other words, the pinning force is strong enough to pin more vortices closer to the surface of the superconductor. Hence, the current density in a superconductor has to be either J_c or zero. Then, according to the critical state model the magnetic flux density relates to the current density by,

$$\nabla \times B = \mu_0 J_c \tag{2.7}$$

To illustrate the critical state model we consider a superconducting slab with the geometry as shown in Figure 2.10, with an applied magnetic field (B_a) parallel to the y-axis. When vortices enter the superconductor from the sides, a current occurs according to Equation (2.7). As there will only be a change in the magnetic field along the x-axis, the corresponding current by Equation (2.8) can be expressed as,

$$\frac{dB_a}{dx} = \pm\mu_0 J_c. \tag{2.8}$$

The slope of the magnetic field (B) in the superconductor will be either $\pm\mu_0 J_c$ or zero along the x-axis, and zero in the y and z-direction.

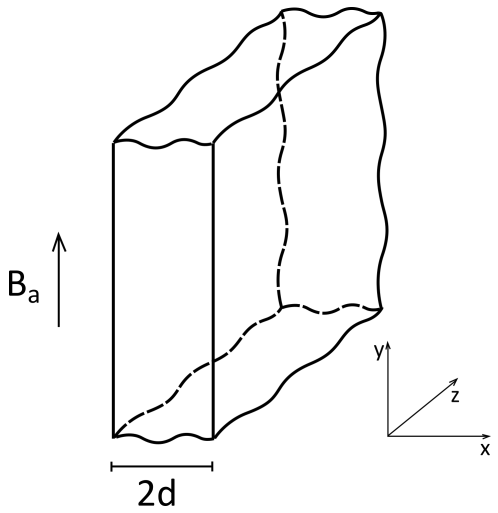

Figure 2.10: A superconducting slab with a thickness of 2d and infinite length in the y and z direction, in an applied magnetic field (B_a) parallel to the y axis.

2.6.2 Hysteresis losses in a superconductor

Figure 2.11 illustrates how the magnetic field and the corresponding currents changes in the superconducting slab, as the applied magnetic field is first increased then decreased. The change in the vortex-density starts at the superconductor boundary and the magnetic field gradient follows the relation in Equation (2.8). Consequently, the magnetic field inside the superconductor depends on the history of the applied magnetic field. The occurring screening currents results in losses as vortices passes through them when the magnetic field penetrating the superconductor changes.

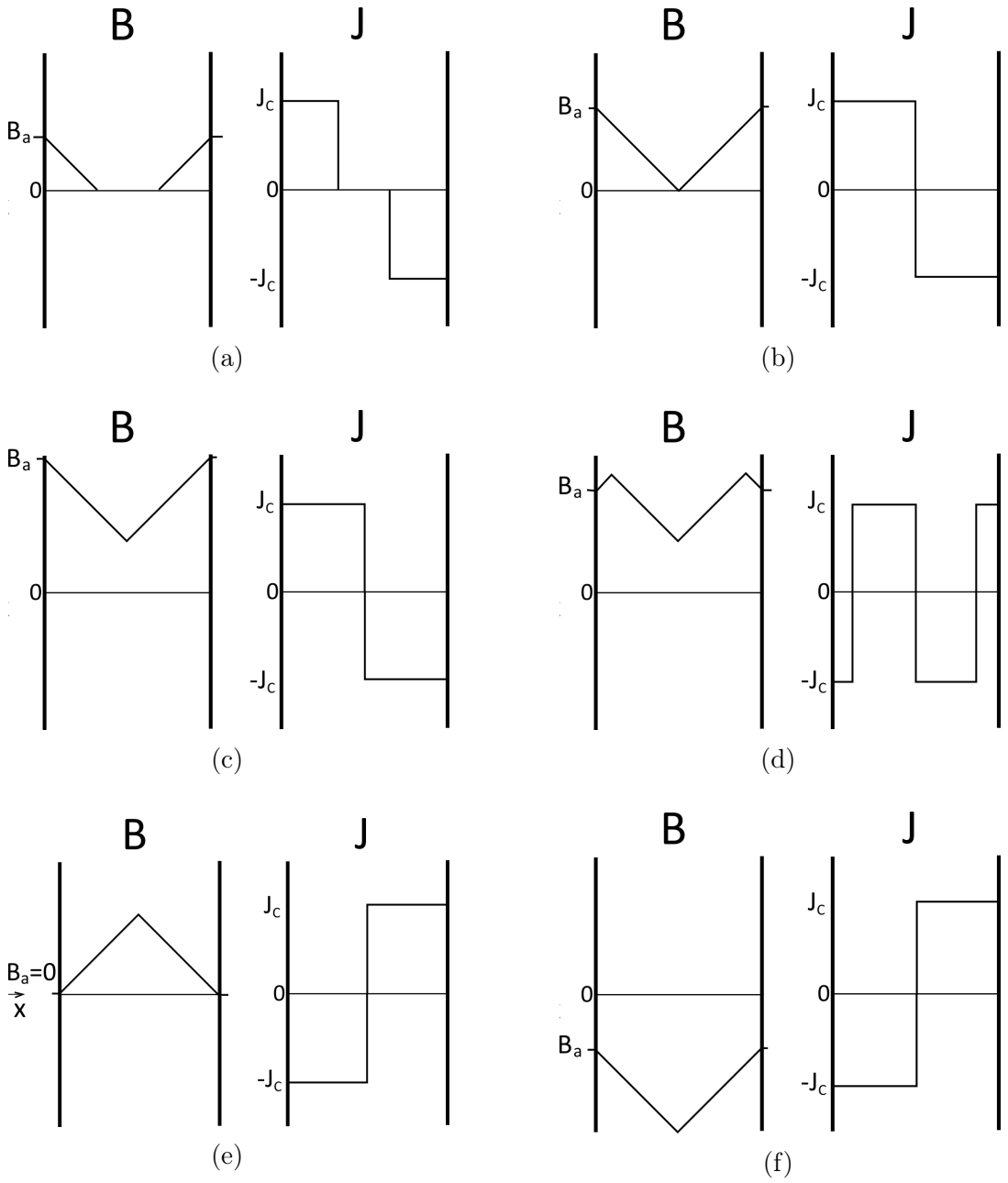

Figure 2.11: Magnetic field and current density in the xy-plane of the slab in Figure 2.10, for a varying applied magnetic field. The graph width equals the thickness of the slab.

2.6.3 Modelled AC losses

Hysteresis losses in a MgB_2 superconductor, of the same type as in this project, is modelled based on the critical state model [10]. The losses are given for a DC magnetic field with an AC ripple, like in the experiments to be executed.

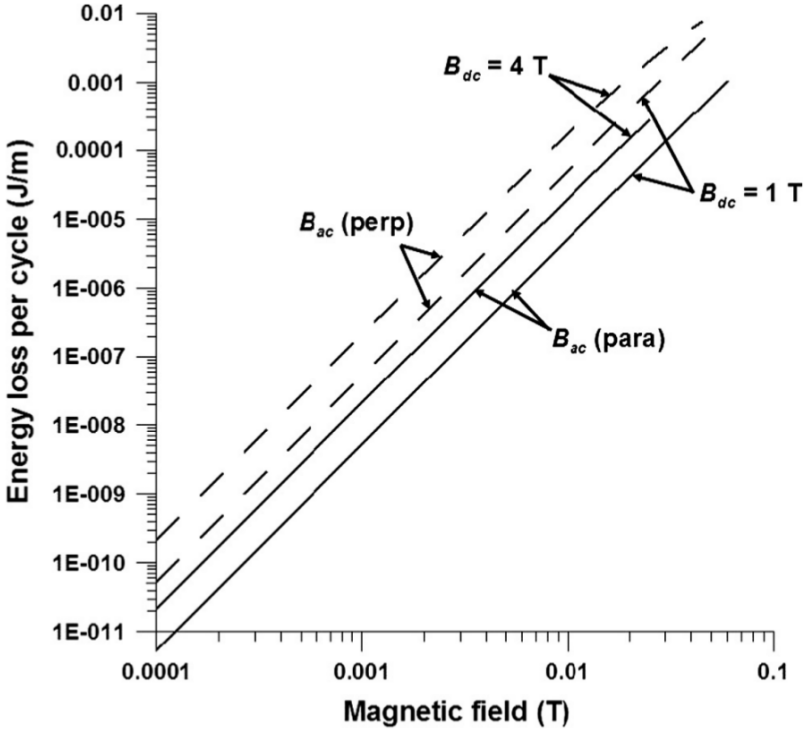

Figure 2.12: Modelled losses in a MgB_2 superconductor per cycle and metre as a function of AC magnetic ripple peak directed parallel (solid lines) and perpendicular (dashed lines) to the wide side of the conductor at 1 T and 4 T DC magnetic field [10].

In this project, losses will be measured with magnetic fields aligned perpendicular to the superconductor. Some values for perpendicular fields with a DC field of 1 T is read from Figure 2.12 and presented in Table 2.1. These modelled values are used to predict the losses in the tests to determine the design of equipment to be used in this project.

Table 2.1: Modelled MgB_2 superconductor AC losses per cycle for different AC magnetic field strength with a 1 T DC background field. Fields aligned perpendicular to the superconductor.

B_{peak}[mT]	$E[\mu$ J/m]
4	4
8	27
11	69
15	176
20	409

2.7 Calorimetric Measurement Method

A calorimetric measurement system is applied to measure the losses in the MgB_2 superconductor when exposed to a strong DC magnetic field with a AC magnetic field ripple. In the calorimetric method, the temperature increase in the superconducting wire test piece is measured to find the power losses in the adiabatic system. The power losses from the AC magnetic field is given by:

$$P_{loss} = cm\frac{\Delta T_{AC}}{\Delta t_{AC}}. \tag{2.9}$$

c is the specific heat capacity and m is the mass of the superconducting wire sample. By multiplying these parameters with the temperature change due to the AC magnetic field (ΔT_{AC}) and dividing it by the duration of the exposure to the AC magnetic field (Δt_{AC}), the power losses are found. As the specific heat capacity of the superconductor sample is not known, a reference heater is applied to determine the power losses. The reference heater is attached to the superconductor, such that the reference heater and the superconductor sample has a shared heat capacity (cm). Using Equation (2.9) it is found that,

$$P_{loss} = \frac{\Delta T_{AC}\Delta t_{ref}}{\Delta t_{AC}\Delta T_{ref}}P_{ref}. \tag{2.10}$$

To determine the power loss from a test, the testing time and the reference heater testing time (Δt_{ref}) are equal. The reference heater is used separately from the AC loss testing to find the temperature change for a certain power in the test piece. The temperature increase in the reference heater is logged during a constant known power injection (P_{ref}), for example for 10 seconds. This operation is performed for a range of power injections. Then, for similar ΔT_{AC} and ΔT_{ref} the P_{loss} equals P_{ref} [16].

2.8 Quench Protection

During operation of the DC field winding, the field winding is protected with a quench protection circuit. If part of the superconductor leaves the superconducting state, resistance appears in the MgB_2 wire, and heat will be generated in the coil. This is called a quench. When a high current is injected, a quench could potentially damage the coil if too much heat is generated in a short amount of time. To prevent such damage, a quench protection system is connected to the winding. In Figure 2.13 the quench protection scheme used in this project is shown.

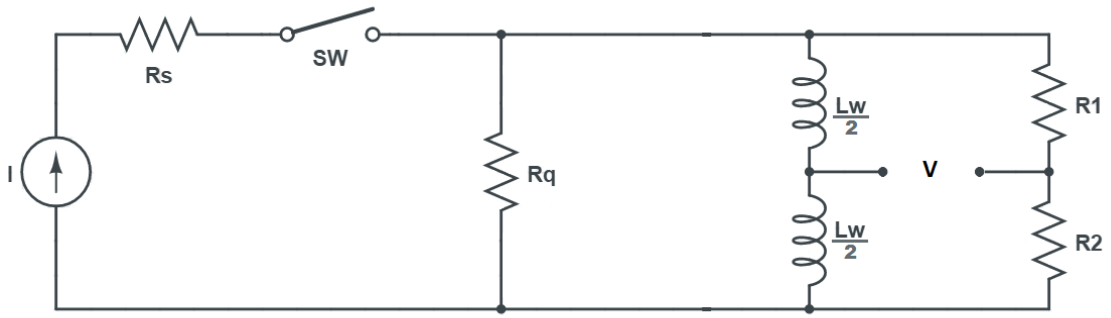

Figure 2.13: Quench protection system.

Under normal operation with the field winding in the superconducting state, there is zero voltage across the field winding (L_w). No current will run in the branches parallel to L_w, as the winding has zero resistance. Accordingly, there will be zero voltage measured in V. For the quench protection, two resistances (R_1 and R_2) are connected in parallel with the MgB_2 winding. If the field winding leaves the superconducting state, a resistance appears in the winding and a fraction of the current will flow through R_1 and R_2. The resistance in the winding in case of a quench will not be distributed evenly in the two halves of the winding, hence a voltage occurs in V. If the voltage in V exceeds a specified limit, e.g. 10 mV, a signal triggers the switch (SW) to open.

When a quench is detected and SW is opened the current will circulate through the winding and the resistance R_q ($R_q << (R_1 + R_2)$). Thereby, the energy in the winding will be consumed mainly by the resistance R_q which is located outside the cryostat, reducing the risk of damaging the winding by overheating.

The energy in the superconducting field winding can be estimated using Equation (2.12) for energy in an inductance. The field winding has an inductance of L=2.9 H. If a current of 100 A is injected into the coil the energy of the coil is W=14.5 kJ. This energy should be released in the resistance Rq in the case of a quench.

2.9 Electromagnetism

2.9.1 Inductance

When a current is injected into an inductor an electromagnetic force is induced opposing the change of current, i.e. direct current will pass an inductor without inducing a voltage. The relation between the current and the voltage in an inductor is given by:

$$V_L = L\frac{di_L}{dt}. \tag{2.11}$$

The voltage of the inductor (V_L) is proportional to the rate of change of the current trough the inductor (I_L). The inductance L is the proportionality constant and is measured in Henry (H). The value of L depends on the inductor. Higher inductance implies a slower rate of change of current. In a coil, L increases with the number of turns.

The inductor does not consume nor produce energy, but it can hold energy. The energy stored in an inductor is proportional to the square of the inductor current. This energy is released when the voltage polarity is negative where the current is injected and the current gradually drops. The energy stored in a inductor is given by Equation (2.12).

$$W_L = \frac{1}{2}LI_L^2 \tag{2.12}$$

2.9.2 The electromagnetic force

In a magnetic field a point charge (q) will experience a magnetic force (F). The force acts on the charge perpendicular to its direction of movement and the magnetic field. The magnitude and direction of the force is given by,

$$F = qv \times B. \tag{2.13}$$

The force by Equation (2.13) can be expressed by a current (I) flowing in a conductor of length (l). F is then given by the sum of the electromagnetic forces acting on all the charges in the conductor.

$$F = Il \times B. \tag{2.14}$$

2.9.3 Hysteresis losses

When a magnetic material experiences an alternating magnetic field, hysteresis losses occur in the material. These losses are due to the lag in the magnetic flux direction when the applied field is reduced. When the material is magnetized, more energy is applied then the energy returned when the material is demagnetized. The remaining energy is converted to heat. In a magnetic material, the hysteresis power losses per cycle per unit volume in a AC magnetic field is expressed as,

$$e' = \int_{period} HdB. \tag{2.15}$$

The integral of the H-field and B-field in Equation (2.15) is illustrated by the hysteresis loop in Figure 2.14. The grey area enclosed by the hysteresis curve equals the energy loss per cycle, and its shape depends on the material. First, the material has no magnetization, following the curve from the origin. When the material has been magnetized, it will follow the path on the outer curves during magnetization and demagnetization. For each magnetic field cycle the path is repeated, giving power losses proportional to the frequency of the magnetic field.

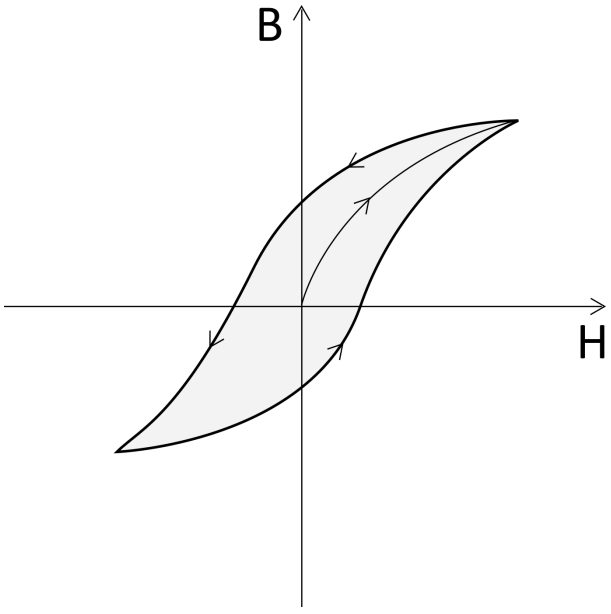

Figure 2.14: Generic hysteresis loop of a magnetic material.

2.9.4 Eddy Current Losses

Eddy current losses arise in conducting material when exposed to an alternating magnetic flux. The alternating flux induces a voltage in the material according to Faradays law, opposing the change in flux. These induced voltages produce circulating currents in the material perpendicular to the magnetic flux, called eddy currents. A power loss by RI^2 accompanies the circulating currents, called eddy current losses. The eddy current losses increase with the square of the magnitude of the magnetic flux and with the square of the magnetic flux frequency.

2.10 Heat transfer

Whenever there is a temperature difference between media or in a medium, energy transit will occur until thermal equilibrium is reached. There are three modes of heat transfer; conduction, convection and thermal radiation. In the cryostat used in this project, there are heat transfer by conduction and thermal radiation. Convection is eliminated as there are only stationary media in the cryostat.

2.10.1 Thermal radiation

Any material with a temperature above the absolute zero emits energy to its surroundings by radiation. Contrary to conduction and convection, radiation do not require a medium to transfer heat. In fact, radiation is more efficient in vacuum. The rate at which radiation is emitted from the surface of the material is called the emissive power [W/m^2] and is given by,

$$E = \epsilon \sigma T_s^4 \tag{2.16}$$

where ϵ is the emissivity, σ is the Boltzmanns constant ($5,670 \cdot 10^{-8}$[$W/(m^2 \cdot K^4$]) and T[K] is the temperature of the surface. The emissivity of different materials varies in the range of 0 to 1, where a value of 1 corresponds to the ideal black body emissive power, which is the maximum.

By multiplying the emissive power by the surface area (A) of the emitting material, the total emitted power can be found as,

$$P = \epsilon \sigma T_s^4 A. \tag{2.17}$$

2.10.2 Conduction

In any medium with a temperature gradient, heat will be transported in the direction of decreasing temperature. Between two isotherm surfaces of temperature T_1 and T_2, the magnitude of the heat transfer from conduction can be calculated using Fourier's law:

$$q_x = -kA\frac{\Delta T}{\Delta x} = -kA\frac{T_2 - T_1}{L}. \tag{2.18}$$

The heat transfer (q_x) is proportional to the temperature difference between the surfaces (ΔT), the surface area (A) and the inverse of the distance between the surfaces (L). k is the proportionality parameter, known as the thermal conductivity (W/(m· K)). The thermal conductivity depends on the type of material.

Chapter 3

Hardware Design And Production

In this chapter, the testing hardware is described in detail. Pre-produced equipment are presented with essential specifications, and the custom made equipment are presented with the design considerations and specifications.

There are two prominent complicating aspects of preparing experimental tests at temperatures close to the absolute zero. Firstly, material properties such as thermal conductivity, electrical conductivity and mechanical strength often change significantly at cryogenic temperatures, and the exact data for the properties is of often difficult to obtain or unavailable. The second aspect is the time consuming processes of assembling, cooling and heating the cryogenic environment, to perform tests in the cooled state. While unknown material parameters requires testing of new hardware in the cooled state to determine its functionality, the time consuming testing process suggests to limit the number of tests. As a result, the hardware design is based on a thoroughly theoretical elaboration without intermediate testing in the production process. At the same time, the theoretical elaboration relies on a series of assumptions and approximations.

3.1 Overview of test equipment

This section presents a visual overview of the test equipment, and the positions of different components inside the cryostat. For readers that are not familiar with the test equipment it is suggested to look up equipment positions in Figure 3.1 while reading the report, for a better understanding. (When using the term left and right regarding equipment positioning in the report it is referred to this figure.)

Table 3.1: Equipment numbering referring to Figure 3.1.

Number	**Equipment**
1	Cold head stage 1 (50K)
2	Cold head stage 2 (15K)
3	Superinsulation
4	Copper screen
5	Support bolts
6	HTS/BSCCO superconductors
7	Copper current leads (Field winding)
8	Mechanical support (Field winding)
9	DC field winding
10	Thermal interface
11	AC current leads
12	AC coil
13	AC coil mount
14	AC coil cooling
15	MgB_2 superconducting wire sample
16	Wire sample holder
17	Reference heater
18	Wire sample cooling/ Litz wire

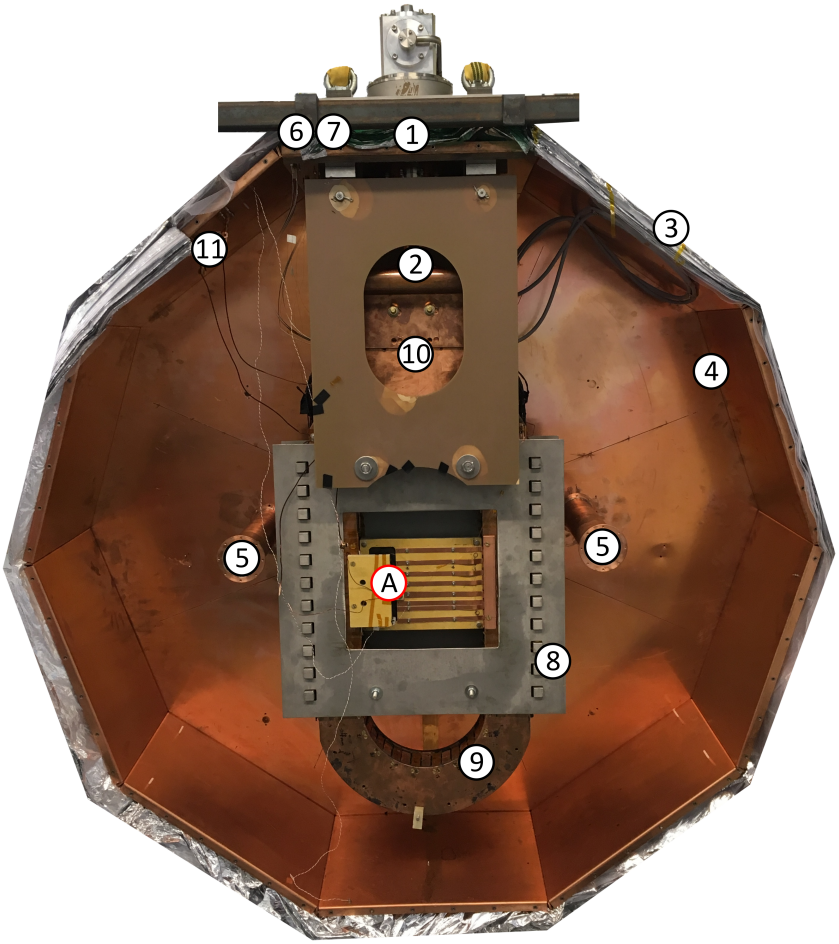

Figure 3.1: Positions of test equipment inside the cryostat. Referring to equipment numbers in Table 3.1.

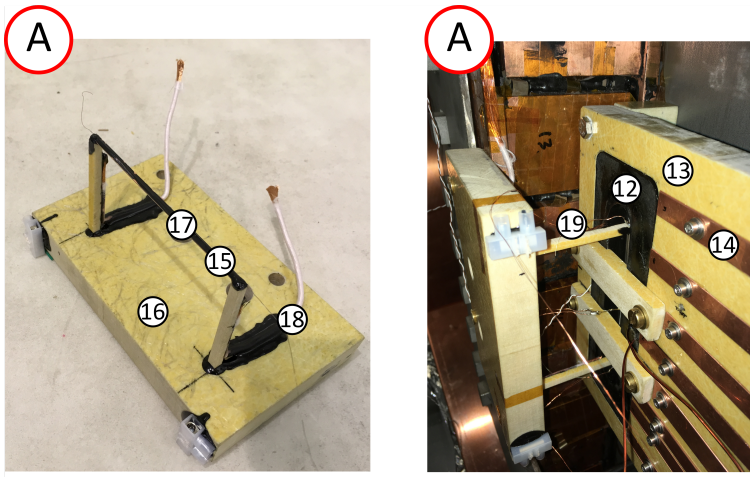

(a) (b)

Figure 3.2: AC loss test equipment. (a) Wire sample holder. (b)Wire sample holder mounted. Position is indicated in the overview picture in Figure 3.1.

3.1.1 Magnetic field for testing

Figure 3.3 illustrates the magnetic field to be set up in the cross section of the wire sample of the superconducting MgB_2 wire. The field winding applies a constant DC field, while an AC coil sets up an alternating field. The superconducting wire sample is exposed to a magnetic field (B) given by the superposition of the DC and the AC magnetic field. The AC field and DC field are both aligned parallel to each other, perpendicular to the wire sample.

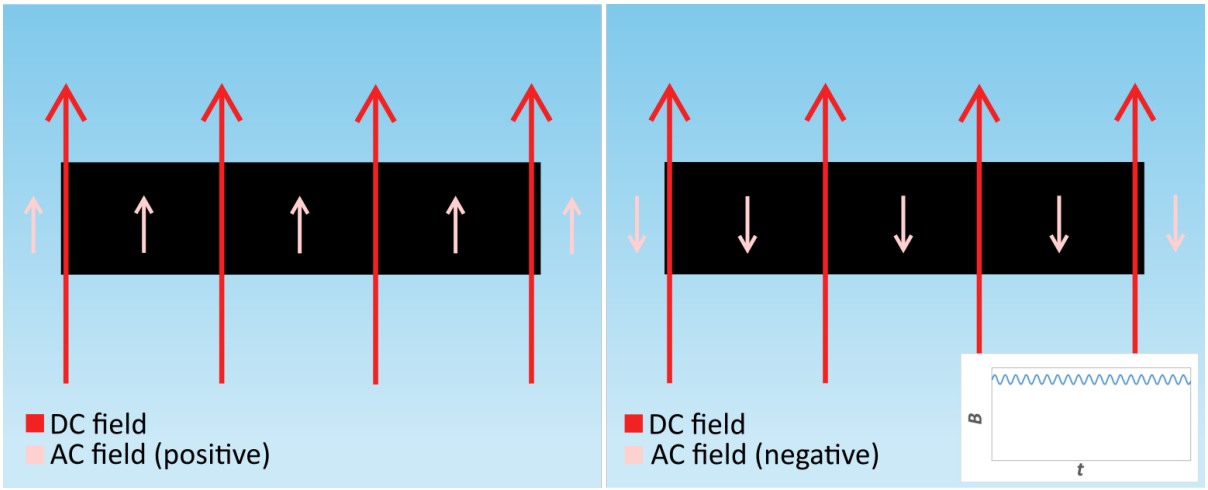

Figure 3.3: Illustration of the magnetic field in the cross-section of the test wire.

3.2 MgB_2 superconducting wire sample

A sample of MgB_2 superconductor was used to experimentally determine the losses when exposed to a DC magnetic field with an AC magnetic field ripple. The power losses per unit length are assumed to be independent of the length of the superconductor. It was chosen to use a 10 cm long sample of the superconductor. The short sample length simplifies the mounting rig and reduces the required size of the AC coil. Furthermore, a small AC coil incur less resistive losses in the coil, i.e. less heat dissipation inside the cryostat. The DC magnetic field from the field winding are not homogeneous throughout the air gap, hence a short wire sample will experience less variation in the magnetic field across its length. This is assumed to give a more constant power loss all over the wire sample and a more accurate prediction of the magnetic field in the wire sample. The wire sample was placed in such a way that both the DC and the AC magnetic field were aligned perpendicular to the MgB_2 wire sample. A parallel alignment to the magnetic fields was also considered, but this is estimated to give only one tenth of the superconductive losses [10]. For this reason, a perpendicular alignment of the magnetic fields was chosen, to make it possible to measure losses at lower field strengths. The test equipment is designed for testing with no current injection in the wire sample.

Figure 3.4: MgB_2 wire sample with the reference heater resistance attached with epoxy.

3.2.1 Wire sample mass and expected ΔT

To be able to design a proper AC winding for the test, it is necessary to know the required magnitude of the AC ripple field to obtain a measurable temperature increase in the wire sample. The required ripple field magnitude could be determined by knowing the amount of energy needed to increase the temperature in the wire sample by a certain degree. It was decided to do the design estimations regarding a temperature change of ΔT=0.5 K.

To estimate the amount of energy necessary, the wire sample was assumed to consist of copper and nickel only, neglecting the MgB_2 filaments in the nickel. Furthermore,

the additional mass from the reference heater and the epoxy attaching it was neglected. Parameters and calculated values for the copper and the nickel are presented in 3.2.

Table 3.2: Wire sample physics. Simplified to estimate required energy for ΔT=0.5 K.

	Copper	**Nickel**	**Unit**
Length	10.00	10.00	cm
Width	3.00	3.00	mm
Depth	0.20	0.50	mm
Specific mass	8960.0	8900.0	kg/m^3
Specific heat capacity (15 K)G.0.1	0.36	0.22	J/mol K
Mol weight	63.55	58.69	g/mol
Mass	0.54	1.34	g
Mol	0.0085	0.0227	mol
Energy$_{\Delta T}$	1.53	2.42	mJ

It was estimated that to increase the temperature by 0.5 K, starting at a temperature of 15 K, it requires a total energy of approximately,

$$E = 1.53\text{mJ} + 2.42\text{mJ} = 3.95\text{mJ}. \tag{3.1}$$

This amount of energy from power losses was assumed to be necessary to increase the wire sample temperature by 0.5 K.

3.2.2 Power losses to be obtained in the wire sample

To estimate the required AC magnetic field, the power loss needed for a 0.5 K temperature raise in the wire sample was estimated. Thermal radiation from the wire sample during operation was assumed to be zero due to the small surface area and the small temperature difference to the surrounding equipment. Heat transfer from the wire sample mainly occurs from conduction through the two epoxy sticks holding it and through the wires attached to it. The thermal conductivity of epoxy is low, hence heat transfer though epoxy was assumed to be negligible within a 10 second test period. For simplicity, the conduction through the wires attached to the wire sample was also assumed negligible in this estimation. Hence, it was assumed that a 10 second adiabatic heating of the wire sample could be achieved. The required power loss was estimated to,

$$P_{0.5K} = \frac{E_{0.5K}}{\Delta t} = \frac{3.95\text{mJ}}{10\text{s}} = 0.395\text{mW}. \tag{3.2}$$

To estimate the required AC magnetic field ripple for power losses in that order of magnitude, a theoretical model of the AC losses in the wire was used (Figure 2.12).

At a 1 T DC field, it is found that an AC magnetic field frequency of $f = 50$ Hz would require a peak ripple of approximately a 11 mT to obtain losses of $P_{0.5\mathrm{K}} = 0.395$ mW. The power losses in a 0.5 T field are expected to be lower than at 1 T. However, the AC coil design was based on the value from the modelled power losses at 1 T background field.

3.2.3 MgB_2 wire sample holder

A custom-made holder was designed to position the wire sample precisely in the center of the AC coil. The holder was made of epoxy to mechanically withstand the low temperatures. Furthermore, the low conductivity of epoxy is beneficial as it assures that power losses in the wire sample do not dissipate in the holder before a measurable temperature increase occurs. At the same time, a too limited heat transfer to the wire sample could make the testing time consuming, as the wire sample needs to return to steady state temperature between each test. To assure a reasonable cool-down time, two copper litz wires of 3 mm diameter were attached to the epoxy holder (Figure 3.5). One end of each litz wire was attached about 1 cm from the wire sample. The other end was attached to the thermal interface of the field winding with Capton tape. It was chosen to use litz copper wires due to their low eddy current losses, which reduces the possibility of disturbing AC losses from the copper wires during testing.

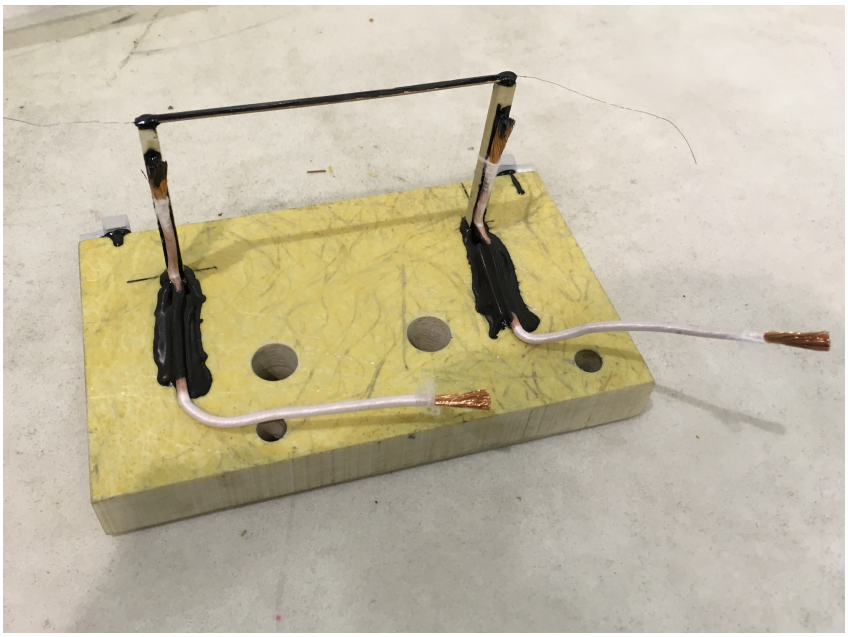

Figure 3.5: Wire sample holder with litz wire for cooling.

3.2.4 Wires attached to the wire sample

There are in total eight copper wires attached to the wire sample. Four of them are connected to the cernox sensor for current injection and voltage measurement, and similarly four are connected to the reference heater. If the copper wires attached to the wire sample are too thick, the energy from the AC losses might dissipate in the wires instead of increasing the temperature of the wire sample. The eight wires used has a diameter of d=0.15 mm and is l=0.7 m long. At T=15 K, the conductivity of copper is approximately $\sigma = 3600$ W/(m·K). By assuming a temperature difference of ΔT=0.5 K between the two ends of each wire during a test, the conducted effect for one wire was estimated to,

$$P_{wire} = \frac{\sigma \cdot \frac{\pi d^2}{4} \cdot \Delta T}{l} = \frac{3600\mathrm{W/(m \cdot K)} \frac{\pi (0.00015m)^2}{4} 0.5\mathrm{K}}{0.7\mathrm{m}} = 45.5\mu\mathrm{W}. \tag{3.3}$$

Thus, at a temperature difference of 0.5 K between the wire sample and the cooling interface, a total power dissipation of 0.364 mW is estimated. Considering the magnitude of the estimated AC power losses (Equation (3.2)), lower wire conduction values would have been preferred. However, due to the practical difficulty of installing thinner copper wires manually without distorting them, 0.15 mm diameter was found to be the thinnest wires applicable for the installation. Considering the current capacity of the wires, copper wires of this cross-section are typically rated for currents of 20 mA at 20 °C. As the resistivity of copper drops to at least one tenth (depending on the purity of the copper) at 15 K, the wire was considered applicable even for the reference heater current of up to 100 mA.

3.2.5 Reference heater

For the calorimetric measurement of the power losses, a reference heater was connected to the wire sample. The reference heater must be able to produce power values in a range similar to the power losses in the wire sample. The test equipment was designed for an AC ripple of 20 mT peak. In a 1 T field this was estimated to induce superconductor power losses per cycle of $p' = 300\mu$J/m (Figure 2.12). With a frequency of $f = 50$ Hz and a superconductor length of $l = 0.10$ m, the upper expected power loss was estimated to,

$$P_{loss\_20mT} = p' \cdot l \cdot f = 300 \frac{\mu\mathrm{J}}{\mathrm{cycle \cdot m}} \cdot 0.10\mathrm{m} \cdot 50\mathrm{Hz} = 1500\mu\mathrm{W}. \tag{3.4}$$

The reference heater consists of a single resistance wire stretched across the 10 cm length of the MgB_2 piece. A constantan wire was chosen as its resistance is almost independent of the temperature. A wire of 16 cm was glued to the surface of the wire sample by a thin layer of epoxy. The 16 cm length left 3 cm outside the wire sample on each side to solder them to copper conductors. The epoxy used was Locktite Stycast 2850 FT. The resistance

was attached to the copper side of the wire sample. This was chosen to benefit from the high thermal conductivity of copper, to quickly distribute the thermal energy from the resistance throughout the wire sample. The resistance of the reference heater wire was measured across the wire sample length. The resistance was measured to $R_{ref} = 3.15\Omega$ at 20°C. By assuming an upper power to be produced of 1500 μW, this requires a voltage of 69 mV and a current of 22 mA in the reference heater resistance. To cover a wide range of possible power loss values, the reference heater was designed to produce power as low as 100 μW. This will require a voltage of 17 mV and a voltage of 6 mA. These values are all within the range of the Rodhe &Schwarz HMC 8042 power source used, and higher power values than 17 mV could be injected if necessary.

3.3 The superconducting field winding

A superconducting field winding is used to induce the background DC magnetic field. The field winding is made by SINTEF in a prior project as a downscaled hardware demonstrator for a superconducting generator design. Due to the limitation to the length of MgB_2 wire provided by manufacturers, the field winding consists of sub-coils spliced by soldering. Two out of ten sub-coils was disconnected due to damage in a previous test, hence the field winding consists of eight sub-coils wounded as double pancakes. The inductance of the field winding was estimated to 2.9 H. The estimation is based on simulations of the field winding in accordance with the measured inductance before disconnecting two sub-coils [14]. Each double pancake consists of 208 turns, adding to a total of 1664 turns for the complete winding.

Figure 3.6: Complete field winding with thermal interface [14].

A thermal copper interface assures good thermal connection between the cryocooler and the field winding. Copper has a high conductivity, thus the thermal interface will effectively transfer heat from the winding to the 2nd stage of the cryocooler. The bottom and top of the thermal interface are flat pieces of copper resembling the shape of the coil, with extensions on one side for mechanical and thermal connection (Figure 3.6). The thermal interface also consists of copper teeth around the air gap to align the pancakes precisely on top of each other, and to obtain contact between every pancake and the thermal interface.

Table 3.3: MgB_2 field winding data

Double pancake coils	8
Turns per double pancake	208
Total number of turns	1664
Total wire length	4000 m
Inductance	2.9 H
Full width	47 cm
Height	106 cm
Depth	8 cm
Conductor width	9 cm
Superconductor	MgB_2
Insulation	Epoxy

3.3.1 Magnetic field simulation (COMSOL)

A 3D simulation model of the field winding was made according to the parameters in Table 3.3. By simulating with a DC current in the winding, the flux density around the winding was analysed. Based on the analysis it was decided to place the wire sample 6 cm from center center on the left long edge, as shown in Figure 3.7. At this position the wire sample is exposed to a strong DC magnetic field. The distance to the field winding of 6 cm is necessary to limit the power losses in the field winding from the AC magnetic field to be set up.

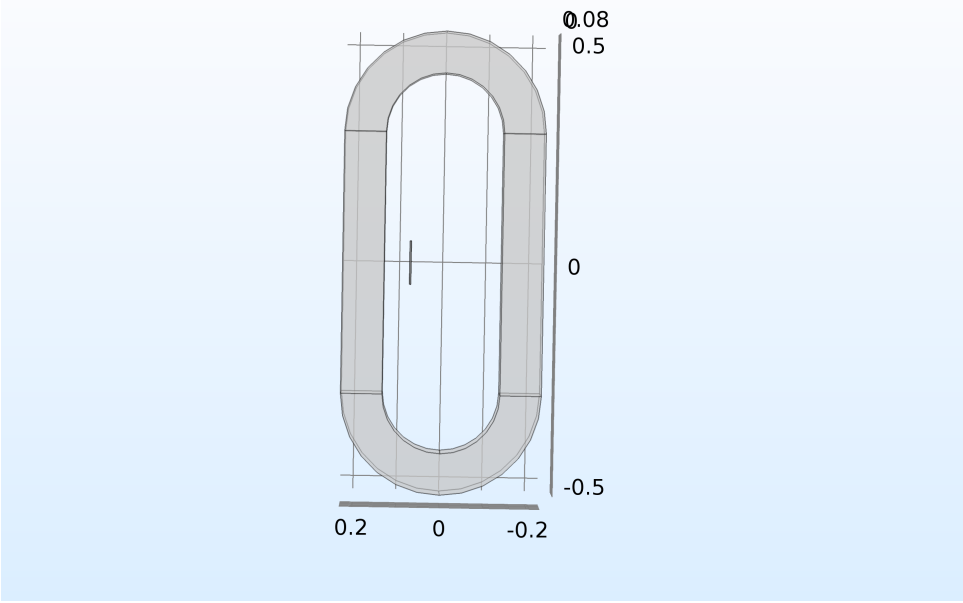

Figure 3.7: Wire sample position in the air gap of the DC field winding.

A 2D simulation of the winding cross-section was used to evaluate the magnetic field in the cross-section of the wire sample when positioned in the air gap of the field winding. The simulated flux density distribution from the field winding is shown in Figure 3.8.

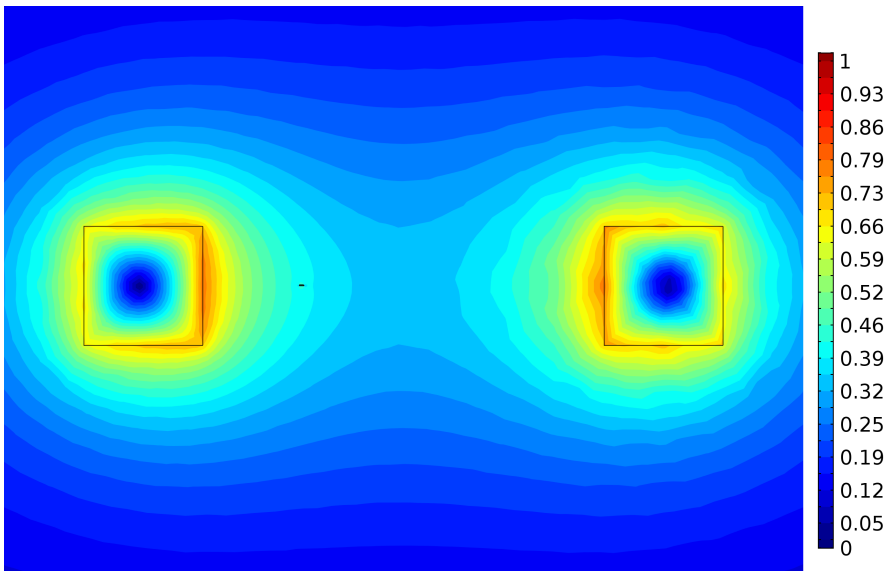

Figure 3.8: Simulated magnetic flux density [T] in the cross-section of the field winding with a current of 100 A. Wire sample cross-section is included on the left side of the air gap.

It was simulated with different winding currents in the range of zero to 100 A, to find the background field in the wire sample. During testing, these values were used to determine the necessary current for a certain background field. Corresponding current and magnetic field values are listed in Table 3.4.

Table 3.4: DC background field in the cross-section of the wire sample at given field winding current.

I_{dc}[A]	B_{dc}[T]
0	0
20	0.1
40	0.2
60	0.3
80	0.4
100	0.5

3.3.2 Forces on the field winding

The magnetic field induced by the DC field winding exerts an electromagnetic force on the winding itself, as the magnetic flux induced by one side of the winding crosses the current conductors on the other side. E.g. the current flowing in the left long side of the winding induces a magnetic flux that crosses the conductors on the right long side. This force increases with the conductor length, the current, and the magnetic flux density. The simulation of the magnetic field was used to estimate the strength of the forces.

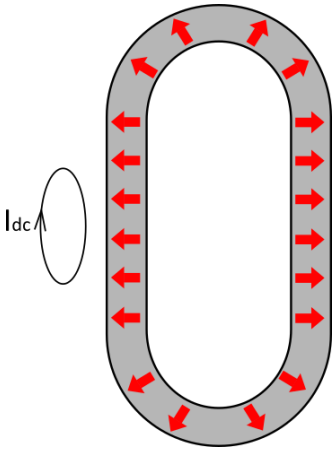

Figure 3.9: Direction of the forces on the field winding. The net magnetic field in the winding cross-section is pointing into the paper.

Figure 3.8 illustrates all the magnetic flux in the cross-section of the winding. To find the forces, only the net magnetic field in the cross-section needs to be counted for, as the rest cancels out. The net magnetic field on one side of the winding is given by the magnetic flux induced by the current flowing in the conductors on the other side. By simulating a current of $I_{DC} = 100$ A in one side of the coil, the average flux density in the other was found to be $B_{net} = 0.087$ T. By the right hand rule, the net force exerted on the winding is pointing outwards from the center of the coil. The long edges will experience the strongest forces, due the length of the long edges and the short distance between them. To estimate this force on one long edge, the magnetic field was assumed uniform in its length $l = 0.6$ m. The number of wires is $N = 1664$. The electro magnetic force on one long edge was estimated to (Equation (2.14)),

$$F_{DC} = B_{net} \times I_{DC} l N = 0.087\text{T} \cdot 100\text{A} \cdot 0.6\text{m} \cdot 1664 = 8.7\text{kN}. \tag{3.5}$$

This force will be exerted on both the long edges of the winding. At the same time forces will act outwards on the top and bottom of the winding. These forces will partly counteract the outward forces on the long edges through the winding tension, but as the forces on the long edges are assumed to be significantly higher, an additional mechanical support is required outside the long edges.

3.3.3 Mechanical support

A mechanical support designed in a previous project [14] was used to withstand the forces on the long edges of the DC field winding during operation. The support is made of stainless steel due to its non-magnetic properties to affect the magnetic field the least. The sides of the support fit perfectly up to the long sides of the winding, and two plates are connected flat on the top and the bottom of the winding, holding the side support together. For the purpose of the testing in this project, the original mechanical support was customized by cutting a hole in the front plate. The assembly of additional AC loss testing equipment (Figure 3.1) is mounted inside the hole. The hole is positioned in the center of the plate and is 30 cm high and 33 cm wide. This is assumed to reduce the mechanical withstand strength of the mechanical support, but as the original mechanical support was dimensioned for a force of 500 kN, the mechanical support will still take the forces estimated to less than 20 kN from the planned testing.

The AC coil mount was attached in the back plate of the mechanical support by four bolts. Due to the precision requirements of the wire sample positioning inside the AC coil, two new bolts was inserted in the bottom part to hold the mechanical support plates in a fixed position.

3.4 The AC coil

An AC coil was designed to be placed inside the field winding to produce a controlled AC ripple to the background DC field. The design of the AC coil was elaborated considering size, power losses, field strength, mechanical forces and positioning relative to the field winding.

According to the estimations, the AC coil needs to set up an AC magnetic field with an amplitude of at least 11 mT in the center of the AC coil air gap. It was decided to dimension the AC coil for a magnetic field up to 20 mT amplitude. To induce a magnetic field that is homogeneous across the wire sample length, the AC coil needs to have two parallel edges longer than 10 cm. The width of the air gap must be wide enough to place the 3 mm wide MgB_2 wire sample in the center without any contact with the AC coil or the AC coil mount, to avoid heat transfer. Furthermore, the gap between the copper conductors must have space for a mechanical support to withstand the electro magnetic force on the copper conductors during operation.

3.4.1 Magnetic field simulation (COMSOL)

A design to meet the requirements for the AC coil was found by an iterative simulation process in COMSOL. An air gap of 2.5 cm from side to side was considered sufficiently large to fit 2 mm mechanical support on each side, and have a distance of vacuum to the wire sample. The long edge inside the AC coil was set to 13 cm, to fit the 10 cm wire sample with some margin at each end. From a 3D simulation (Figure 3.10) of the magnetic field, it was found that with such a coil design it would be induced an approximately homogeneous magnetic field across the 10 cm wire sample length. The simulation gave only a 5 % variation in the magnetic field referred to the center of the coil.

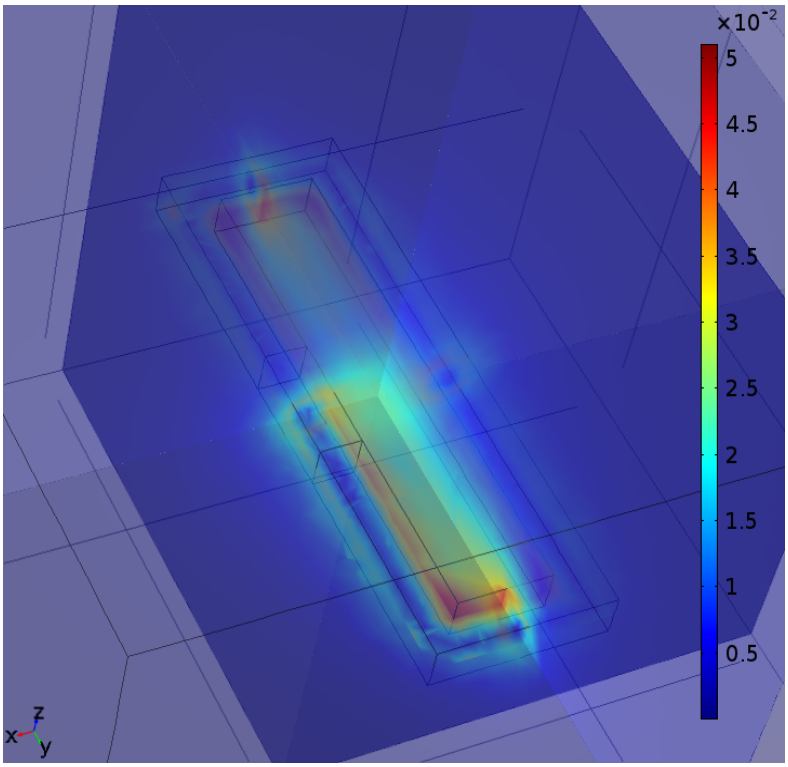

Figure 3.10: 3D simulation of the magnetic field [T] induced by the AC winding with a current of 10 A.

According to the simulation, it was decided to produce an AC coil with N=100 turns, dimensioned for a current of 10 A. This was chosen as it was found to induce the required magnetic field of 20 mT in the wire sample.

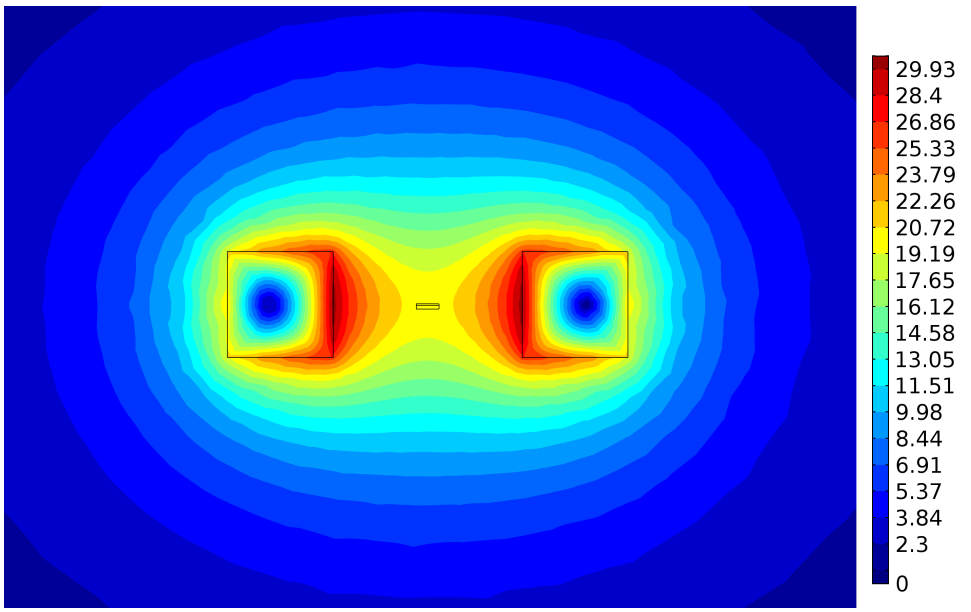

Figure 3.11: 2D simulation of the magnetic field [mT] in the wire sample induced by the AC winding with a current of 10 A.

The 2D coil simulation was used to find the corresponding magnetic field for different current injections in the AC coil (Table 3.5). These values was used to find the corresponding AC current values for a certain AC magnetic field in the cross-section of the wire sample during testing.

Table 3.5: Simulated magnetic flux density in the wire sample of the AC coil for different currents injected.

I_{peak}[A]	I_{rms}[A]	B_{peak}[mT]
1.0	0.71	2.2
2.0	1.41	4.3
3.0	2.12	6.5
4.0	2.83	8.7
5.0	3.54	10.8
6.0	4.24	13.0
7.0	4.95	15.1
8.0	5.66	17.3
9.0	6.36	19.5
10.0	7.07	21.6

3.4.2 AC coil production

100 turns of an enamelled copper wire was wounded with an air gap of 2.5 cm. A copper wire with a diameter of 1.12 mm was used to carry the 10 A AC current with low resistive losses (Section 3.4.3).

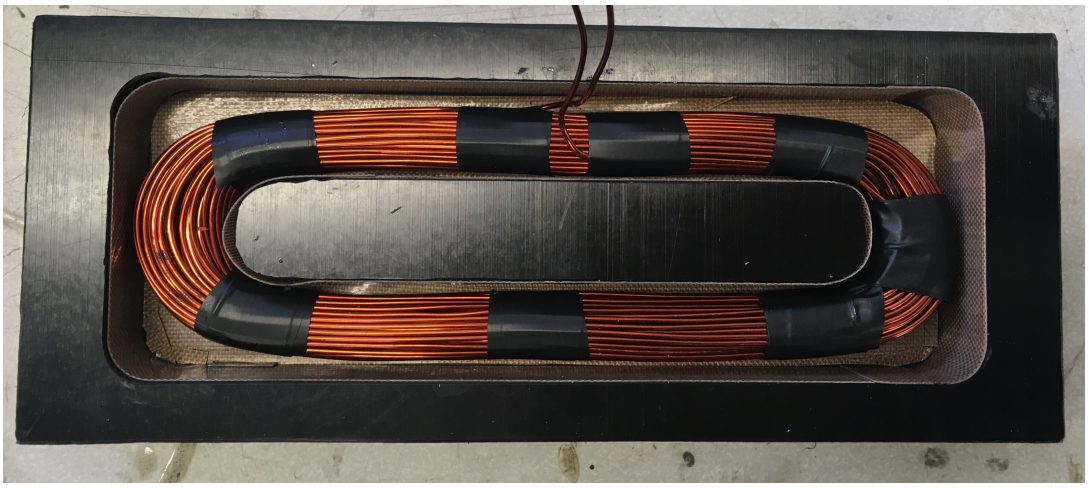

Figure 3.12: AC coil windings in the casting mold.

In Figure 3.12 the copper windings was placed in a custom made casting mold. The center piece of the mold was 2 cm wide. This assured a 2-3 mm epoxy thickness on the inside of the windings on each side for mechanical support. The final air gap of the AC coil then became 2 cm. The casting mold further assured 2-3 mm of epoxy around the outsides for mechanical support against the outward pointing forces.

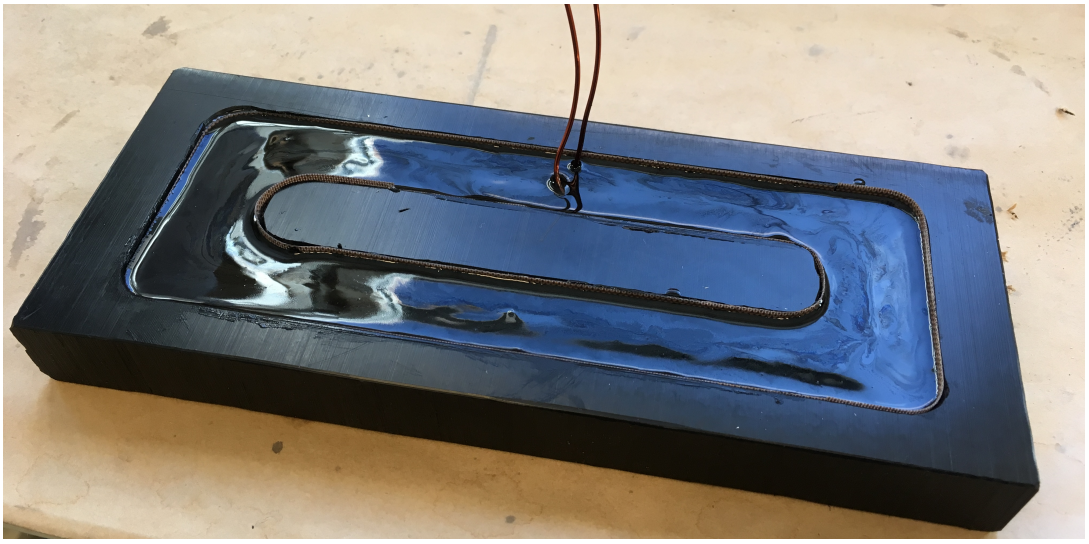

Figure 3.13: AC coil in casting mold filled with epoxy.

Next, the casting mold with the windings in place was filled with epoxy (Figure 3.13). The epoxy used was Stycast 2850 FT mixed with the hardener Cat 24 LV (weight mixing ratio 100:7). This epoxy was chosen due to good mechanical strength at cryogenic temperatures. After hardening, the AC coil was cut out of the mold. The finished AC coil is presented in Figure 3.14.

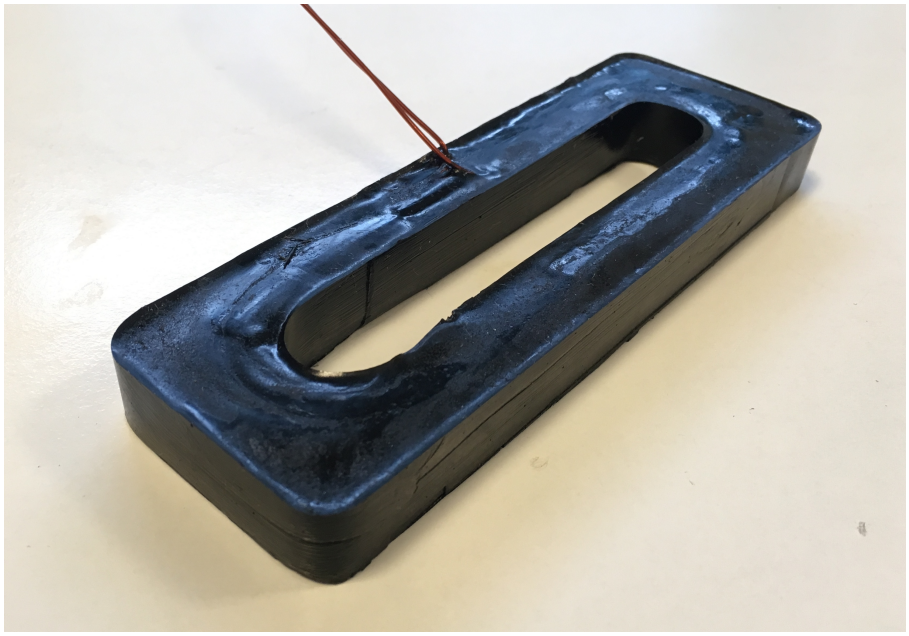

Figure 3.14: The AC coil.

3.4.3 Estimated power loss in the AC coil

During the 10 second testing time, when an AC current flows in the AC coil, there are losses in the copper wires in the coil. There are resistive losses, eddy current losses and hysteresis losses. The AC coil is cooled by the same thermal interface as the field winding. If the AC coil losses are high enough to increase the temperature of the thermal interface and thereby the field winding, the critical temperature of the superconductor in the field winding might be exceeded in some zones. Furthermore, if parts of the superconducting wire in the field winding leaves the superconductive state during a test, the test will not be successful and the field winding might be damaged. It is assumed that the resistive losses will dominate in the AC coil. Hence, to predict the magnitude of the AC coil losses the resistive losses was estimated.

The AC coil has N=100 turns with an average turn length of l_t=0.32 m. The copper wire has a diameter of d=1.12 mm. The copper resistance at 15 K depends on the purity of the copper. The RRR value (the measure of purity) of the copper is not given for the wire used. Hence, a value of RRR=200 is assumed. At a temperature of 15 K the resistivity

of the copper is found to be $\rho_{cu} = 8.0 \cdot 10^{-11}\Omega$m (Appendix F). This suggests a total resistance of the AC coil copper wire at 15 K of,

$$R_{AC} = \frac{\rho_{cu} \cdot N \cdot l_t}{\pi(\frac{d}{2})^2} = \frac{8.0 \cdot 10^{-11}\Omega\text{m} \cdot 100 \cdot 0.32\text{m}}{\pi(\frac{1.12 \cdot 10^{-3}\text{m}}{2})^2} = 2.60\text{m}\Omega. \tag{3.6}$$

To estimate the power dissipation in the coil the resistive losses in the AC coil was estimated to,

$$P_{AC} = R_{AC} \cdot I_{rms}^2 = 2.60\text{m}\Omega \cdot (\frac{10\text{A}}{\sqrt{2}})^2 = 130\text{mW} \tag{3.7}$$

Additional heating of 130 mW in the inner of the cryostat could be handled by the cryocooler stage 2 with a temperature increase of less than 1 K (Appendix E). From the estimation of the resistive losses, the heat from the power loss in the AC coil could be assumed not to influence the operation of the field winding, and the heat from the power losses can be transferred through the thermal interface of the field winding.

3.4.4 AC coil cooling interface

To assure similar conditions in each test, the AC coil must return to the steady state temperature between each test. The AC coil epoxy mount is attached to the mechanical support made of stainless steel with low thermal conductivity, hence additional cooling of the AC coil is applied. The cooling is chosen to be obtained by strips of copper, attached to the thermal interface of the field winding. Copper is chosen as it is a non-magnetic metal with high thermal conductivity. To prevent the heat from the AC coil to influence the heat transfer from the wire sample on the left side of the field winding, the AC coil cooling is attached to the right side of the field winding air gap. It is decided to attach 7 copper strips of 1 cm width and a thickness of 0.5 mm for cooling. Using strips of copper reduces the eddy current losses in the copper, compared to using a single plate of copper. The copper strips are attached to the AC coil mount using screws of stainless steel, as shown in Figure 3.18. A layer of Apiezon grease is applied between the epoxy and the copper strips to assure thermal connection.

3.4.5 Forces on the AC coil

During the AC loss tests with a strong background magnetic field, a strong electromagnetic force will act on the AC coil windings. As the AC current is alternating with a frequency of f =50 Hz, so does the electromagnetic force on the ($N = 100$) copper wires in the coil. The small self field from the AC coil is neglected in this estimation. The long edges of the AC coil experience the weakest mechanical counterforce by the coil construction and is the longest sections with an approximately uniform electromagnetic force. Thus, the long edges is assumed to be most prone to distortion from the electromagnetic forces. The long edge length is $l = 0.13$m. The electromagnetic force on the winding is strongest when the strongest background field is applied and the AC current is highest. By assuming an AC current of $I_{AC} = 10$ A and a DC magnetic field of $B_{DC} = 0.5$T, the electromagnetic force on one long edge was estimated to,

$$F = B_{DC} \times I_{AC} \cdot l \cdot N = 0.5\text{T} \cdot 10\text{A} \cdot 0.13\text{m} \cdot 100 = 65\text{N} \tag{3.8}$$

Over each current cycle this force will alternate between pointing inwards and outwards as illustrated in Figure 3.15.

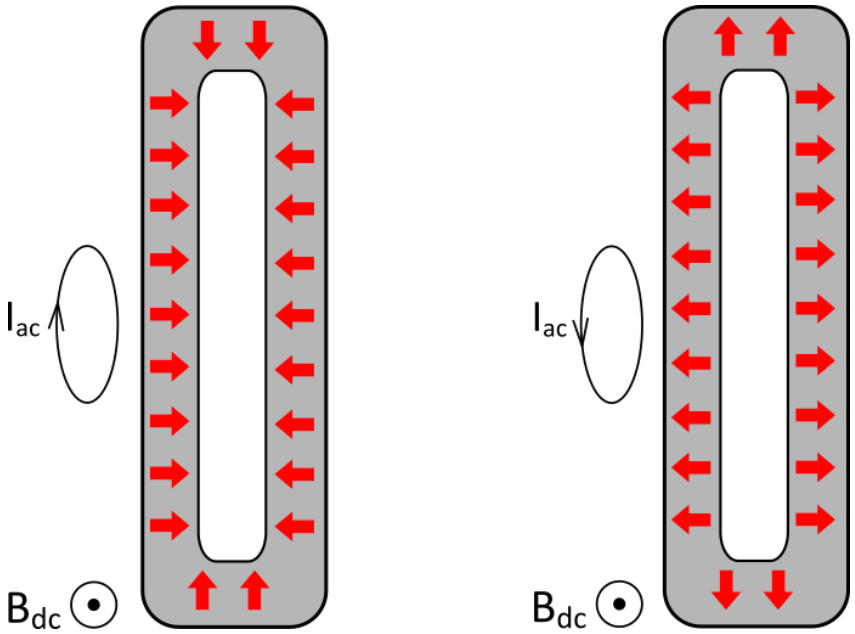

Figure 3.15: Electromagnetic force on the AC coil due to the background magnetic field, given a positive and negative current in the AC coil.

For the AC coil to withstand these forces and maintain its shape throughout all the tests, the coil windings was covered in epoxy. The epoxy is assumed to withstand the forces. However, additional mechanical support is added in the AC coil mount to further ensure that the AC coil do not break down in the cooled state.

3.4.6 AC coil mount

From the COMSOL simulation of the DC magnetic field, the field strength was found to be stronger closer to the inside of the field winding. In that regard, the AC coil should be placed as close to the field winding as possible. On the other hand, if the AC coil is placed close to the field winding the AC field might impose significant AC losses in the field winding. Based on the simulations, the AC mount was decided to be designed for a distance of 6 cm from the inside of the field winding to the center of the AC coil air gap. This distance of 6 cm was considered sufficiently far from the DC field winding not to risk damaging AC losses in the field winding during testing. At a distance of 6 cm the background field is still about 0.5 T for a current of 100 A, which is less than 5 % lower than the highest obtainable DC field in the AC coil air gap. Figure 3.16 illustrates how the AC coil is positioned inside the DC field winding.

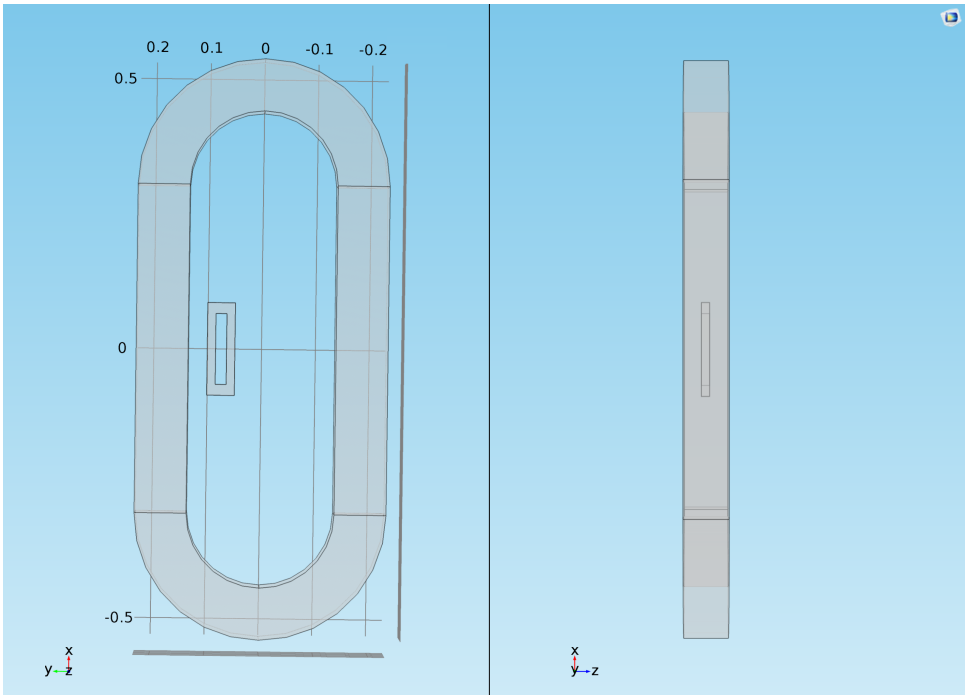

Figure 3.16: Position of the AC coil inside the DC field winding, from the front (left figure) and from the left side (right figure)

.

To mechanically support the AC coil from the outside, the coil is recessed into a plate of epoxy. The hole in the epoxy plate is milled in the exact shape of the coil. Inside the AC coil air gap, it must be assured that the wire sample could fit without touching anything in contact with the AC coil, hence the the space for mechanical support is limited. It was chosen to leave a 2 mm elevated rectangle with a width equal to the air gap, to hold back forces from the sides (Figure 3.17). Similarly, on the two attachment pieces on top, there are a 2 mm elevation into the air gap reaching from side to side.

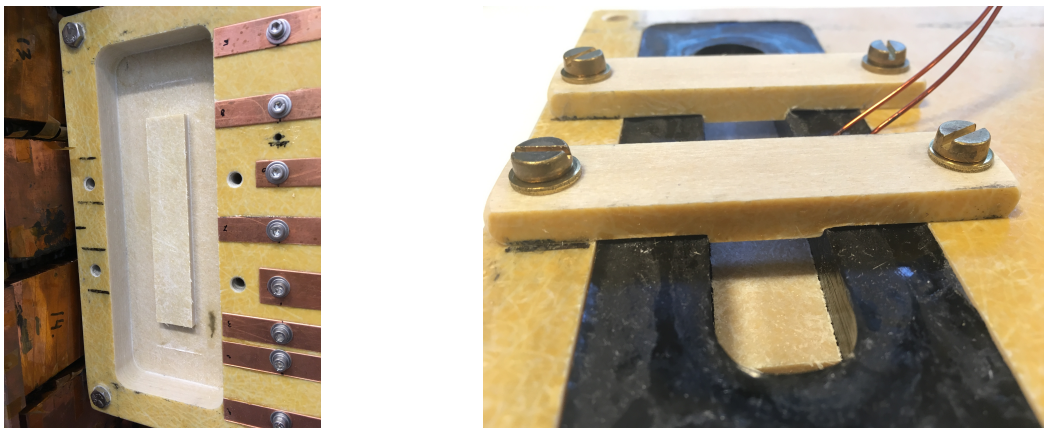

(a) AC mount (b) AC mount with AC coil

Figure 3.17: The mount provides mechanical support to the AC coil both inside and outside the air gap.

In Figure 3.18 the complete AC mount is shown, mounted inside the field winding. The AC coil cooling is attached to the AC mount and to the thermal interface of the field winding on the right side.

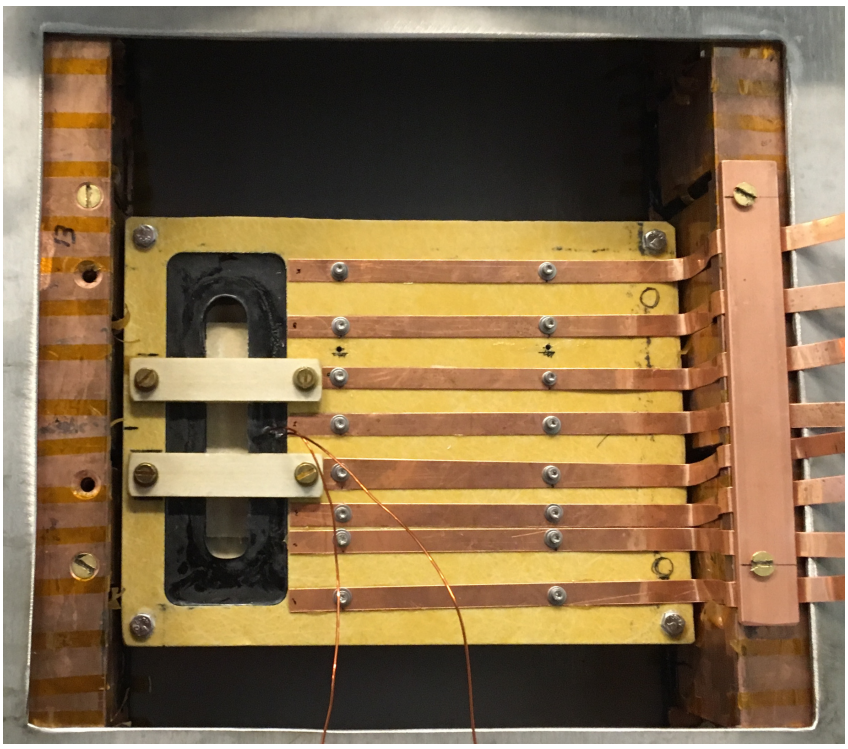

Figure 3.18: AC coil mount attached to the mechanical support of the field winding in the back.

3.4.7 Current leads

For the AC coil current injection, two copper current leads are installed. The current leads are entering the cryostat through a vacuum gate on the top left. Inside the cryostat they are attached just below the gate to the copper screen for cooling and they enter into the screen through two holes (Figure 3.19). The current leads need to be connected while the cryostat top is elevated. As a result, is was necessary with a wire length of 1.5 m from the vacuum gate to the copper screen connections, where they are cooled.

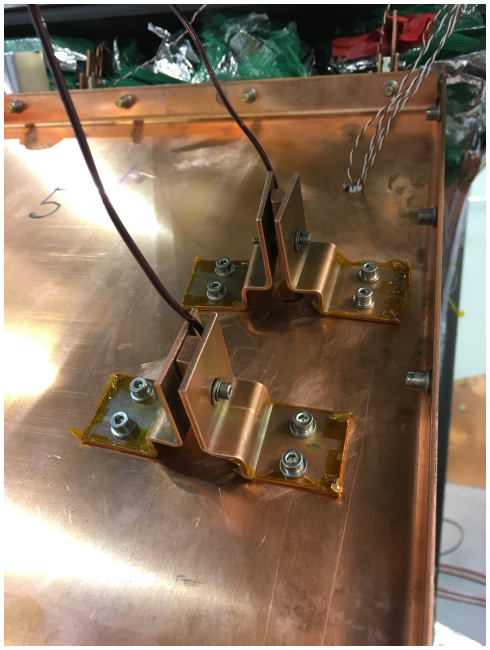

Figure 3.19: AC wire copper screen entrance. The wires are thermally connected to the copper screen for cooling.

The current leads transfer heat into the cryostat in two ways: The copper conductors are transferring heat from the ambient through conduction, and the resistance of the wire leads to power losses as current is injected into the copper leads. The resistive losses could be reduced by increasing the wire diameter, while the conductive heat transfer is proportional to the cross-sections of the current leads. The optimal current lead cross section are determined by minimizing the sum of these losses. For current injection into a cryogenic device, the optimal wire cross section (A) for a DC current of 1000 A is estimated as a function of the wire length (L) [15].

$$A = \frac{L}{3700 \frac{\mathrm{m}}{\mathrm{m}^2}} \tag{3.9}$$

The current leads in this project are dimensioned to inject an AC current up to 10 A peak, i.e. a peak value of one 100th of the current optimized for in (3.9). By assuming

that the optimal wire cross section by Equation 3.9 depends on the current density in the wire, the relation between A and the wire length becomes,

$$A = \frac{L}{370000\frac{\mathrm{m}}{\mathrm{m}^2}} = \frac{1.5\mathrm{m}}{370000\frac{\mathrm{m}}{\mathrm{m}^2}} = 4.05 \cdot 10^{-6}\mathrm{m}^2 \tag{3.10}$$

This suggests a wire diameter of 2.27 mm. It was decided to use copper wires of 2.0 mm diameter, as the estimation is based on DC current, not AC peak current which gives lower losses.

3.4.8 Cryostat gate

A vacuum-proof gate into the cryostat was made for the AC current injection. The cap of an existing opening into the cryostat was modified to pass current through it as shown in Figure 3.20. Two 2 mm^2 square copper sticks of 8 cm length are crossing the gate for the current injection. The cylinder of the gate was filled with epoxy cast (Stycast 2850 FT), to make it vacuum proof. The cylinder was designed with a rim on the inside to assure that the epoxy is not pushed into the cryostat due to the higher pressure on the outside during operation.

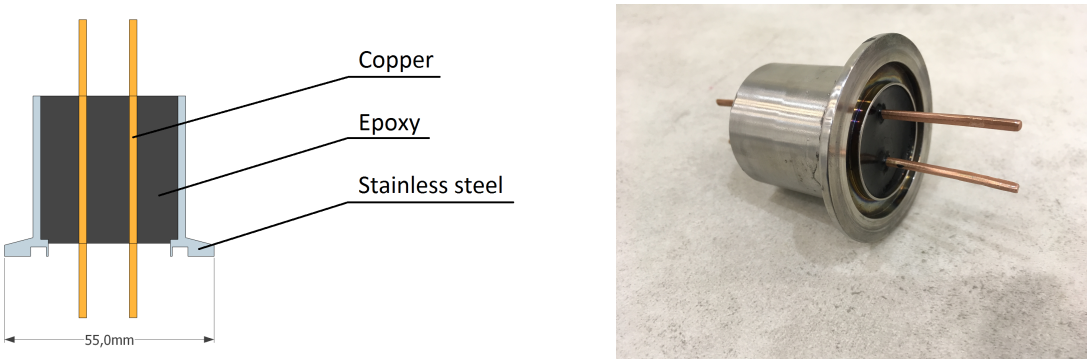

Figure 3.20: Vacuum gate for the AC current injection.

Chapter 4

Cooling System

To operate the superconducting field winding and test the wire sample, it must be obtained a field winding temperature close to the absolute zero. To achieve this, all heat transfer must be kept to a minimum. All materials surrounding the equipment emit thermal radiation that can be intercepted by the surface of the winding and increase the thermal energy of the winding. Furthermore, there are mechanical connections between the winding and the surroundings at a temperature of approximately 20°C. The winding needs to be in contact with the mechanical construction that holds it and with several wires for current injection and measurements. All these connections inflict heat conduction from the surroundings. This chapter includes a brief presentation of the cooling equipment and the temperature measurement system (Further discussed in a previous project report [12]).

4.1 Operating temperature

4.1.1 Field winding and wire sample temperature

The DC field winding requires a temperature below the critical temperature (T_c) of MgB_2 to operate in the superconductive state. Approximately the same temperature is preferred in the wire sample, as the purpose of the loss measurements is to predict operational AC disturbance losses, e.g. in a operating DC field winding. Litz wire and epoxy connects the wire sample to the field winding's thermal interface and assures that the temperature is approximately the same as in the field winding.

MgB_2 superconductors have an upper critical temperature of 39 K. This T_c requires a magnetic field of zero and a current of zero. In this project, the superconductor in the field winding is planned to be operated with a current of 100 A and with a strong magnetic field with an average of 0.6 T in the cross-section of the winding. The temperature must be below the Tc of 39 K to obtain superconductivity under these conditions.

A current of 100 A and a total wire cross-section of 2.1 mm^2 corresponds to an engineering current density J_e=47.6 A/mm^2. In previous testing of the field winding, the cooling system was proven capable of obtaining a temperature of 15 K in the field winding [12]. At a temperature of T=15 K and an engineering current density of 47.6 A/mm^2, superconductivity could be obtained in a magnetic field as strong as B=7.0 T (Figure 2.7). This implies that at 15 K the margins to the critical limits are sufficiently large to expect the superconductor to stay in the superconductive state under normal operation, even in sections where the magnetic field or the temperature is higher than the average.

4.1.2 AC coil temperature

The temperature in the AC coil is not as crucial as in the superconductors, as the AC current is flowing in a copper wire. However, the resistivity of the copper conductors increase with the temperature. Thus, if the temperature is too high a self-reinforcing temperature increase might occur during current injection. A self-reinforcing temperature increase can result in damaging temperatures in the AC coil, or the increased thermal radiation from the AC coil could disrupt the AC loss measurements in the wire sample. To reduce the risk of such temperatures, the AC coil is cooled with copper strips anchored in the field winding's thermal interface for it to hold the same temperature of about 15 K.

4.2 Cryostat

To successfully lower the temperature of the winding to about 15 K, heat transfer to the winding must be minimized and a powerful low temperature cooling system must be applied to transfer heat from the winding. A stainless-steel (non-magnetic) cryostat is used to obtain the required temperature in the test equipment. A vacuum pump and a turbo vacuum pump reduces the pressure in the cryostat to 30 Microns (3.9 Pa). This almost eliminates conduction and convection through air. To reduce the temperature of the equipment, heat is transferred from the field winding using a helium gas cryocooler.

Figure 4.1: The cryostat with the cryocooler coldhead on top and the vacuum pumps connected to the left.

4.2.1 Copper screen

The outside of the cryostat vessel is exposed to air at ambient temperature. Thus, the temperature of the vessel will remain relatively high. As the thermal radiation from a surface is proportional to the forth power of its temperature, the inside of the vessel surface radiates significant amounts of energy. A copper screen is mounted around the winding, to prevent thermal radiation from the cryostat vessel to be intercepted by the winding. The copper screen is only connected in the top, to stage 1 of the cryocooler. The thermal interface of the winding is attached to the copper screen on the inside at the top.

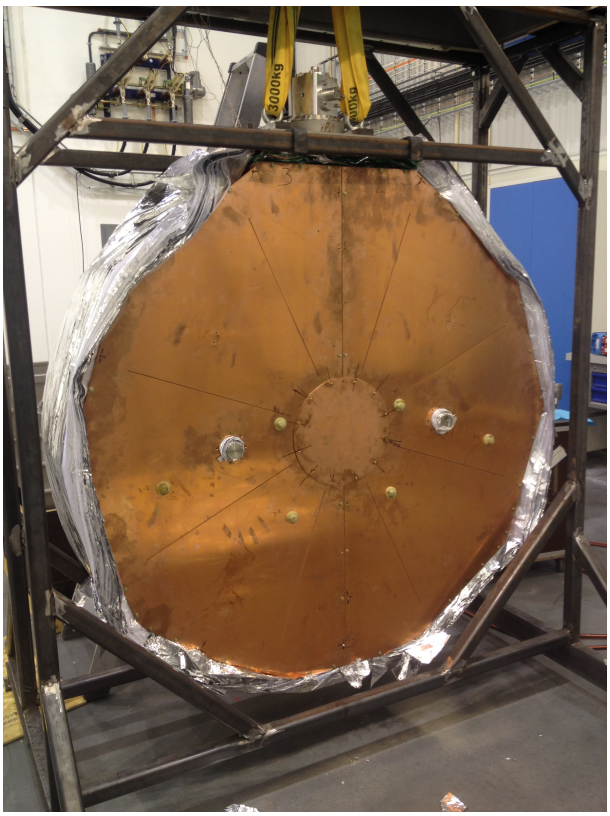

Figure 4.2: The copper screen.

Copper has a high thermal conductivity. This assures that the copper screen is cooled evenly and efficient. Furthermore, polished copper has an emissivity factor of less than 0.05, assuring a limited thermal radiation to the field winding.

4.2.2 Superinsulation

A shroud of superinsulation is wrapped around the copper screen (Figure 4.3). 30 double layers of aluminium foil and mesh fabric constitute the superinsulation. The mesh fabric layers keep the aluminium foil layers separated to reduce heat conduction between layers. Thermal radiation from the cryostat vessel is intercepted by the outer layer of the superinsulation. Only a small fraction of the heat is radiated through all the 30 layers to the inner layer in contact with the copper screen.

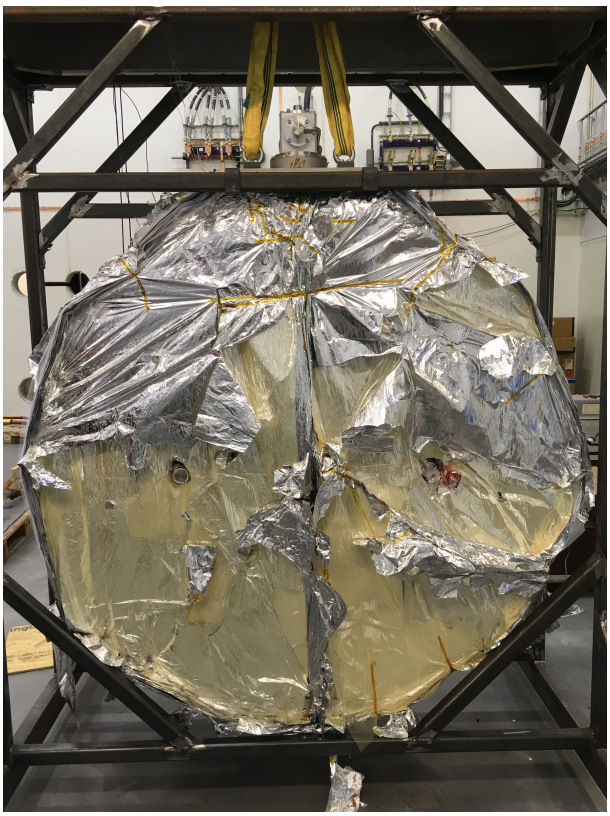

Figure 4.3: The copper screen covered with superinsulation.

4.2.3 Cryocooler

A helium gas cooling system transfers heat from the field winding by conduction. Figure 4.4 shows the coldhead on top of the cryostat. Two tubes are used to circulate helium gas between the helium compressor unit and the coldhead. The cooling system transfers heat from inside the cryostat at two stages. The first stage is just below the coldhead and is connected on top of the copper screen. This stage has the highest refrigeration capacity. Stage 1 mainly conducts heat from the copper screen to reduce the radiation from the copper to the field winding. Indirectly, the cooling of the copper screen also cool the AC current wires, the field winding copper current leads and the HTS wires. Cooling these conductors reduces the conduction of heat to the AC coil through the AC wires and to the field winding through the HTS wires. In addition, it assures that the HTS wires are in the superconductive state (below 110 K). The heat-load capacity of the cryocooler depends on the temperature of both stage 1 and stage 2 of the cryocooler. E.g. at a temperature of 50 K at stage 1 and 15 K at stage 2, the heat load capacity is approximately 40 W at stage 1 and 13 W at stage 2 (Appendix E).

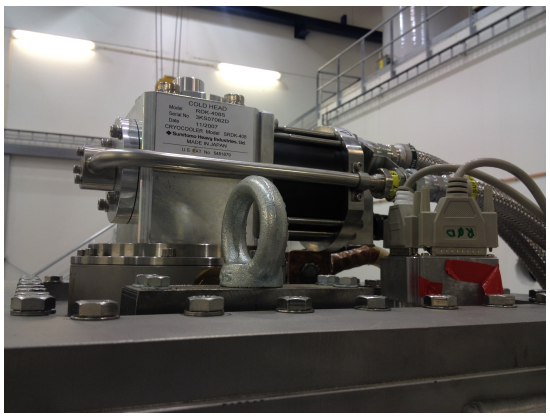

Figure 4.4: : Coldhead of the cryocooler on top of the cryostat vessel.

When vacuum is obtained in the cryostat and the cryocooler is started, the temperature is reduced from about 293 K to below 20 K in about 5 days (Figure 4.5).

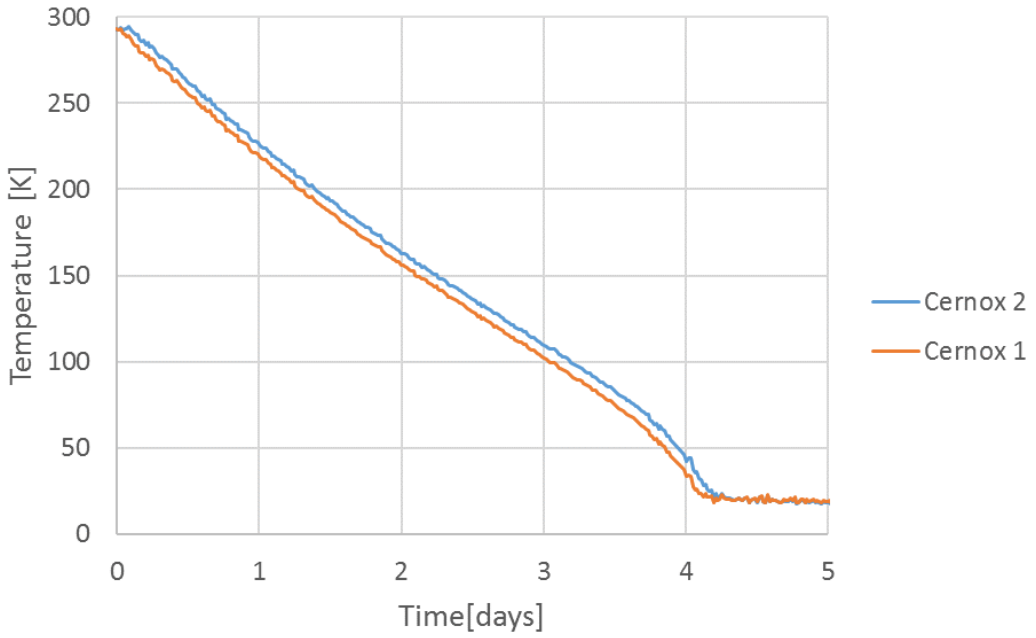

Figure 4.5: Measured cool-down temperatures of the field winding.

4.3 Temperature Measurement

Low enough temperatures inside the cryostat is a premise for successful testing, hence the temperatures need to be measured accurately during testing. When the temperatures reach a stable low value, the measurements are used to verify if the equipment is cold enough for testing. The temperatures measured during testing indicates if the equipment is operating as supposed to, or if there are unexpected power losses. The AC losses in the superconducting wire sample are measured using a calorimetric measurement method. The calorimetric measurement method requires high accuracy measurements of the temperature at cryogenic temperatures, to measure the temperature change in the wire sample during testing. A total of eight temperature measurement sensors are positioned on strategic parts of the equipment. Six of the sensors are thermal elements type T and two are Cernox sensors.

4.3.1 Cernox Sensors

Figure 4.6: Cernox sensor

The two Cernox 1070-SD-HT-4L sensors used are made by Lake Shore Cryotronics. The sensors are cryogenic temperature sensors that can measure temperatures in the range of 100 mK to 400 K. They have high sensitivity at low temperatures. At 20 K the typical sensor accuracy given by the manufacturer is ± 9 mK. The sensors also have low magnetic field induced errors and are proven stable over repeated thermal cycling. Due to the high cost of these sensors, only two Cernox sensors are used in the testing. The Cernox sensors are used where the accuracy of the measurements are most important.

According to the calibration data, the voltage across the cernox sensors should be 2 mV ±25%. At a temperature of 20 K, this requires a current of about 1 μA. It is paramount for the precision of the colorimetric measurements that the Cernox power source delivers a stable current of this value. In this project, the Cernox current was supplied by a Knick Berlin 37 - S140 low voltage power source.

4.3.2 Thermal Elements Type T

Figure 4.7: Thermocouple wire Type T

Thermal elements of type T was used to measure temperatures in the cryostat on locations with lower accuracy requirements and higher temperatures than where the Cernox sensors was placed. During cool down, the temperature was logged on a computer down to the software limit of 100 K. After cool down, when steady state temperature was reached, the temperatures of the type T elements was measured manually with a Fluke 54 II B thermometer. Fluke 54 II B has a temperature range of 23 K to 673 K, for type T sensors. The rated accuracy of type T measurements are $\pm$[0.50% + 0.3°C], which at 50 K equals $\pm$1.4 K.

4.3.3 Sensor positioning

The positions of the sensors are shown in Figure 4.8. The thermal element 1 is positioned on the left side of the AC coil between the coil and the epoxy mount. Thermal element 2 is positioned on the thermal connection between the copper screen and the AC wire furthest away from the cryocooler. The thermal element 3 and 4 are attached respectively to the red and blue thermal connection at the transition between the copper current leads and the HTS wires. These temperatures tell if the HTS superconductors reaches the superconductive state and if they remains superconductive during operation. Thermal element 5 is positioned on the flange of the cryocooler stage 1 to check if the operating temperature is as expected (about 50 K), to be sure the cryocooler is operating properly. The thermal element 6 is attached at the bottom of the copper screen, furthest away from the connection to the cryocooler. This is expected to be the coldest place on the copper screen, thus the temperature indicates if the whole copper screen is cooled sufficiently.

Cernox sensor 1 is positioned on top of the thermal interface of the field winding. The temperature of the thermal interface is critical as it indicates if the temperature of the field winding is sufficiently low for superconductivity. The Cernox sensor 2 is positioned in the center of the 10 cm MgB_2 wire sample. This sensor measures the temperature increase due to the AC losses during testing, and from the current injection in the reference heater.

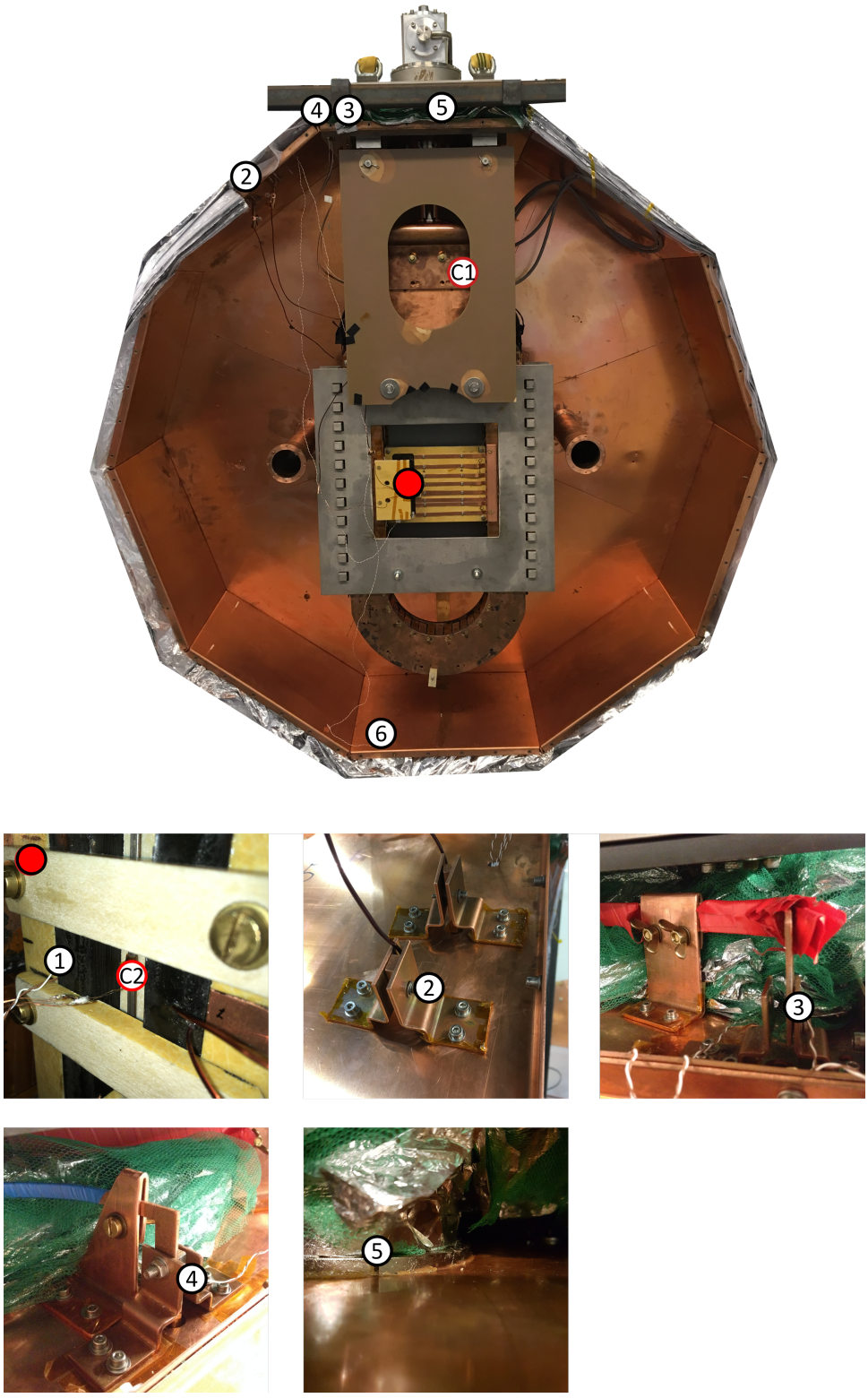

Figure 4.8: Positions of the six thermal elements type T and the two Cernox sensors.

Chapter 5

Generically On Testing In The Cooled State

5.1 Cooling procedure

A four-step cooling procedure needs to be conducted to prepare for testing in the superconductive state. The first step is to assemble the equipment. The copper screen is closed and the superinsulation is attached on the copper screen. Subsequently, the upper part of the cryostat vessel with the winding and the copper screen is submerged into the lower part. The second step is to run the vacuum pump for about 24 hours to reach a pressure below 300 Microns in the cryostat. The third step is to run the turbo vacuum pump, which needs a couple of hours to obtain a pressure of 30 Microns. In the fourth and last step, the cryocooler is started and uses about 5 days to cool the equipment to the lowest temperature. When the temperatures in the cryostat reaches a stable low value of about 15 K, it is set for testing. The whole cooling procedure sums up to a minimum of 6 days.

5.2 Testing procedure

When performing AC loss tests, firstly the field winding needs to be energized to obtain the background magnetic field. The DC magnetic field is constant while running different AC magnetic field tests. An AC test is performed over a 10-second period by injecting a 50 Hz AC current in the AC coil and logging the temperature change in the wire sample. Several 10-second tests is performed with different AC magnetic field. The wire sample must be left for cooling back to the initial steady temperature between each 10-second test.

5.2.1 Field winding energizing

Current is injected in the field winding through an electric circuit with a quench protection as shown in Figure 2.13. To obtain a certain background field, the necessary winding current is given in Table 3.4. A small voltage is applied by a voltage source to inject a current through the winding. By slowly ramping up the voltage applied, a small voltage is maintained across the field winding inductance. This voltage across the inductance leads to a continuous increase of the field winding current, given by the current voltage relation in an inductance (Equation (2.11)). When the required current is reached, the voltage ramping is stopped and the inductive voltages across the winding disappear in a couple of minutes. The high winding inductance of 2.9 H causes this long stabilization time. When the inductive voltage disappears, the remaining resistive voltages in the sub-coils indicate if the coils remain superconductive.

5.2.2 AC coil energizing

Current is only injected in the AC coil during the 10-second testing period. A variac is connected through a transformer to inject a 50 Hz current in the range of 1 A to 10 A peak. The current magnitude is measured using a Fluke 289 multimeter. The corresponding current for a certain peak magnetic field at the wire sample is given in Table 3.5. During the test period, the type T thermal element 1 indicates if the temperature of the AC coil becomes too high.

5.2.3 Reference heater

The power in the reference heater is set by injecting a reference heater current according to Table 6.2. The reference heater current is injected during a 10-second testing period, while the temperature change is measured in the wire sample. Reference heater tests is taken to approximately match the highest and lowest temperature change observed in the AC loss measurements, and with reasonable intervals between these. Interpolation is used between the temperatures measured to find the AC power losses for any temperature change measured. During reference heater measurements, the AC coil and the field winding is disconnected.

Chapter 6

Results

6.1 Temperatures

The steady state temperatures was measured after the cool-down (Table 6.1). Both Cernox sensors measured a temperature below 20 K, indicating that the field winding temperature was low enough for the planned current injection of 100 A. The AC coil had a temperature of 32.7 K (Type T 1(T1)). This was significantly higher than the field winding, but as it remained at the same temperature during the testing this did not cause any problems. Where the AC coil wire is attached to the copper screen for cooling, the temperature was 67.5 K (T2). This was 12 K more than the temperature of the cryocooler stage 1 (T5) where it is cooled. On the bottom of the copper screen it was measured 62.6 K (T6), indicating proper cooling of the whole copper screen. At the connection between and the copper current lead 1 and the HTS 1 wire it is measured a temperature of 83.2 K (T4), well below the critical temperature of 110 K. The temperature sensor at the connection of HTS 2 (T3) had ceased to function after the assembling.

Table 6.1: Steady state temperatures after cool-down.

Sensor	**Temperature [K]**
Cernox 1 (field winding)	19.8
Cernox 2 (wire sample)	18.8
Type T 1 (AC coil)	32.7
Type T 2 (AC wire cooling)	67.5
Type T 3 (HTS2)	-
Type T 4 (HTS1)	83.2
Type T 5 (Cryocooler st. 1)	55.4
Type T 6 (Copper screen - bottom)	62.6

6.2 Field winding

The voltages across the field winding was similar to in the previous test. As the current injected was increased, the resistive voltages increased faster than a linear ohmic relation would predict. However, the voltages remained within tolerable levels and did not restrict the current injection. Similar results for the voltages of the sub-coils of the field winding is presented and discussed in a previous project report [12].

The AC magnetic field produced by the AC coil was expected to induce some power losses in the field winding, and to might disturb the field winding during operation. However, even for the highest AC current of 10 A_{peak}, there was no measured changes in the field winding temperature nor the sub-coil voltages of the field winding.

The HTS 2 current lead was replaced prior to the test, due to failure from over heating in the previous test. In the new soldered joint between HTS 2 and the end of coil 8, the resistance measured during operation was as low as in the eight other joints, below 0.4 mΩ. During testing, when the field winding current was increased above 20 A, the voltage across HTS 2 started to increase. First, this restricted the field winding current to an upper limit of 27 A. Above 27 A the voltage started to run away too fast, and the current had to be lowered immediately to prevent damage to the HTS 2 due to over heating. To overcome this problem without disassembling the cryostat, insulation was applied around the current injection cable leading to HTS 2, to reduce the conduction through the wire. This reduced the temperature on the cable just outside the cryostat from 15°C to 0°C. This temperature decrease allowed for a current up to 34 A to be injected. To reduce the temperature further, a custom made dry ice cooling system was mounted on the current cable connection point on top of the cryostat (Appendix B). This reduced the temperature at the current inlet to the HTS 2 to -41.6°C. Now, the HTS 2 voltage was sufficiently stable to run tests with field winding currents up to 70 A. The increasing voltage across the HTS 2 was the single factor limiting the current of the field winding to a maximum of 70 A, i.e. limiting the background magnetic field to 0.35 T.

6.3 AC loss measurements in the MgB_2 wire sample

6.3.1 Reference heater measurements

A series of tests was performed with the reference heater to obtain data pairs of corresponding power injections and temperature increases in the wire sample. A total of 11 data pair values in the range of zero to 10 mW was considered to be sufficient to do a linear interpolation between measured values. The reference heater tests was performed at a zero background field. In that way the field winding did not need to be energized more than necessary, with a risk of damnation. The temperature curves from the reference heater tests is assumed to be independent of the background field. The tests was performed

by injecting a current in the reference heater using a low voltage DC power supply (Rohde&Schwarz HMC 8042).

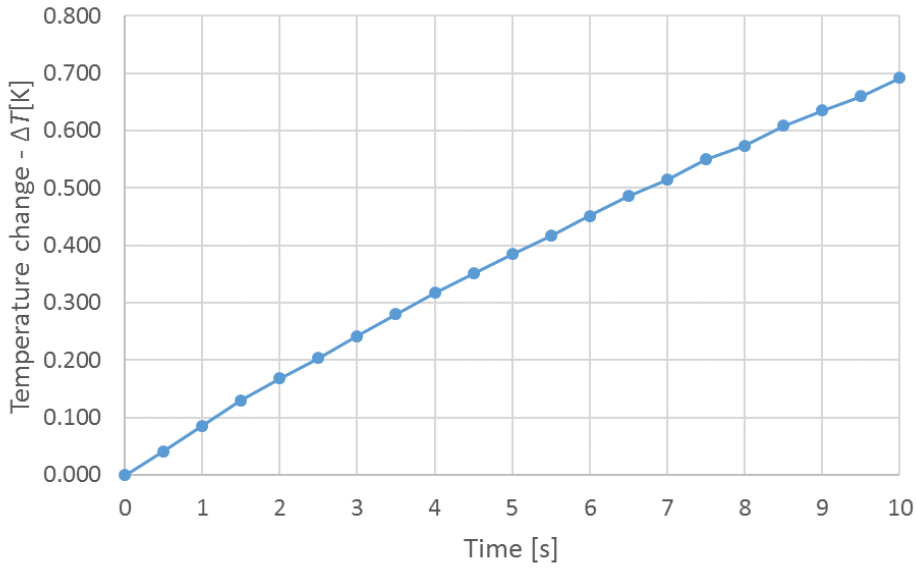

Figure 6.1: Example of a temperature change curve in the wire sample from the reference heater. These temperatures were measured over a 10 second period with a power of 2500 μW (29 mA current injection).

In the cooled state, the reference heater was measured to have a resistance of $R_{ref} = 2.93\Omega$. The power current relation, $P = RI^2$, was used to find the power from the reference heater for a certain current. During the tests, the reference heater current was measured with a multimeter (Fluke 289). Figure 6.1 shows an example curve for one of the reference heater tests. The final ΔT values from each test is used to make an index table of corresponding power and temperature increase (Table 6.2). For a certain temperature increase from a 10 second AC loss test, the corresponding power loss is found from the index table.

Table 6.2: Measured temperature increase in the wire sample from a 10 second constant power injection from the reference heater.

Power [μW]	**ΔT[K]**
0	0.000
47	0.011
99	0.029
293	0.082
887	0.260
1773	0.480
2464	0.693
2944	0.821
3925	1.035
5881	1.572
7832	1.982
9789	2.439

The values from Table 6.2 is plotted in Figure 6.2. The curve of the plot shows that the $P-\Delta T$ relation is approximately linear, thus a linear interpolation between the measured values is expected to give accurate estimates of the AC power losses.

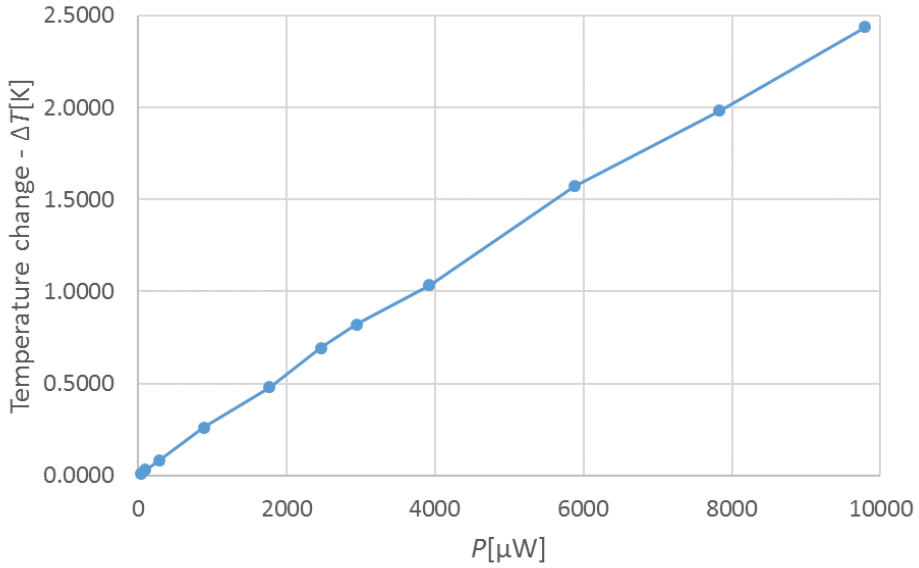

Figure 6.2: Plot of the measured temperature increase in the wire sample after 10 seconds of constant power injections from the reference heater. Dots indicate the measured values in each of the 11 tests.

6.3.2 AC loss measurements

The AC losses was measured by a series of tests with varying values of the AC magnetic field strength, with different background fields. During the tests, a peak current in the range of 1 A to 10 A was injected in the AC coil, which induces a peak AC magnetic field in the range of 2.2 mT to 21.8 mT. The background field strength from the field winding was in the range of zero to 0.35 T, obtained by current injections from zero to 70 A. In the presented results, currents are converted to magnetic fields according to the simulations of the AC coil and the field winding. All presented loss values are estimated from the measured temperature increase in the wire sample, according to the reference heater values in Table 6.2. The frequency of the AC current used was f=50 Hz.

AC losses with zero background field

The starting temperature measured in the wire sample for each of these tests was in the range of 18.96 K to 18.97 K. No current was injected in the field winding during the test, i.e. there was no DC magnetic field exposure to the wire sample.

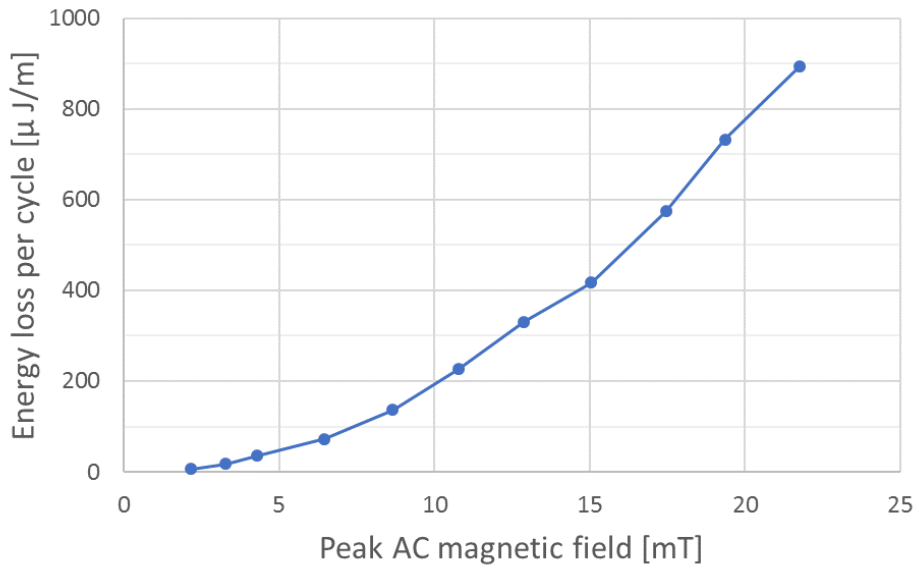

Figure 6.3: AC losses in a MgB_2-superconductor with zero background field.

The results from 11 tests are presented in Figure 6.3. It is found that the power losses increases exponentially with the peak magnetic field. The power losses increase as an exponential function of the AC magnetic field with an exponent of 2.1.

AC losses with 0.13 T background field

The temperature of the wire sample was in the range of 19.14 K to 19.17 K at the beginning of each of these tests. The DC magnetic background field of 0.13 T was obtained by injecting a current of 25 A in the field winding.

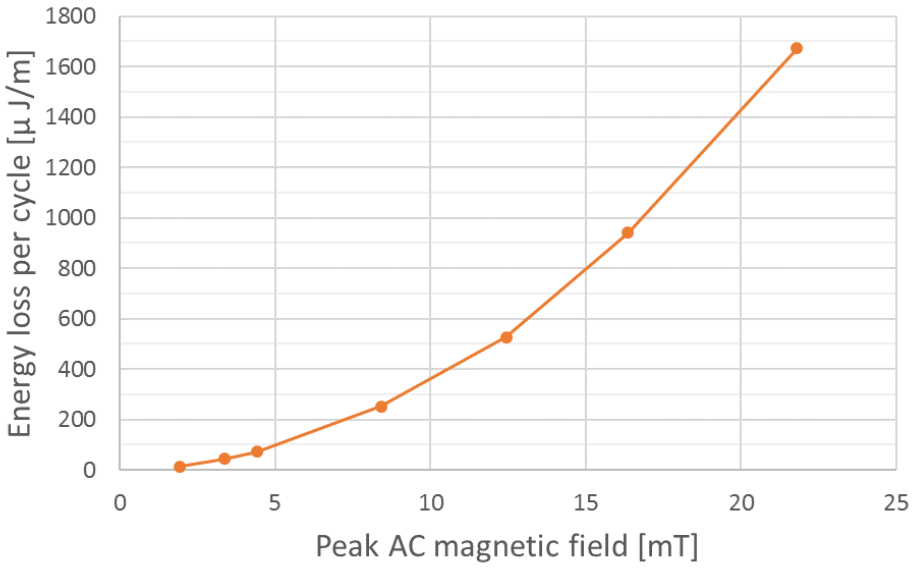

Figure 6.4: AC losses in a MgB_2-superconductor with a 0.13 T background field.

It was found that the AC power loss values could be approximated as en exponential function of the AC peak magnetic field with an exponent of 2.0 (Figure 6.4). The background field of 0.13 T resulted in approximately twice as high losses as when the wire sample was not exposed to a magnetic field. E.g. for an AC magnetic field of 21.8 mT it was measured losses of 900μJ/m per cycle with zero background field and 1670μJ/m per cycle with 0.13 T background field.

AC losses with 0.25 T background field

The wire sample had a temperature in the range of 19.09 K to 19.12 K at the beginning of each test. A background magnetic field of 0.25 T was obtained by a field winding current of 50 A.

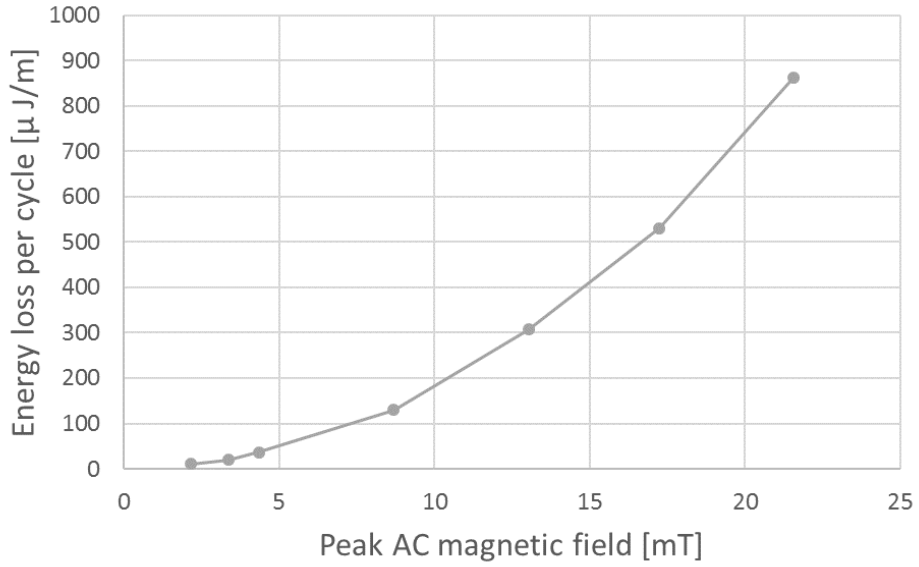

Figure 6.5: AC losses in a MgB_2-superconductor with a 0.25 T background field.

The results for different AC magnetic fields and a background field of 0.25 T are presented in Figure 6.5. The results could be approximated as an exponential function of the AC magnetic field with an exponent of 1.9. The magnitude of the losses measured with 0.25 T background field are similar to the losses measured at zero background field, approximately half of the losses measured with 0.13 T background field.

AC losses with 0.35 T background field

The starting temperature of the wire sample before each test was in the range of 19.11 K to 19.17 K. The current in the field winding was 70 A to obtain the 0.35 T background field. At this current the HTS 2 current lead did not become stable. The voltage across HTS 2 was slowly growing and after a while the growth became faster and the ohmic power dissipation eventually threatened to damage the HTS 2 wire. To avoid the risk of damnation, the test had to be aborted after about 30 minutes. Due to this, only 4 different AC magnetic field values was tested for with 0.35 T background field.

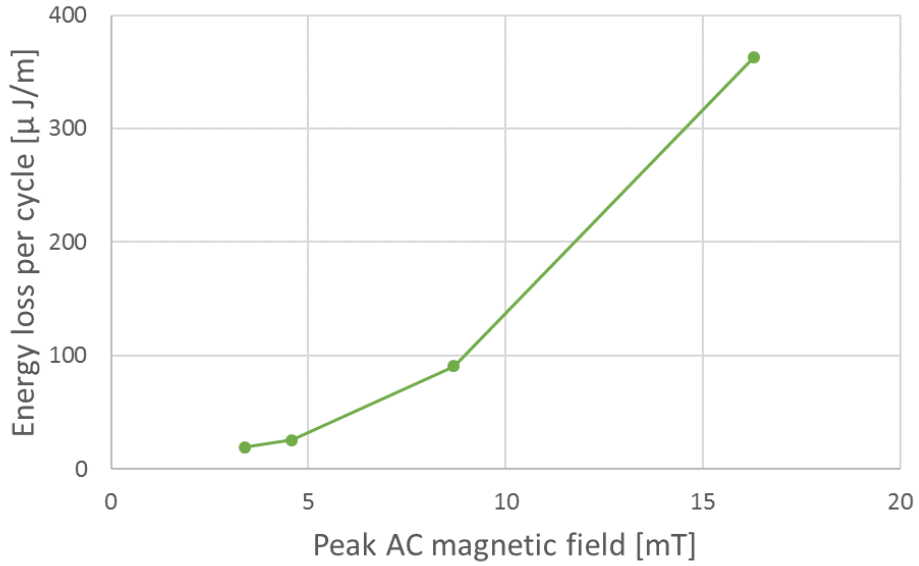

Figure 6.6: AC losses in a MgB_2-superconductor with a 0.35 T background field.

The AC losses measured increases as an exponential function of the AC magnetic field with an exponent of 1.9 (6.6). At 0.35 T background field it was measured the lowest AC losses, approximately 30 % lower than with zero background field.

Comparison of losses with different background fields

In Figure 6.7 the loss measurements at the four different background fields are plotted on logarithmic axes. A plot of the modelled superconductor losses for 1 T background field is also included.

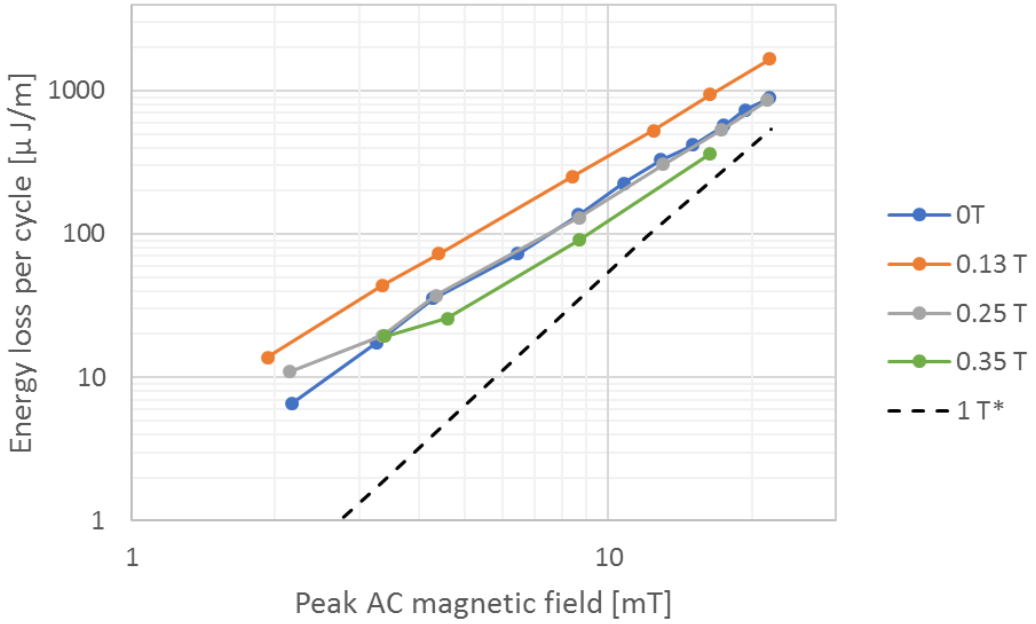

Figure 6.7: Plot of AC losses in a MgB_2-superconductor with different background fields (Logarithmic axes). *Modelled superconductor losses at 1 T (Figure 2.12).

The losses measured, with all the different background fields, can be fitted to an exponential function of the AC field magnitude with an exponent of approximately 2. This could be seen from the parallel slopes in the log-log plot in Figure 6.7. The modelled superconductor losses has a steeper slope as it increases with the third power of the AC magnetic field.

AC power losses as a function of background field strength

To be able to study the effect of the strength of the DC magnetic background field, tests was performed for three AC magnetic fields at every increment of 50 mT background field. Losses was measured for peak AC magnetic fields of 3.4 mT, 4.3 mT and 8.6 mT. The AC power losses measured is presented in in Figure 6.8.

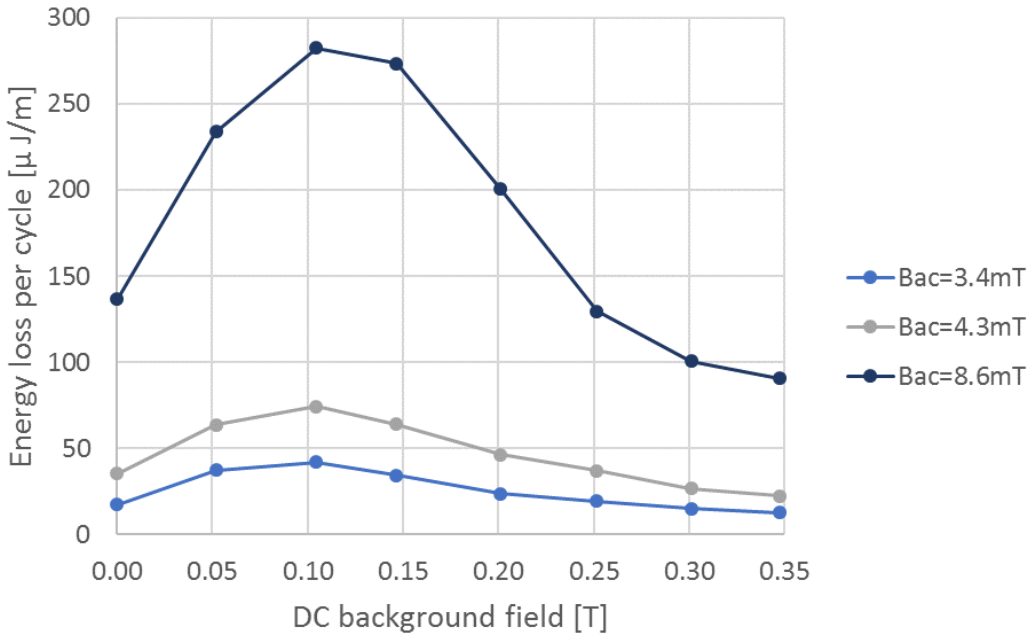

Figure 6.8: Energy losses per cycle per unit length for different background fields. AC magnetic field strengths are given in peak values.

The losses measured for all three AC field magnitudes follows the same pattern. As the background field is increased from zero, the losses are increasing until reaching a peak at about 0.1 T. Above this value, the AC losses decrease with an increasing background field. At a background field of about 0.25 T, the losses are of the same magnitude as with zero background field. As the background field is increased further, the losses continue to decrease. For all the AC fields, the lowest losses are measured with the strongest background field of 0.35 T. When reaching this background field, the loss curve starts to level out.

Loss deviation from the pre-test to the final test

In this subsection, it will be presented results from a similar series of tests executed before all the test results presented this far. After the first series of tests (pre-test), the temperature measurement accuracy on the wire sample was significantly improved. This was achieved by measuring the AC coil current with a Fluke 289 multimeter, instead of with the same datalogger as the temperature sensor voltage. As the improvement made the temperature measurements significantly more stable, it was decided to perform all the tests a second time (final test, presented above). The following results from the pre-test are presented as it was found a remarkable difference in the power losses compared to the final test. The magnitude of the differences measured are significant regardless of the lower accuracy in the first test. The tests and the results are listed chronologically in Appendix A.

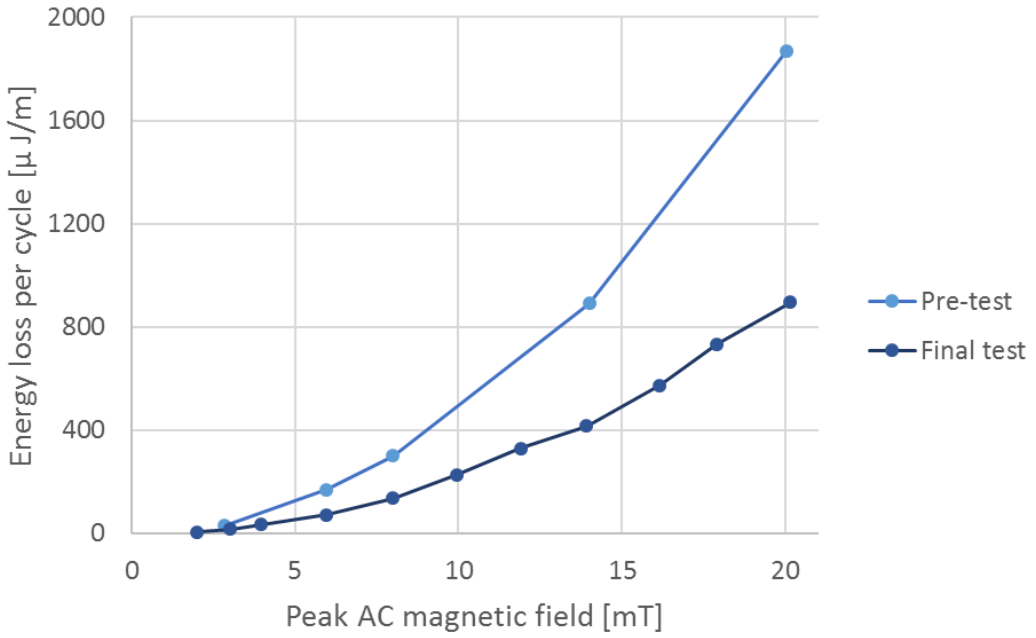

Figure 6.9: Comparison of results in pre-test and final test. Energy losses per cycle per unit length with zero background field for different AC magnetic fields.

In the pre-test, the power losses as a function of the AC magnetic field, was increasing exponentially with the square of the magnetic field, like in the final tests. This pattern is the same for all the four background fields applied in the pre-test. In Figure 6.9 it is present the results for different AC fields at zero background field. The pattern of exponential growing losses is the same as in the final test, but the magnitude is different. Furthermore, the magnitude of the losses in the pre-test varied strongly with the background field. The loss variation for some AC field strengths as a function of background field is shown in Figure 6.10.

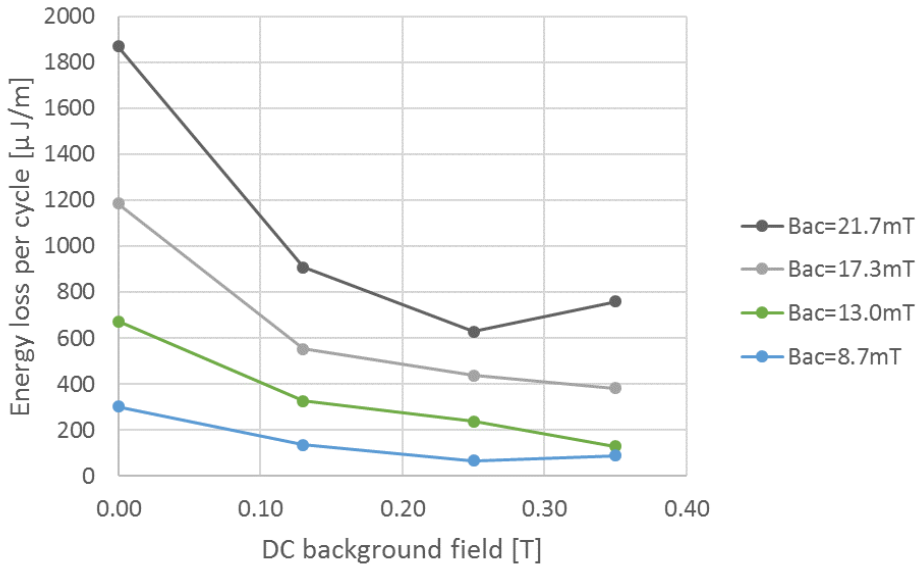

Figure 6.10: Pre-test results for energy losses per cycle per unit length with different background fields.

The pattern is approximately similar for different AC fields (Figure 6.10). The variation at 0.25 T and 0.35 T, could be assumed to be due to the low accuracy of the pre-test measurements. It is shown that as the background field increases, the magnitude of the losses in the pre-test was varying in a different pattern than in the final test (Figure 6.11).

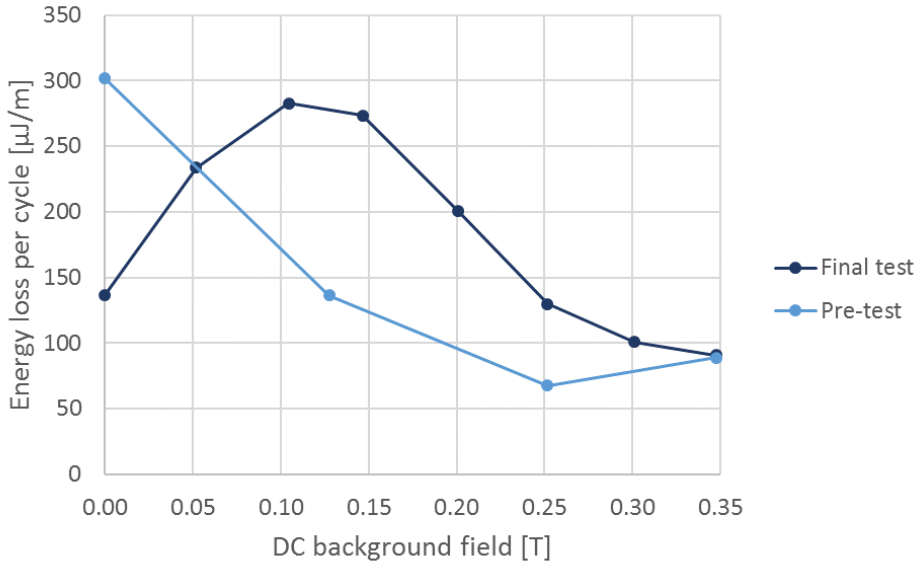

Figure 6.11: Comparison of results in pre-test and final test. Energy losses per cycle per unit length with an AC magnetic field of 8.6 mT peak and different background fields.

Chapter 7

Discussion

7.1 Field winding operation

The field winding operation has been a continuous challenge throughout this project. As the assemble of the cryostat and cool down is necessary to fully test the result of a repair, a trial and error process takes about three weeks plus the time of the repair. To reduce the number of cool downs, it was decided to both replace the HTS 2 and design, produce and install the AC loss testing equipment, before cooling and testing. Due to the limited time of this master thesis project, it was only time for one cool-down and testing with the AC loss measurement equipment.

During testing, the sub-coils was operating satisfactory, but the HTS 2 current lead restricted the current injection. The HTS 2 was replaced before this testing, but a similar voltage increase as observed in the replaced HTS 2 was observed in the new HTS 2. Before the replacement it was assumed that the old HTS 2 had been damaged somehow while working on the field winding, and due to this degraded its superconductive properties. Insufficient cooling of HTS 2 was assumed less likely, as the voltage across HTS 2 was constant for currents up to 149 A in a previous test, with the same cooling equipment installed. During testing of the new HTS 2, as the injected current was increased above 19 A, the voltage increased as if it was leaving the superconductive state. This indicated that it was the cooling of the HTS 2 that was limiting its performance. This assumption was confirmed as the dry ice cooling system was installed, and current up to 70 A could be injected before the same voltage increase occurred. The temperature of HTS 2 was not measurable as the thermal element 6 had lost connection during assembling. However, by decreasing the temperature of the current cable outside the cryostat, the critical current was increased by approximately 50 K. By improving the cooling of the HTS 2 it is assumed that currents higher than 70 A could be injected in the field winding.

7.2 Temperature measurements

The steady state temperatures measured on top of the field winding (C1) and on the wire sample (C2) after cool down, was 19.6 K and 18.7 K respectively. In a previous test, it was measured 14.2 K on top of the field winding (C1) and 11.0 K on the bottom (C2) [12]. The only new equipment installed in this latest test was the AC loss measurement system. It is assumed that the increased temperature was caused by conduction through the AC wires. When stage 1 of the cryocooler has a temperature of 55 K, the capacity of stage 2 is about 4 W higher at a temperature of 19 K than at 14 K (Appendix E). Hence, it could be assumed that the conduction through the AC wire was approximately 4 W. However, the temperature of the field winding reached below 20 K, and was cold enough for the planned testing.

In the cooled state, the C1 sensor on top of the field winding measured 0.9 K higher temperature than C2, which is located further from the connection to the cryocooler. As stage 2 of the cryocooler is connected on top of the thermal interface of the field winding, it is expected that the temperatures increase further down on the field winding. It might be that one of the cernox sensors is damaged, such that the resistance-temperature relation from the calibration is no longer exact. Another possibility is that the voltage measurements across the sensors by the Agilent datalogger is not as precise as necessary, or that there are some errors from the voltage measurement circuits. The current in the Cernox sensors were the same, as they were connected in series. Thus, the current measurement can not explain the unexpected temperature difference. During heating of the cryostat, after finished testing, it was observed an irregularity in the measurements of C1. From time to time the temperature measured was leaping and dropping by up to 15%. If the measured value of 19.6 K was erroneous 15 % higher than the actual value, the value of C1 in relation to C2 would be reasonable. Furthermore, higher measured temperatures could occur due to a insufficient thermal contact between the sensor and the equipment to be measured.

Despite the uncertainty regarding the exact temperatures from the Cernox measurements, this do not reduce the quality of the AC loss measurements. Using the calorimetric measurement method, it is the measured temperature differences that are used to measure the losses, not the exact temperatures. The Cernox sensor 2 on the wire sample was proven to measure stable values throughout the reference heater and AC loss testing, which is the requirement to measure the AC power losses.

7.3 AC losses

The losses in the wire sample during exposure to different AC magnetic fields and background fields did not follow a pattern that could be explained by the modelled AC losses in the MgB_2. With a fixed background field, the losses was increasing as an exponential function of the AC magnetic field with an exponent of 2 (Figure 6.3 - Figure

6.6). This pattern was similar for all the background fields applied. AC losses in the MgB_2 are expected to increase as an exponential function of the AC field with an exponent of 3, according to the modelled losses (Figure 2.12). Furthermore, the modelled losses is higher with stronger background field. From the measurement it is found a completely different pattern for the losses as a function of the background field (Figure 6.8). As the background field increases, the losses first increase until reaching a peak around 0.1 T, then decreasing towards 0.35 T.

The losses measured are assumed to not be superconductor AC losses in the MgB_2, but rather eddy current losses and hysteresis losses in the copper and the nickel in the wire. Theoretically, eddy current losses are proportional to the square of the AC magnetic field applied, which fits the losses measured. Eddy current losses might occur both in the copper and in the nickel of the wire sample. Hysteresis losses might occur in the nickel of the wire sample, as the nickel is magnetic. To determine the origin of the measured losses, it was sought a theoretical estimation of the magnitude of the eddy currents and the hysteresis losses.

A simulation of the AC losses in the wire sample was conducted to compare with the measured losses (Described in Appendix D). The losses was simulated with different relative permeability (μ_{Ni}) of the nickel, to investigate if the saturation of the nickel due to a remanent field influences the losses. However, the simulation do not include hysteresis losses. In the first simulations, it is applied a high relative permeability of the nickel of μ_{Ni}=600, to simulate the pre-test (with no prior magnetization of the wire sample). This corresponds to typical magnetic behaviour near the origin of the B-H graph (Figure 2.14). In the next simulations, the relative permeability of nickel is set to μ_{Ni}=1, to simulate the losses in the final test with an assumed high remanent field. A relative permeability of 1 corresponds to full magnetic saturation (upper right point on the hysteresis loop). The results from the simulations are plotted with the test results with zero background field in Figure 7.1.

From the simulations, the losses are estimated to be smaller with μ_{Ni}=1 than with μ_{Ni}=600. This indicates that a remanent field in the wire sample nickel might reduce the AC losses. However, the simulated loss reduction is only about 10 %. This is significantly less than the 50 % reduction from the pre-test to the final test with zero background field. 98 % of the simulated losses are found to occur in the wire sample copper, while only 2 % in the nickel. Furthermore, the simulated losses increase with the square of the AC field, suggesting that the simulated losses are mainly eddy current losses in the copper.

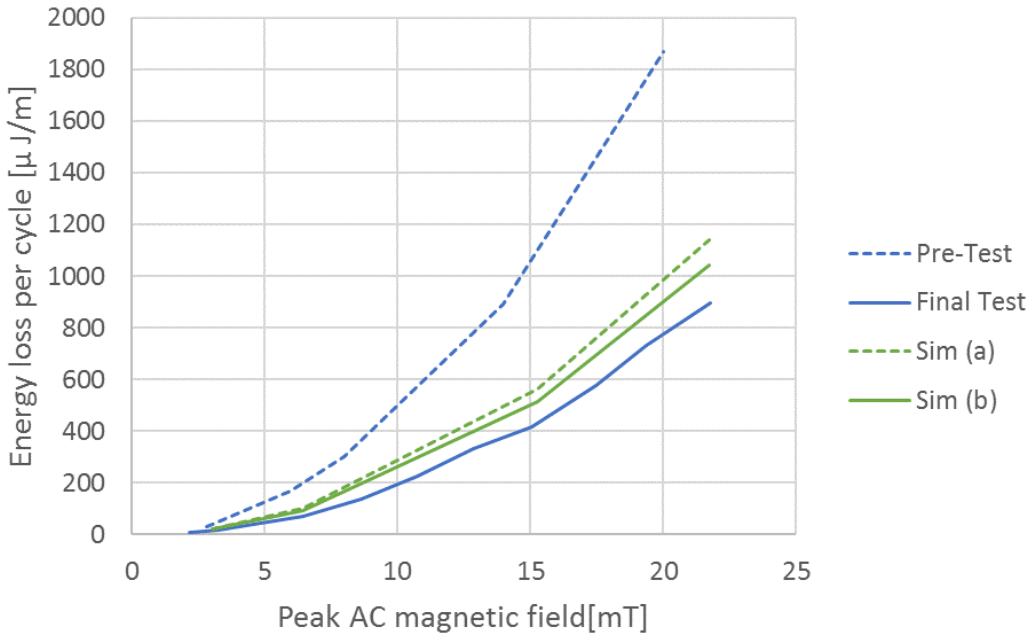

Figure 7.1: Simulation of AC losses in the wire sample and measured values in the pre-test and the final test with zero background field. Sim (a):μ_{Ni}=600. Sim (b):μ_{Ni}=1.

The simulations match the measurements in the final test with zero background field, with a deviation of less than 30 %. Considering all the sources of error in the models and in the measurements, the simulation is assumed to imitate the actual losses well and that the losses measured in the final test at zero background field are dominated by eddy current losses. According to the simulation, when increasing the background field from zero to 0.35 T, it could be expected a reduction in eddy current losses. However, the origin to the measured loss pattern for different background fields could not be determined by the simulation alone, nor can the deviation from the pre-test to the final test.

To theoretically estimate the hysteresis losses, it is necessary to know the magnetization curve of the nickel (the B-H curve). This is not known for the nickel in the superconducting wire. However, if there are hysteresis losses these will approach zero if the nickel is magnetically saturated by a strong background field. Furthermore, the magnetization of the nickel could cause different hysteresis losses with the same applied field. The comparison of the test results from the pre-test and from the final test with zero background field (Figure 6.9), shows that the losses was approximately 50 % lower in the final test than in the pre-test. According to the hysteresis loop (Figure 2.14), after exposing a magnetic material to a magnetic field and than reducing the applied field to zero (H=0), a magnetic flux (B) remains in the material due to magnetization. This remanent field in the nickel makes the measurements history dependent, which might explain the deviation in the losses measured from the pre-test to the final test. Before the pre-test, the wire sample had not experienced exposure to a strong magnetic field. In the end of the pre-test, the wire sample is exposed to a DC magnetic field of 0.35 T for the first time. Lower AC

losses in the final test might be due to a remanent field from the DC magnetic field applied in the pre-test. At zero background field in the final test, the nickel might be close to saturation from the remanent field, which gives a different B-H curve and corresponding different AC losses.

At a background field of 0.35 T in the final test the results are similar to the losses in the pre-test (Figure 6.11). As the applied field is increased to 0.35 T in the final test, the magnetic field in the nickel returns to the previous upper point (from the pre-test) on the BH-curve. Hence, it is expected that hysteresis losses at 0.35 T background field are similar in the pre-test and the final test.

On the basis of the difference in measured losses from the pre-test to the final test (Figure 6.11), it is sketched a possible B-H curve of the nickel. According to the simulations above it is assumed that the eddy current losses maintain at a relatively stable value regardless of the background field. This value is assumed to be just below the value measured at 0.35 T background field (Figure 6.8). It is assumed that the remaining losses are hysteresis losses in the nickel.

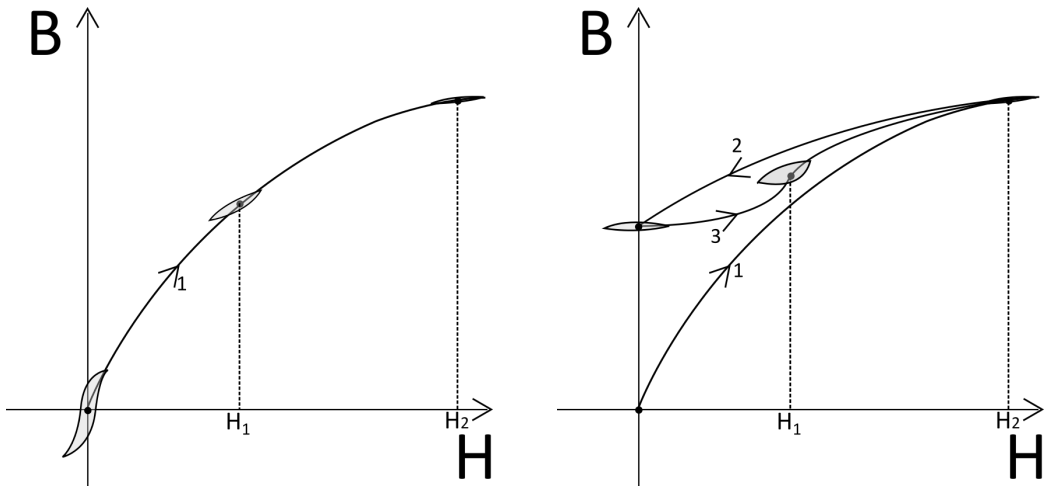

(a) Pre-test (b) Final test

Figure 7.2: Sketch of a possible B-H curve for the nickel based on the test results. Gray areas enclosed by hysteresis loops from a AC magnetic field indicate losses, and is illustrated at three different background fields. 1: DC magnetic field path during first magnetization. 2: Applied DC magnetic field is removed between pre-test and final test. 3: DC magnetic field path in the final test.

In a magnetic material, the magnetization is reduced slower than the applied field (H). As a consequence, the hysteresis losses become high where the slope of the B-H curve is steep. Figure 7.2a shows a curve that causes a reduction of the loop area for stronger background fields, corresponding to the reduced losses for higher background fields in the pre-test (first magnetization). As the nickel gets closer to magnetic saturation, the losses approach zero. Path 3 corresponds to the background field in the final test. The

peak of measured losses at about 0.1 T background field suggests a B-H curve with the steepest slope at H_1, between zero and the strongest field. A B-H curve like path 3 could also explain low losses at zero background field, and lower losses at the highest magnetic saturation at H_2.

When the background field reaches the highest value in the final test, the nickel is expected to have returned to the same point on the B-H curve, as seen in Figure 7.2b. The losses measured are about the same in the pre-test and in the final test at the highest background field. This is a strong indication that the measurements are reliable, and that a difference in the magnetization path for the first an second magnetization causes the different patterns of losses.

A B-H curve for pure nickel with a shape like path 3 is found in literature [4], but to determine how this curve corresponds to the curve of the nickel in the superconducting wire it is required further studies. However, the curve found for pure nickel confirms that the a curve shape like the sketched curve based on the final test (path 3) is realistic. Further, it is found that magnetic saturation of nickel occurs in the range of 0.61 - 0.64 A/m [4]. Depending of the magnetization curve, this could comply with the assumption that the hysteresis losses are approaching zero as the measured losses levels out at 0.35 T background field (Figure 6.8).

7.4 Consideration of field winding losses

If the superconducting field winding is operated at max current of 200 A, the average flux density in the cross-section is simulated to be about 1 T. With such background field, the AC losses in MgB_2 is expected to have a greater influence on the total losses (Figure 2.12). However, even with an average background field of 1 T there could be flux densities below 0.35 T in a section near the center of the cross-section (Similar to the field variations simulated in Figure 3.8). Depending on the strength of the AC magnetic field and the background field, the eddy current losses and the hysteresis losses in these sections could have a significant impact on the total losses of the field winding. E.g. with a background field of 1 T and a AC magnetic field of 11 mT the modelled superconductor losses are 69 μJ/m per cycle (Table 2.1), while from the measurements at a background field of 0.1 T and an AC field of 11 mT the losses are measured to 400 μJ/m per cycle.

From the loss simulations, eddy current losses in the copper seem to remain high regardless of the background field. This could also be supported by the measured losses (Figure 6.8), as the losses start to level out at a finite value above zero as the background field reaches 0.35 T. These results could suggest to limit the amount of copper used in the superconducting wire. Further, it could be considered to produce superconducting wire with strips of laminated copper on the superconductor to reduce the eddy current losses.

7.5 Uncertainty Analysis

The numerical results from the experiments are subject to several sources of systematic errors. These are errors from measured values and human factors. In this section, different sources of uncertainty in the results are discussed.

The magnetic field values for the AC coil and the field winding are approximated with simulations. The currents measured during test have been converted to the corresponding magnetic field values found in simulations. Deviations in the physics and dimensions between the models and the actual field winding and AC coil will produce errors in the conversion from the current to the magnetic field. Furthermore, there could be errors in the measured AC coil current and the field winding current by the measurement tools that could result in further discrepancy between actual and estimated magnetic fields.

For exact measurements of the temperature with the cernox sensors, it is required exact calibration and accurate measurements of both the cernox current and voltage. The typical accuracy of a Cernox sensor at 20 K is $\pm$ 9 mT. For the purpose of the experiments the exact temperature is not crucial, as long as the sensor gave stable measurements to determine minor temperature changes. From a series of 100 measurements with presumed constant temperature at C2, the temperature measured was found to have a standard deviation of 2.6 mK. The stability of the measurements was considered sufficiently accurate to measure a temperature increase of 45 mK (in a 10 second test), corresponding to a power of 150 μW. However, at the lowest values it was observed that even human movement next to the measurement equipment distorted the voltage measurements. Waving an arm above the data logger provoked voltage pulses equivalent to a temperature change of more than 100 mK. This indicates that the Cernox temperature measurements was prone to significant disturbance. However, all temperature curves used for the results was considered to be reasonable by inspection.

The reference heater resistance was soldered to the copper wires for current injection and voltage measurement on each side of the wire sample. To avoid any electrical connection from the solder lead to the copper or nickel in the superconductor, it had to be a small distance from the soldered joint to the wire sample. As a result, the reference heater resistance wire is 1-3 mm longer than the 10 cm wire sample on each side. The power in the exceeding resistance wire could be assumed to partly dissipate in the copper wires. I.e. as the wire sample length is 100 mm, 2-6 % of the reference heater power might not dissipate in the wire sample. This results in some error in the power conversion table from the reference heater.

Chapter 8

Conclusion

Hardware for experimental testing of AC losses in a sample of a MgB_2 superconducting wire have been designed, produced and tested. During testing, the cryogenic cooling system obtained temperatures below 20 K in the test equipment. The field winding was capable of carrying currents up to 70 A, i.e. setting up DC magnetic fields up to 0.35 T. The custom-made AC coil installed was operating properly and induced 50 Hz AC magnetic fields up to 21 mT peak. The calorimetric measurement system installed was proven capable of measuring the AC losses in the 10 cm wire sample in the range of 150 μW to 10 mW.

The AC losses measured in the superconducting wire sample increased as an exponential function of the AC magnetic field applied with an exponent of 2. This relation between AC losses and the magnitude of the AC magnetic field was the same for all the background fields applied. However, the magnitude of the losses was found to strongly depend on the background field. In the final test series, the losses measured increased when the applied background field was increasing until reaching a peak at a background field of 0.1 T. For stronger background fields, the losses decreased and started levelling out as the background field reached 0.35 T.

From the measured AC losses, it is assumed that within the range of the magnetic fields applied, the dominating losses in the superconducting wire are not AC losses in the MgB_2. The loss patterns found suggest that the losses are a combination of eddy current losses and hysteresis losses in the copper and nickel in the superconducting wire. The losses was found to increase with the square of the AC magnetic field, which complies with theory and conducted simulations of eddy current losses. However, it was found a pattern of the measured losses as a function of the background field that could not be explained by eddy current losses. The different magnitude of the losses with different background fields could be caused by hysteresis losses. It was measured a significant change in the pattern of the losses as a function of the background field from similar testing in the pre-test to the final test. These different patterns suggests that the losses depend on the magnetization of the nickel.

It was not obtained a background field of 0.5 T as planned in the testing. However, the results could be relevant to determine AC losses in a superconducting field winding in sections subject to weaker background fields. The losses measured for up to 0.35 T background field were significantly higher than the modelled superconductor AC losses. Hence, losses from sections with lower background fields in a field winding could strongly impact the total losses. For a complete estimation of AC losses in a superconducting field winding, further testing of AC losses and a precise determination of the magnetic field distribution in a field winding is necessary.

Chapter 9

Recommendations For Further Work

To determine the superconductor AC losses in the MgB_2, it is necessary to obtain stronger magnetic fields. The superconductor AC losses increase with the 3rd power of the AC magnetic field. Hence, these are expected to become dominant with stronger AC fields. Such strong AC fields might be obtained with the AC coil installed, as it is expected to be capable of carrying a current up to 20 A peak, which corresponds to an AC field of 43 mT peak. Testing this would require a change in the AC coil circuit outside the cryostat and the measurement tools, for them to handle a 20 A current. However, this would impose a higher risk of damnation to the AC coil, due to the electromagnetic forces or overheating.

A stronger background field could presumably be achieved with the field winding. The current injection in the field winding was limited to 70 A, by the temperature of the HTS 2. The eight remaining sub- coils in the field winding have in previous testing been proven capable of carrying a current of 146 A [12]. This corresponds to a magnetic field in the wire sample greater than 0.7 T. Thus, by enhancing the HTS 2 cooling, the field winding could be capable of producing twice the magnetic field that was obtained in this project. This could be expected to reduce the eddy current and hysteresis losses (Figure 6.7) and increase the MgB_2 superconductor losses, allowing for the superconductor losses to have a greater impact on the total losses measured.

The measured losses are assumed to be mainly eddy current losses and hysteresis losses. To further investigate the unexpected pattern of losses as a function of the background field, more test series on the installed equipment could be executed. Due to the significant change in measured losses from the pre-test to the final test, it is suggested to run a third similar series of tests to verify the results from the final tests. Furthermore, the wire sample could be demagnetized before another series of tests, trying to replicate the pre-test results. To determine the origins of the losses, the copper on the wire sample could be separated from the nickel and similar tests could be executed on the copper and nickel separately.

The simulations of the field winding and the AC magnetic field have been subject to several simplifications. By investigating the magnetic field distribution in a more thoroughly developed model of the physics in the field winding, a more exact estimation of the magnetic field could be obtained. Furthermore, a more exact model could be used to precisely simulate the magnetic field in the cross- section of the field winding. This would enable to estimate the losses from AC disturbance in a field winding, with respect to the strength of the background field, in different parts of the field winding cross-section.

Bibliography

[1] Columbus Superconductors. Wire Proposal. Power point slides received on mail from N. Magnusson. October, 2016.

[2] The European Wind Energy Association. Wind in power - European statistics 2015. 2016. [Online]. Available: `http://www.ewea.org/fileadmin/files/library/publications/statistics/EWEA-Annual-Statistics-2015.pdf`.

[3] Roland Berger. Offshore wind towards 2020 - On the pathway to cost competitiveness. 2013. [Online] Available: `https://www.rolandberger.com/nl/Publications/pub_offshore_wind_power_central_to_the_transformation_of_germany_s_energy_system.html`.

[4] B. H. Billings and D. E. Gray. *American Institute of Physics Handbook*. McGraw-Hill, New York, 3rd edition, 1972.

[5] Global Wind Energy Council. Global wind report - Annual marked update 2016. 2017. [Online]. Available: `http://www.gwec.net/publications/global-wind-report-2/`.

[6] Copper Development Association Inc. Cryogenic properties of copper. [Online] Available: `https://www.copper.org/resources/properties/cryogenic/`.

[7] Sumitomo Electric Industries. BSCCO characteristics. [Online] Available: `http://global-sei.com/super/hts_e/`.

[8] C. Kittel. *Introduction to Solid State Physics*. Wiley, Hoboken, N.J, 8th edition, 2005.

[9] N. Magnusson. *AC losses in high-temperature superconducting tapes : calorimetric measurement system and semi-empirical modelling*. Thesis, Royal Institute of Technology, Sweden, 2000.

[10] N. Magnusson, A. B. Abrahamsen, D. Liu, M. Runde, and H. Polinder. Hysteresis losses in MgB_2 superconductors exposed to combinations of low AC and high DC magnetic fields and transport currents. *Physica C: Superconductivity and its applications*, 506:133–137, 2014.

[11] I. Marino, A. Pujana, G. Sarmiento, S. Sanz, J. M. Merino, M. Tropeano, J. Sun,

and T. Canosa. Lightweight MgB_2 superconducting 10 MW wind generator. *Superconductor Science and Technology*, 29(2):024005, 2016.

[12] L. Moslått. Cooling and testing of superconducting MgB_2 field winding, 2017. Specialization project TET 4520, NTNU.

[13] University of Cambridge. MgB_2 molecule structure. `http://www.phy.cam.ac.uk/research/research-groups/qm/novelsc`.

[14] M. Paulsen. Assembly and testing of superconducting field winding. Report, NTNU, Norway, 2016.

[15] C. N. Rasmussen and C. Rasmussen. Optimization of termination for a high-temperature superconducting cable with a room temperature dielectric design. *IEEE Transactions on Applied Superconductivity*, 9(1):45–49, 1999.

[16] H. Ta, N. Runde, M. Ta, M. Magnusson, and M. Runde. Apparatus for calorimetric measurements of losses in MgB_2 superconductors exposed to alternating currents and external magnetic fields. *Cryogenics*, 54:44–49, 2013.

Appendices

Appendix A

Measured data

The measurement data from the tests, presented chronologically.

Table A.0.1: Pre-test measurements. AC coil rms current, field winding DC current, 10 second temperature change and calculated power loss from the reference heater table.

08.mai	I_{dc}=0	I_{ac}[A]	1.41	2.11	2.83	3.56	4.24	4.95	5.64	6.38	7.08
		ΔT[K]	0.102	0.248	0.414	0.656	0.913	1.181	1.581	1.895	2.335
		P[μW]	358	845	1507	2344	3366	4457	5924	7417	9343
09.mai	I_{dc}=25.5A	I_{ac}[A]	1.41	2.11	2.88	3.61	4.25	4.86	5.75	6.35	7.17
		ΔT[K]	0.087	0.131	0.199	0.276	0.446	0.602	0.772	0.930	1.204
		P[μW]	308	455	681	951	1634	2169	2759	3446	4539
10.mai	I_{dc}=50.3A	I_{ac}[A]	1.45	2.13	2.86	3.54	4.3	4.91	5.7	6.35	7.02
		ΔT[K]	0.068	0.089	0.095	0.213	0.336	0.401	0.608	0.777	0.865
		P[μW]	241	316	337	727	1193	1452	2188	2778	3145
10.mai	I_{dc}=69.7A	I_{ac}[A]	1.43	2.13	2.85	3.57	4.22	4.85	5.67	6.4	7.13
		ΔT[K]	0.042	0.098	0.128	0.239	0.188	0.551	0.521	0.555	1.006
		P[μW]	144	344	444	814	644	2002	1905	2017	3794

Table A.0.2: Reference heater measurements.

10.mai	I_{dc}=0	$P[\mu W]$	0	47	99	293	887	1773
		ΔT[K]	0.000	0.011	0.029	0.082	0.260	0.480
		$P[\mu W]$	2464	2944	3925	5881	7832	9789
		ΔT[K]	0.693	0.821	1.035	1.572	1.982	2.439

Table A.0.3: Final test measurements. AC coil rms current, field winding DC current, 10 second temperature change and calculated power loss from the reference heater table.

10.mai	I_{dc}=0	I_{ac}[A]	0.71	1.07	1.4	2.83	4.21	5.71	7.12
		ΔT[K]	0.007	0.026	0.051	0.199	0.451	0.802	1.186
		$P[\mu W]$	33	88	177	683	1654	2874	4474
12.mai	I_{dc}=10.4A	I_{ac}[A]		1.03	1.41	2.84			
		ΔT[K]		0.054	0.090	0.330			
		$P[\mu W]$		187	318	1168			
12.mai	I_{dc}=20.9A	I_{ac}[A]		1.05	1.42	2.84			
		ΔT[K]		0.060	0.106	0.391			
		$P[\mu W]$		210	372	1413			
12.mai	I_{dc}=29.3A	I_{ac}[A]		1.01	1.36	2.84			
		ΔT[K]		0.049	0.091	0.379			
		$P[\mu W]$		171	321	1367			
12.mai	I_{dc}=40.2A	I_{ac}[A]		1.01	1.37	2.86			
		ΔT[K]		0.035	0.066	0.289			
		$P[\mu W]$		119	233	1003			
12.mai	I_{dc}=50.3A	I_{ac}[A]	0.70	1.10	1.42	2.84	4.26	5.64	7.05
		ΔT[K]	0.014	0.029	0.053	0.189	0.422	0.744	1.140
		$P[\mu W]$	55	98	185	648	1538	2655	4309
12.mai	I_{dc}=60.2A	I_{ac}[A]		1.07	1.35	2.86			
		ΔT[K]		0.021	0.039	0.145			
		$P[\mu W]$		76	133	503			
12.mai	I_{dc}=69.5A	I_{ac}[A]		1.11	1.50	2.84		5.33	
		ΔT[K]		0.017	0.038	0.131		0.493	
		$P[\mu W]$		63	128	454		1815	
12.mai	I_{dc}=25.2A	I_{ac}[A]	0.63	1.10	1.44	2.75	4.07	5.35	7.13
		ΔT[K]	0.019	0.062	0.104	0.353	0.740	1.250	2.106
		$P[\mu W]$	69	219	364	1260	2638	4707	8361

Appendix B

Dry ice cooling equipment

External cooling of the copper current lead 2, to lower the temperature of the HTS 2 inside the cryostat. A small aluminium container is attached with a copper bracket to the copper conductor on top of the cryostat. During operation of the DC field winding, about 1 liter of dry ice was maintained in the container.

Figure B.0.1: Dry ice cooling system.

Appendix C

Cernox calibration data

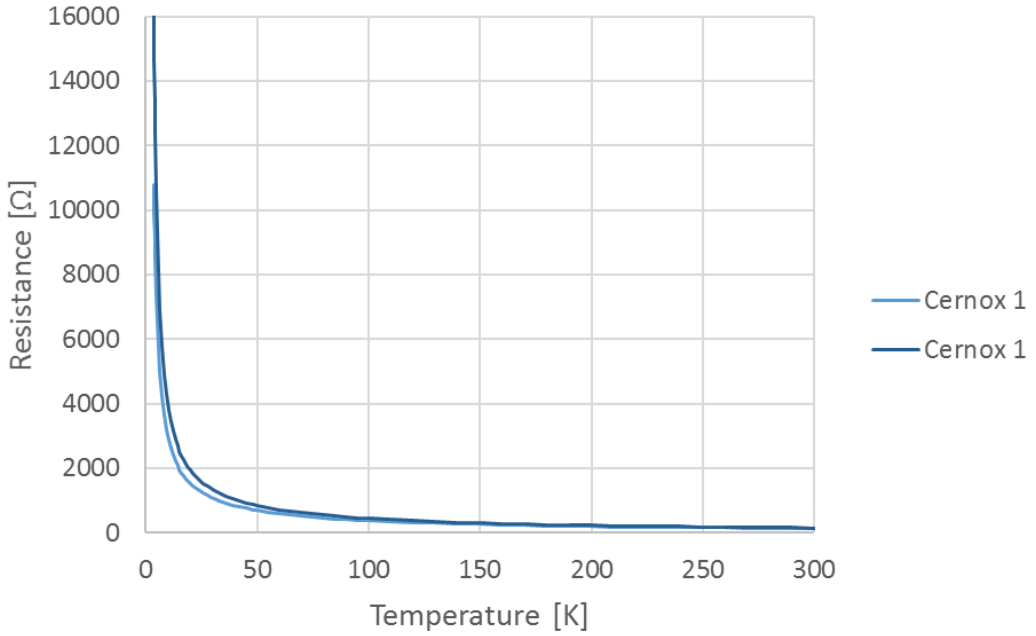

Figure C.0.1: Cernox calibration data.

Appendix D

Simulation of eddy current losses

This chapter presents the properties and settings used in the simulation of the eddy current losses, presented in Figure 7.1. It was executed a 2D simulation of the cross section of the wire sample and the AC coil, that was studied in the frequency domain.

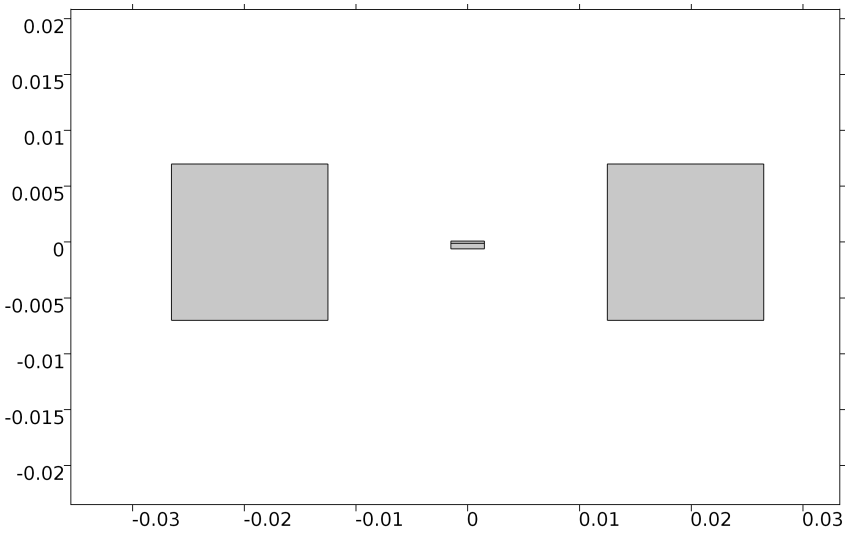

Figure D.0.1: Comsol geometry of the wire sample in the air-gap of the AC coil.

Table D.0.1: Parameters used in the simulation.

Parameter	Value
AC coil sides	14 mm
AC coil air-gap	25 mm
Wire sample width	3 mm
Wire sample copper height	0.2 mm
Wire sample nickel heigth	0.5 mm
Electrical conductivity - Copper	1.25e10 S/m
Electrical conductivity - Nickel	8.33e7 S/m
Relative permeability - Nickel	1 / 600
Frequency	50 Hz

The wire sample is center in the air-gap of the AC coil, and the AC coil is centered in a 30 cm simulation box of air. The cross-sections of the AC coil resemble the area of the copper wires only, and is defined as copper. The upper part of the wire sample is set to copper while the lower is set to nickel.

The AC coil cross-sections is defined as a multi-turn coil with 100 turns. One of the cross-sections is set to be the reverse coil direction. The copper and nickel in the wire sample is defined as a single turn coil with a current of 0 A. This assures that the net current through the wire is 0 A, as in the testing. The mesh is set to *Extremely fine*.

Appendix E

Cryocooler capacity

TYPICAL REFRIGERATION CAPACITY*

***Reference data for new condition.**

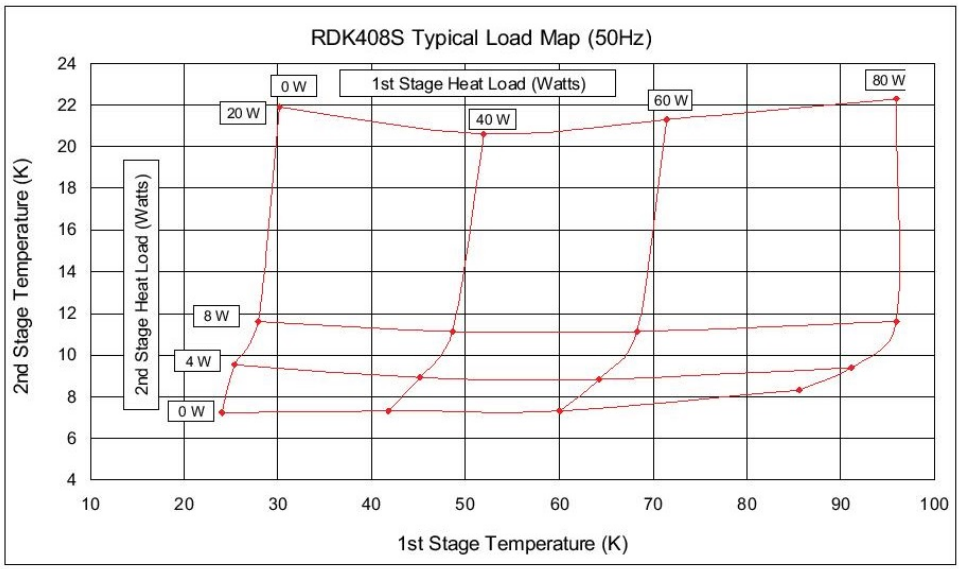

Figure E.0.1: Refrigeration capacity of cryocooler as a function of 1st stage and 2nd stage temperature.

Appendix F

Thermal conductivity of copper

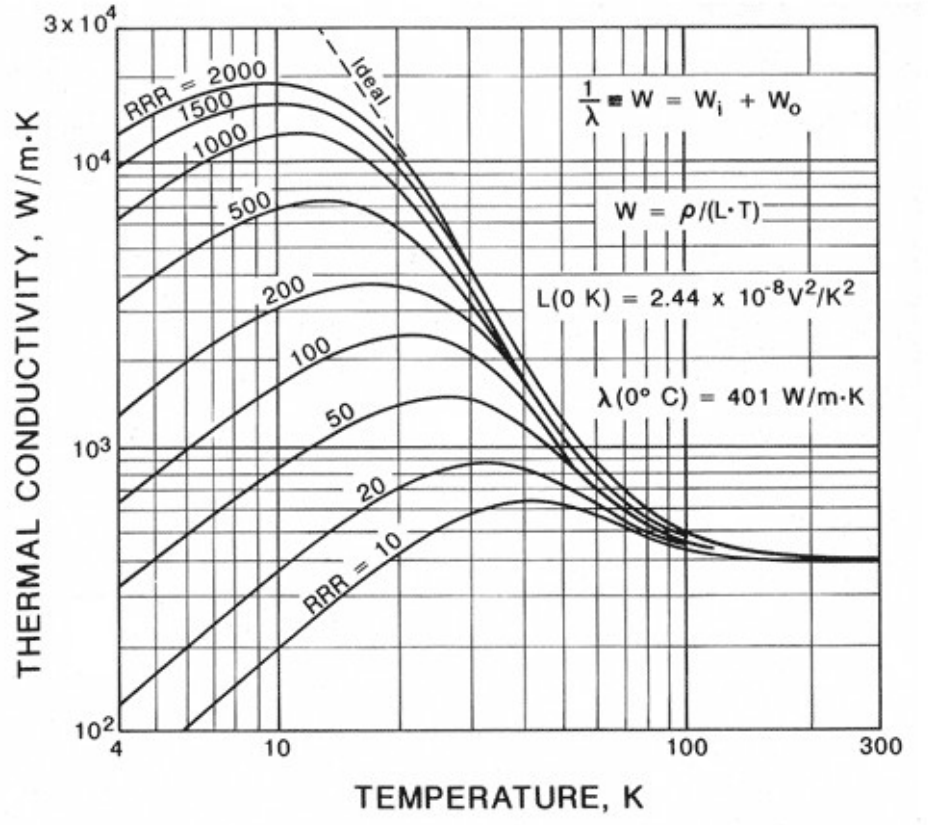

Figure F.0.1: Thermal conductivity of copper as a function of temperature, for different copper RRR-values[6].

Appendix G

Specific heat capacity - Debye curve

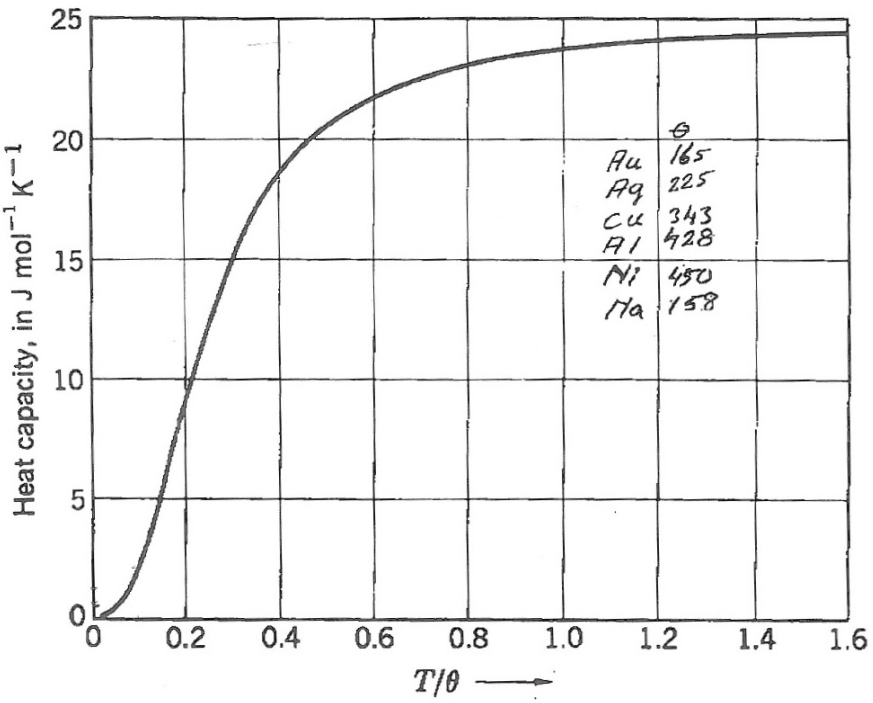

Figure G.0.1: Debye curve. Heat capacity of a solid, according to the Debye approximation. The vertical scale is in J mol^{-1}K^{-1}. The horizantal scale is the temperature normalized to the Debye temperature θ [8].

Appendix H

Resistivity of copper

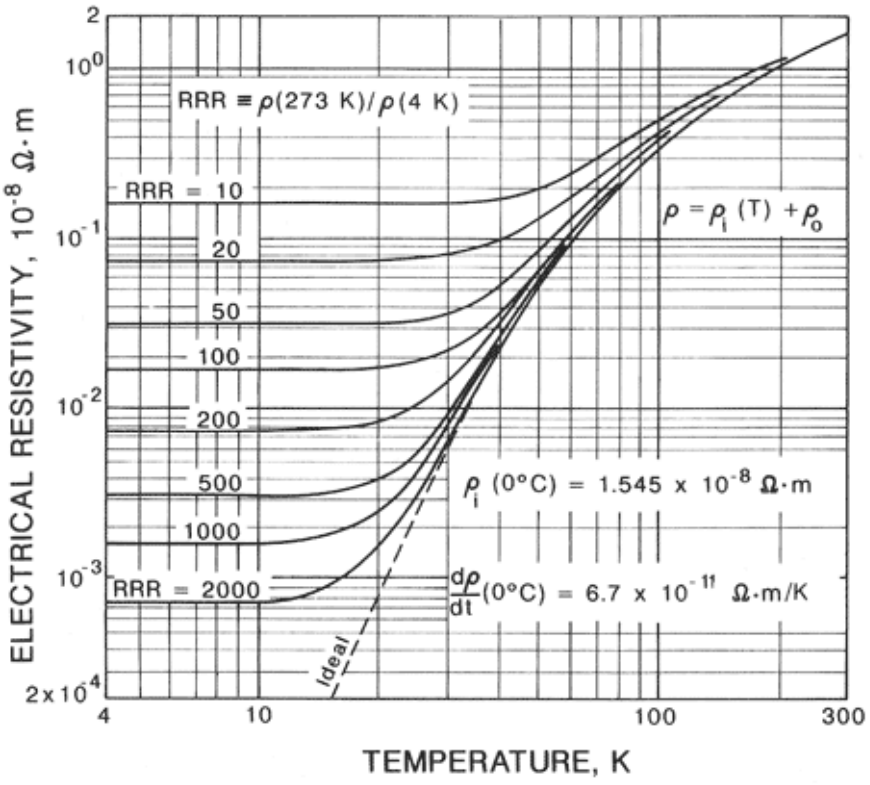

Figure H.0.1: Resistivity of copper at low temperatures for different RRR-values [6].

Appendix I

List of equipment

Table I.0.1: List of equipment

Equipment	**Type**	**Function**	**Mark**
Cryocooler cold head	SUMITOMO RDK-408S	Cold head of the cryocooler	S/N: 47D07334D
Cryocooler compressor unit	SUMITOMO CSW-71D	Compressor unit of the cryocooler	S/N: 3KS07062D
Laptop	Dell Latitude D630	Collect data from datalogger	P07-1481
Datalogger	AGILENT 34970A	Datalogger for quench circuit voltage and circuit break trigger	G05-127
Datalogger	AGILENT 34970A	Data logger for voltage, current and temperature measurements.	G05-0171
Datalogger module	AGILENT 34901A	Data logger module for voltage, current and temperature measurements.	G05-0183-01
Datalogger module	AGILENT 34901A	Data logger module for voltage, current and temperature measurements.	G05-0138-01
Thermometer	FLUKE 54 II B	Temp. measurements from Type T thermal elements below 80K	

Equipment	Type	Function	Mark
Multimeter	FLUKE 175	Resistance measurements	
Multimeter	FLUKE 289	AC current and reference heater current measurements	S03-0446
Multimeter	FLUKE 289	Cernox current measurements	
Vacuum pump	Alcatel 2015	Pre-vacuum pump	
Turbo vacuum pump	PFEIFFER THP200	Turbo vacuum pump	
Power supply	PFEIFFER TCP200	Controller and power supply of turbo vacuum pump	
Exhaust filter	LEYBOLD AF 16-25	Vacuum pump exhaust filter	P05-0068
Current source	Agilent 6661A	Current source of the field winding	B02-0503
DC power supply	Knick Berlin 37 - S140	High precision DC power supply for the Cernox sensors	B02-0212
DC power supply	Rohde&Schwarz - HMC 8042	High precision DC power supply for the reference heater	
Trafo variac	Lubecke - 2R54-220HP	AC current supply for the AC coil	
Trafo	Eltrafo	Voltage reduction for higher AC current accuracy	B01-0203